ENGINEERING QUANTUM SYSTEMS WITH COHERENT FEEDBACK CONTROL

A DISSERTATION
SUBMITTED TO THE DEPARTMENT OF APPLIED PHYSICS
AND THE COMMITTEE ON GRADUATE STUDIES
OF STANFORD UNIVERSITY
IN PARTIAL FULFILLMENT OF THE REQUIREMENTS
FOR THE DEGREE OF
DOCTOR OF PHILOSOPHY

Gopal Pudipeddi Sarma
June 2013

This dissertation is online at: http://purl.stanford.edu/fy745rc4572

I certify that I have read this dissertation and that, in my opinion, it is fully adequate in scope and quality as a dissertation for the degree of Doctor of Philosophy.

Hideo Mabuchi, Primary Adviser

I certify that I have read this dissertation and that, in my opinion, it is fully adequate in scope and quality as a dissertation for the degree of Doctor of Philosophy.

Surya Ganguli

I certify that I have read this dissertation and that, in my opinion, it is fully adequate in scope and quality as a dissertation for the degree of Doctor of Philosophy.

Yoshihisa Yamamoto

Approved for the Stanford University Committee on Graduate Studies.

Patricia J. Gumport, Vice Provost Graduate Education

This signature page was generated electronically upon submission of this dissertation in electronic format. An original signed hard copy of the signature page is on file in University Archives.

Abstract

The control of quantum dynamics in which feedback is accomplished via coherent, all-optical signal processing suggests the possibility of mature, engineered quantum systems that are technologically homogeneous and in which both plant and controller are quantum systems. In this thesis, I give a focused case study of several systems in which feedback control of the system dynamics is accomplished entirely through field-mediated, coherent signal processing. After introducing some recently developed theoretical tools for modeling individual and networks of open quantum systems, I analyze a proposal for generating polarization-squeezed light by double-passing a coherent drive twice through an atomic ensemble. This setup represents a simple, deterministic feedback system and I illustrate it here primarily to give a detailed, side-by-side comparison of two different quantum optical input/output formalisms. Building on the intuition gained from analyzing this system, I then present an extensive analysis of autonomous quantum memories for quantum error correction. After a review of recent proposals for continuous-time relaxations of the 3-qubit bit-flip/phase-flip and 9-qubit Bacon-Shor codes, I describe an automated workflow for synthesis and analysis of quantum networks in the Gough-James formalism for cascaded quantum networks. Using this workflow, I construct the Gough-James network model, and quantitatively analyze the effects of propagation losses on the 3-qubit and 9-qubit codes. In order to extend this analysis to arbitrary stabilizer codes, I then present a class of phenomenological master equations for autonomous quantum memories, and demonstrate several critical cases in which the structure of the error correcting code is manifest in the physical dynamics of the corresponding photonic implementation. In particular, I show that *separability* of the stabilizer generators,

that is, independent detectability of Pauli-X and Pauli-Z errors can simplify feedback mechanisms for protection from Pauli-Y errors. Then I show how the presence of the gauge qubits in subsystem codes can allow for optimally routing probe beams so that loss induced errors lie entirely on the gauge space, thus increasing the storage fidelity of the encoded state. Finally, I examine the fine grained behavior of these devices and propose a modified fidelity metric for quantifying the performance of realistic quantum memories.

Acknowledgements

I am deeply grateful to my advisor, Hideo Mabuchi, my brilliant colleagues in Mabuchi-Lab, and the many remarkable individuals I encountered during my time at Harvard, Caltech, and Stanford. I feel truly fortunate for having received such an outstanding education. Most of all, I would like to thank my family, without whom, this work simply would not have been possible.

Contents

List of Tables

List of Figures

Chapter 1

Introduction

Strictly speaking, this thesis is about engineering– hence the title. Several decades of research in quantum optics, atomic physics, and related fields has given us an incredible degree of control over atomic dynamics (in both real and artificial atoms) that allows us to envision a future of truly quantum engineered systems, achieving the degree of maturity that we have today with classical electrical engineering systems.

It is common when people hear about quantum engineering to immediately associate the idea with building a quantum computer. But our perspective in the feedback control community is that a quantum computer is just one of many devices that one may want to engineer with a more sophisticated understanding of how to control quantum dynamics, and consequently, the viewpoint that we advocate places a substantial emphasis on extending basic ideas from classical feedback control theory to the quantum domain. Of course, building a quantum computer would be a heroic and worthwhile achievement, and furthermore, we can expect that a mature discipline of quantum engineering would bring about advances in ultra low-power (e.g. attojoule scale) signal processing, interconnects, and sensor networks. And given the broadly applicable nature of some of these technologies, it would be reasonable to suppose that environmental and medical applications may also be on the horizon.

In quantum feedback control, there are what amount to two distinct types of control

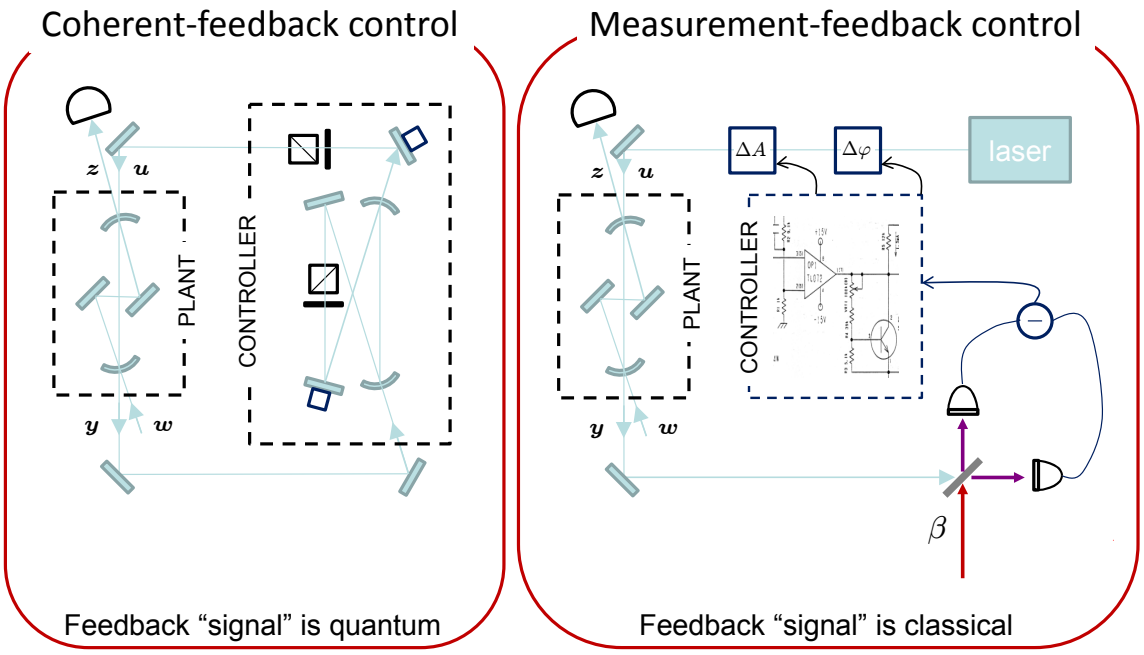

Figure 1.1: Comparison of a coherent feedback setup with its measurement-based counterpart. Although the plant is assumed to be a quantum system in both cases, in the coherent feedback setup, the controller is assumed to be a quantum mechanical system as well, whereas in the measurement-based feedback setup, the controller is a classical device. (*Image courtesy of Hideo Mabuchi*)

systems that merit investigation: measurement-based and coherent feedback control (see Figure 1). As the name implies, measurement-based feedback control consists of a hybrid quantum-classical setup in which active measurement and signal processing is part of the feedback control loop. I call this setup a "hybrid setup" because in measurement-based feedback control, a large part of the system is strictly classical. That is, we presume what amounts to macroscopic or at least mesoscopic apparatus playing the role of an actual computer that is responsible for processing measurement records and then deciding what to do with it.

On the other hand, coherent feedback control refers to those systems in which both plant and controller and fully quantum mechanical systems. There are two primary

reasons to consider coherent quantum feedback over its measurement-based counterparts. The first is technological homogeneity. While there may be some cases where the odd marriage between a hot classical computer and a cold, quantum register is appropriate, in envisioning a future of mature quantum engineered systems, one would naturally suppose that the control systems involved would remain at the nanoscale where the information is being processed.

On the other hand, there may be inherent performance advantages to keeping information at the quantum level- see for example recent work on the advantages of coherent feedback for cooling nano-mechanical oscillators [29]. Indeed, one way of motivating the research agenda of coherent feedback control is to think of it as an engineering analogue to quantum information theory. Historically, the result that launched the field of quantum information and quantum computation was Peter Shor's factoring algorithm, which demonstrated an exponential speedup over the best known classical algorithms for prime factorization [62, 50]. With the intuition then that quantum mechanics can, in the abstract, give rise to performance advantages for certain types of problems, it seems reasonable to ask a related question motivated not from the algorithmic perspective, but rather from the engineering perspective. That is, we can ask if instead of starting with a quantum algorithm and trying to work backwards to engineer a system tailored to that particular algorithm's performance requirements, whether we can develop an understanding of quantum mechanical performance advantages from an engineering perspective by starting with the basic principles of feedback control and working from the bottom up.

In this thesis, I will concentrate on the former set of motivations for why one might consider purely quantum feedback without the need for classical measurement and signal processing apparatus, although, in the context of quantum memories, I will mention how we might think about taking advantage of coherent feedback to achieve performance objectives that may not be possible in the classical case.

With these motivations in mind, I want to briefly discuss the methodology and fundamental analytical tools which are the building blocks of the theoretical work that I present in this thesis. It took a few years for me to understand that in theoretical physics, there is often a rich interplay between researchers who are firmly on the physics side and those firmly on the mathematics side. When fundamentally new mathematical techniques are developed, it can take a few years for these new methods to be integrated into the day to day workflow of the practicing physicist, at which point this work often ceases to have its original mathematical character. The reason I mention all of this, is that on the one hand, the work I describe in this thesis would simply not have been possible without recent developments that qualify as first rate mathematics. On the other hand, what I present here is not in any way, shape, or form, research mathematics.

Therefore, while much of the background material on quantum stochastic calculus can be described in a much more earthy, theoretical physics kind of language– this was developed by among others Gardiner, Zoller, Collet, and Parkins– there are several techniques, notably the adiabatic elimination theory that plays a prominent role in the analysis of quantum error correcting circuits I describe in Chapter 4, that represent genuinely new mathematics that required much of the machinery that was laid down in previous years by researchers in the mathematical physics community. Then again, having applied those techniques, we can often fall back on our physicist's intuition and for example, the work I describe in Section 4.4 starts from a phenomenological master equation for stabilizer codes, without at any point invoking QSDE's or the adiabatic elimination result.

So while this is certainly not a mathematics thesis, it owes a serious debt to mathematics– the references I've included in the introduction should be sufficient for the interested reader to make his or her way to the more mathematical literature that underlies this work. There is no doubt more serious mathematics to be done for coherent feedback control to truly blossom, and when the time is right, I hope the right people will jump in. Perhaps some of the old masters will come back and take another look.

Here then is an outline of what follows. In the first chapter, I give an exposition of quantum optical modeling with quantum stochastic differential equations. In Chapter 2, using two different formalisms– the Gardiner-Collett input/output formalism and also the QSDE-based methods described in the introduction– I analyze a simple, deterministic coherent feedback system for generating polarization-squeezed light. Finally, building on the intuition gained in the preceding chapters, I describe recent work on designing autonomous quantum memories, and give a detailed analysis of robustness issues for stabilizer quantum error correction. Along the way, I describe an engineering-oriented methodology for automating QSDE-based calculations in a workflow that suggests a photonics analogue of classical electrical circuit theory. Finally, I examine a class of phenomenological master equations for continuous-time relaxations of stabilizer quantum error correction, and analyze some general features of stabilizer codes which suggest practical implications for the required control mechanisms and circuit layout for autonomous quantum memories.

As one final point about the exposition, I should state that this thesis should be thought of as an edited volume of original results presented in the references [8, 58, 65, 56, 57]. Additional material both from classic textbooks and more recent research literature is included to form a coherent and self-contained exposition and is not intended to represent original work.

Chapter 2

Quantum optics and quantum stochastic calculus

For the most part, the formalism that underlies the work I present in this thesis can be thought of as arising from the heuristic methods of quantum stochastic calculus that were developed over the course of several decades in the quantum optics community, combined with the series and concatenation products of Gough and James, and the adiabatic elimination theory of Bouten, van Handel, and Silberfarb– the latter of which came about through substantially more rigorous methods in functional analysis and probability theory. However, given that those methods are not necessary to understand the material I present here, I will give a physics-centered introduction to the quantum stochastic calculus, following quite strictly, the exposition of Gardiner, Parkins, and Zoller in [20] and Gardiner and Zoller in [21]. I will then discuss the series and concatenation products for QSDE's and present the basic mechanics of applying the adiabatic elimination techniques in practical computations.

2.1 Quantizing the electromagnetic field

It is remarkable that the formalism we will use to model the coherent quantum networks in the latter sections of this thesis can be derived from first principles starting from Maxwell's equations. Our ultimate goal in this section, which is an intermediate

one, is to find an expression for the independent variables of the field. We will then construct new quantities which are linear combinations of these independent variables (the normal modes), which we will then replace with quantum mechanical operators to arrive at a quantized magnetic vector potential. This will be the starting point in the next section, in which I give a physically motivated derivation of the quantum stochastic calculus.

It is quite common in textbooks on quantum optics or quantum field theory to introduce second quantization of the electromagnetic field by assuming periodic boundary conditions, so that the field/vector potential can be expanded into a discrete set of normal modes. This is a convenient pedagogical tool, and it is of course mentioned as an afterthought, that one can recover a dense set of normal modes by taking the $L \to \infty$ limit. Of course, in the quantum optical case, where we ultimately will want to model the electromagnetic field as a reservoir, we will need a dense set of modes, so the approach I've chosen here follows that of Cohen-Tannoudji [12] where we do not at any point assume periodic boundary conditions in order to quantize the vector potential in the Coulomb gauge. From this point, we can employ the opposite procedure, and impose periodic boundary conditions to recover the more familiar discrete normal mode expansion.

We begin with Maxwell's equations in their familiar form:

$$\begin{aligned}
\nabla \cdot \mathbf{E}(\mathbf{r},t) &= \frac{1}{\epsilon_0}\rho(\mathbf{r},t) \\
\nabla \cdot \mathbf{B}(\mathbf{r},t) &= 0 \\
\nabla \times \mathbf{E}(\mathbf{r},t) &= \frac{\partial}{\partial t}\mathbf{B}(\mathbf{r},t) \\
\nabla \times \mathbf{B}(\mathbf{r},t) &= \frac{1}{c^2}\mathbf{E}(\mathbf{r},t) + \frac{1}{\epsilon_0 c^2}\mathbf{j}(\mathbf{r},t)
\end{aligned}$$

where $\rho(\mathbf{r},t)$ and $\mathbf{j}(\mathbf{r},t)$ are charge and current densities. We will ultimately take these to be 0 (as we are interested in a free field), but will keep them for now for generality. Taking a spatial Fourier transform, we can write these equations in the

following form:

$$\begin{aligned} i\mathbf{k}\cdot\mathscr{E}(\mathbf{k},t) &= \frac{1}{\epsilon_0}\rho(\mathbf{k},t) \\ i\mathbf{k}\cdot\mathscr{B}(\mathbf{k},t) &= = 0 \\ i\mathbf{k}\times\mathscr{E}(\mathbf{k},t) &= \frac{\partial}{\partial t}\mathscr{B}(\mathbf{k},t) \\ i\mathbf{k}\times\mathscr{B}(\mathbf{k},t) &= \frac{1}{c^2}\mathscr{E}(\mathbf{k},t) + \frac{1}{\epsilon_0 c^2}\mathscr{J}(\mathbf{k},t) \end{aligned}$$

From the above equations, we can see that the longitudinal components of the electric and magnetic field are not independent variables. That is, note that

$$\mathscr{E}_{||}(\mathbf{k},t) = -\frac{i\mathbf{k}}{\epsilon_0 k^2}\rho(\mathbf{k},t) \tag{2.1}$$

$$\mathscr{B}_{||}(\mathbf{k},t) = 0 \tag{2.2}$$

However, the transverse components are independent variables, with the following equations of motion:

$$\begin{aligned} \frac{\partial}{\partial t}\mathscr{B}_{\perp}(\mathbf{k},t) &= -i\mathbf{k}\times\mathscr{E}_{\perp}(\mathbf{k},t) \\ \frac{\partial}{\partial t}\mathscr{E}_{\perp}(\mathbf{k},t) &= c^2 i\mathbf{k}\times\mathscr{B}_{\perp}(\mathbf{k},t) - \frac{1}{\epsilon_0}\mathscr{J}_{\perp}(\mathbf{k},t) \end{aligned}$$

We now introduce the vector and scalar potentials $\mathbf{A}$ and U and write the electric and magnetic field in the following familiar form (in real space):

$$\begin{aligned} \mathbf{E}(\mathbf{r},t) &= -\nabla U - \frac{\partial \mathbf{A}(\mathbf{r},t)}{\partial t} \\ \mathbf{B}(\mathbf{r},t) &= \nabla\times\mathbf{A}(\mathbf{r},t) \end{aligned}$$

In $\mathbf{k}$ space, of course, these become:

$$\mathscr{E}(\mathbf{k},t) = -i\mathbf{k}\mathscr{U}(\mathbf{k},t) - \frac{\partial\mathscr{A}(\mathbf{k},t)}{\partial t} \tag{2.3}$$

$$\mathscr{B}(\mathbf{k},t) = i\mathbf{k}\times\mathscr{A}(\mathbf{k},t) \tag{2.4}$$

From elementary electrodynamics, we recall that the $\mathbf{E}$ and $\mathbf{B}$ fields are invariant under a gauge transformation where the vector and scalar potential are modified as:

$$\begin{aligned} \mathbf{A}(\mathbf{r},t) &\longrightarrow \mathbf{A}(\mathbf{r},t) + \nabla\mathbf{G}(\mathbf{r},t) \\ U(\mathbf{r},t) &\longrightarrow U(\mathbf{r},t) - \frac{\partial G(\mathbf{r},t)}{\partial t} \end{aligned}$$

Again, in reciprocal space, we can express the gauge transformation as:

$$\begin{aligned} \mathscr{A}(\mathbf{k},t) &\longrightarrow \mathscr{A}(\mathbf{k},t) + i\mathbf{k}\mathbf{G}(\mathbf{k},t) \\ U(\mathbf{k},t) &\longrightarrow U(\mathbf{k},t) - \frac{\partial G(\mathbf{k},t)}{\partial t} \end{aligned}$$

Thus we see that while the longitudinal component of the vector potential $\mathscr{A}_{||}$ and the scalar potential $\mathscr{U}$ are modified under a gauge transformation, the transverse component of the vector potential is invariant, i.e. $\mathscr{A}'_{\perp}(\mathbf{k},t) = \mathscr{A}(\mathbf{k},t)$.

We also see from above (Equations 2.3 and 2.4), that the transverse field $\mathscr{E} = \mathscr{E}_{\perp}$ and $\mathscr{B} = \mathscr{B}_{\perp}$ only depend on $\mathscr{A}_{\perp}$:

$$\begin{aligned} \mathscr{E}(\mathbf{k},t) &= -\frac{\partial}{\partial t}\mathscr{A}_{\perp}(\mathbf{k},t) \\ \mathscr{B}(\mathbf{k},t) &= i\mathbf{k} \times \mathscr{A}_{\perp}(\mathbf{k},t) \end{aligned}$$

So far, we haven't taken advantage of the gauge freedom afforded to us by the function $\mathbf{G}(\mathbf{r},t)$ above. We now choose the *Coulomb gauge*, which corresponds to the condition $\nabla \cdot \mathbf{A} = 0$, or equivalently $\nabla^2\mathbf{G} = -\nabla \cdot \mathbf{A}$. This implies that the longitudinal component of the vector potential is identically 0 (both in real space and reciprocal space, of course), that is, $\mathbf{A}(\mathbf{r},t) = \mathscr{A}(\mathbf{k},t) = 0$.

We can then find an expression for the scalar potential in terms of the charge density

ρ (see Equations 2.1 and 2.3):

$$\begin{aligned} \mathscr{U}(\mathbf{k},t) &= \frac{1}{k^2\epsilon_0}\rho(\mathbf{k},t) \\ U(\mathbf{r},t) &= \frac{1}{4\epsilon_0}\int d^3r' \frac{\rho(\mathbf{r}',t)}{|\mathbf{r}-\mathbf{r}'|} \end{aligned}$$

Thus we see that in the Coulomb gauge, the independent variables of the field are $\mathscr{A}_\perp(\mathbf{k},t)$ and $\dot{\mathscr{A}}_\perp(\mathbf{k},t) = \mathscr{E}_\perp(\mathbf{k},t)$, the transverse vector potential and its first derivative (the transverse electric field). We will now introduce, as fundamental quantities, convenient linear combinations of these independent fields:

$$\begin{aligned} \alpha(\mathbf{k},t) &= -i\sqrt{\frac{\epsilon_0}{2\hbar\omega}}\left[-\dot{\mathscr{A}}_\perp(\mathbf{k},t) + i\omega\mathscr{A}_\perp(\mathbf{k},t)\right] \\ &= -i\sqrt{\frac{\epsilon_0}{2\hbar\omega}}\left[\mathscr{E}_\perp(\mathbf{k},t) - c\frac{\mathbf{k}}{k}\times\mathscr{B}(\mathbf{k},t)\right] \end{aligned}$$

Note that we can now express the transverse vector potential $\mathscr{A}_\perp$ in terms of the quantity $\alpha(\mathbf{k},t)$ and its Hermitian conjugate:

$$\begin{aligned} \mathscr{A}_\perp(\mathbf{k},t) &= \frac{\alpha(\mathbf{k},t)+\alpha^\dagger(\mathbf{k},t)}{\omega\sqrt{\frac{\epsilon_0}{2\hbar\omega}}} \\ &= \sqrt{\frac{2\hbar}{\epsilon_0\omega}}\left(\alpha(\mathbf{k},t)+\alpha^\dagger(\mathbf{k},t)\right) \end{aligned}$$

Finally, taking the Fourier transform, and using the relationship $\alpha^\dagger(\mathbf{k},t) = \alpha(-\mathbf{k},t)$ we can express the transverse vector potential in real space, expanded into a continuous spectrum of normal modes which can be replaced by their quantum mechanical operator counterparts:

$$\mathbf{A}_\perp(\mathbf{r},\mathbf{t}) = \int d^3k \sum_\epsilon \sqrt{\frac{2\hbar}{\epsilon_0\omega}}\left[\epsilon a_\epsilon(\mathbf{k})e^{i(\mathbf{k}\cdot\mathbf{r}+\omega t)} + \epsilon a_\epsilon^\dagger(\mathbf{k})e^{-i(\mathbf{k}\cdot\mathbf{r}-\omega t)}\right]$$

2.2 Quantum noise processes

To derive the quantum noise processes, we begin with the usual system-bath Hamiltonian representation of an open quantum system:

$$H = H_{sys} + H_b + H_{int} \tag{2.5}$$

We leave H_{sys} unspecified and can write the bath Hamiltonian as:

$$H_b = \frac{1}{2}\int_0^\infty dx \left\{ \dot{A}(x,t)^2 + c^2[\partial_x A(x,t)]^2] \right\} \tag{2.6}$$

and the interaction Hamiltonian as:

$$H_{int} = \int_0^\infty dx \kappa(x)\{c^\dagger \dot{A}^{(+)}(x,t) + c\dot{A}^{(-)}(x,t)\} \tag{2.7}$$

The motivation to choose a linear coupling is that it is the simplest possible interaction between the system and the bath– there is no additional fundamental principle at work here. $A(x,t)$ is a one-dimensional form of the vector potential derived in the previous section, with expansion

$$A(x,t) = A^{(+)}(x,t) + A^{(-)}(x,t) \tag{2.8}$$

with

$$A^{(+)}(x,t) = \int_0^\infty d\omega \sqrt{\frac{\hbar}{2\pi\omega c}} \cos(\frac{\omega x}{c}) b(\omega) e^{-i\omega t}, \tag{2.9}$$

where the operators b and $b^\dagger$ satisfy the canonical commutation relations:

$$[b(\omega), b^\dagger(\omega')] = \delta(\omega - \omega') \tag{2.10}$$

Note that we have made several approximations in this description– the rotating wave approximation to eliminate the non-energy conserving terms $c^\dagger A^{(-)}$ and $cA^{(+)}$ and also we have assumed that there is no system recoil from its interaction with the bath. Typically, where the system is considered to be an atom, this amounts to

neglecting the center of mass motion. The physical assumption behind the rotating wave approximation is that the coupling terms that we have neglected oscillate at much higher frequencies than the slower dynamics that we are interested in. This is a reasonable approximation in quantum optics, where the coupling rates operate on the GHz-MHz frequency scales and the system/bath operators oscillate at optical frequencies (100's of THz) [20, 21, 12].

If we perform the x integration, and let

$$\tilde{\kappa}(\omega) = -\sqrt{\frac{\omega}{2\pi\hbar c}}\int_0^\infty dx\kappa(x)\cos(\frac{\omega x}{c}), \tag{2.11}$$

we arrive at familiar looking interaction and bath Hamiltonians. In fact, this is often the starting point in deriving the quantum stochastic calculus (see, for example, [21]):

$$H_{int} = i\hbar\int_0^\infty d\omega\tilde{\kappa}(\omega)\{c^\dagger b(\omega) - cb^\dagger(\omega)\} \tag{2.12}$$

$$H_b = \int_0^\infty d\omega\hbar\omega b^\dagger(\omega)b(\omega) \tag{2.13}$$

Now, let us consider the equation of motion for this system in the Schrödinger picture:

$$\frac{d|\psi,t\rangle_s}{dt} = \left\{\frac{i}{\hbar}[H_{sys}+H_B] + \int_0^\infty d\omega\tilde{\kappa}(\omega)[cb^\dagger(\omega) - c^\dagger b(\omega)]\right\}|\psi,t\rangle_s \tag{2.14}$$

Moving to an interaction picture with respect to the system and bath Hamiltonians, we obtain:

$$|\psi,t\rangle = \exp\left[\frac{i}{\hbar}[H_{sys}+H_B](t-t_0)\right]|\psi,t\rangle_s \tag{2.15}$$

Then, for operators $X_m^\pm$ such that $[H_{sys}, X_m^\pm] = \pm\hbar\omega_m X_m^\pm$, we incorporate time dependence as follows:

$$\begin{aligned} X_m^\pm(t) &= \exp[\pm i\omega_m(t-t_0)]X_m^\pm \\ c(t) &= \exp[-i\Omega(t-t_0)]c \\ b(\omega,t)_I &= \exp[-i\omega(t-t_0)]b(\omega) \end{aligned}$$

In this new picture, the system and bath Hamiltonian are eliminated from the Schrödinger equation and we are simply left with the second of the above terms– of course, the operators now being time-dependent:

$$\frac{d|\psi,t\rangle}{dt} = \int_0^\infty d\omega\tilde{\kappa}(\omega)[c(t)b(\omega,t)_I^\dagger - c(t)^\dagger b(\omega,t)_I]|\psi,t\rangle \tag{2.16}$$

Substituting the time dependent operators $b(\omega,t)$ and $c(t)$ into our Schrödinger picture representation, we have the following:

$$\frac{d}{dt}|\psi,t\rangle = \sqrt{\gamma}[cb^\dagger(t) - c^\dagger b(t)]|\psi,t\rangle, \tag{2.17}$$

where, recalling the previous equations, we have that the operator $b(t)$ can be expressed as

$$b(t) = \frac{1}{\sqrt{\gamma}}\int_0^\infty \tilde{\kappa}(\omega)b(\omega)e^{-i(\omega-\Omega)(t-t_0)}d\omega \tag{2.18}$$

2.2.1 Markov approximation

Note that while we have assumed that our raising and lowering operators are delta correlated in the frequency domain, a priori, we cannot assume the same in the time domain [63]. Our goal now is to show that we can arrive at delta correlated operators if we make several assumptions, usually lumped together under the heading of a *Markov approximation*. Let us now compute the commutator of $b(t)$ at different times. From our previous expression, we can write this formally as:

$$[b(t), b(t')] = \int_0^\infty d\omega e^{i\omega(t-t')}e^{-i\Omega(t-t')}|\kappa(\omega)|^2/\gamma \tag{2.19}$$

We now proceed in the following manner: first we assume that the interaction picture equation of motion is a slowly varying function of time. In other words, we assume that there is a characteristic time scale τ_D, denoting a damping time, such that $\tau_D \gg \frac{1}{\omega_m}$ (in particular $\tau_D \gg \frac{1}{\Omega}$). We also make a long wavelength approximation [20, 12], that is, we assume that the system (presumably an atom) is much smaller than the distance light can travel in one unit τ_D. This places a constraint on the function

$|\tilde{\kappa}(\omega)|^2$, implying in particular, that $\kappa(x)$ is sharply peaked in a range $x/c \sim \tau_D$. This being the case we can approximate $|\tilde{\kappa}(\omega)|^2$ by $|\tilde{\kappa}(\Omega)|^2 = \gamma/2\pi$. We also extend the lower integral to $-\infty$, and evaluate the commutator as:

$$[b(t), b(t')] \approx \int_{-\infty}^{\infty} d\omega e^{i\omega(t-t')} e^{-i\Omega(t-t')} |\kappa(\omega)|^2/\gamma \approx \delta(t-t') \tag{2.20}$$

The operators $b(t)$ are traditionally thought of as *quantum noise processes*, with the variable t representing the time at which an infinitesimal segment of the field interacts with the system, rather than the free parameter of a time-dependent operator. We can think of these operators as "inputs" to the quantum system– with an input / output theory in mind, let us denote our operators $b(t) \equiv b_{in}(t)$. Now, for a time $t > t_1$, let us take

$$b_{out}(t) = \frac{1}{\sqrt{2\pi}} \int_{-\infty}^{\infty} d\omega e^{-i(\omega-\Omega)(t-t_1)} b(\omega, t_1) \tag{2.21}$$

which is defined analogously to $b_{in}(t)$, but at a future time t_1. In the Heisenberg picture, it can be shown [21] that for all t_1, $b_{out}(t)$ is given by

$$b_{out}(t) = b_{in}(t) + \sqrt{2\pi\kappa(\Omega)} c(t) \tag{2.22}$$

Thus we see that the output field $b_{out}(t)$ consists of two terms– the input field, plus a contribution arising from the quantum noise process interacting at time t with the system.

2.2.2 Quantum stochastic calculus

Suppose we assume that the field is initially in a vacuum state. Then we have that $b(t')|0\rangle = 0$ and furthermore that:

$$\langle 0|b(t')b^\dagger(t)|0\rangle = \langle 0|b(t')b^\dagger(t) - b^\dagger(t)b(t')|0\rangle = \langle 0|[b(t'), b^\dagger(t)]|0\rangle = \delta(t-t') \tag{2.23}$$

As this is a singular quantity and not a proper function, we have to resort to the techniques from classical stochastic calculus (see for example, [52]) in order to properly

handle integration of the white noise processes $b(t)$. Like classical white noise $\xi(t)$, our field operators are delta correlated.

So in analogy to the case of integration with respect to classical white noise, we can think of our field operators as a derivative of the integral expressions:

$$B_t - B_{t_0} \equiv \int_{t_0}^{t} dt' b(t') \equiv \int_{t_0}^{t} dB_t \tag{2.24}$$

$$B_t^\dagger - B_{t_0}^\dagger \equiv \int_{t_0}^{t} dt' b^\dagger(t') \equiv \int_{t_0}^{t} dB_t^\dagger \tag{2.25}$$

The operators B_t and $B^\dagger(t)$ are traditionally called the *annihilation* and *creation processes*, respectively. Later in this chapter, when we examine how to extend the single-mode treatment developed here to the case of multiple modes, we will introduce the *gauge process* [5, 9]:

$$\Lambda_t - \Lambda_0 \equiv \int_{t_0}^{t} dt' b^\dagger(t') b(t') \equiv \int_{t_0}^{t} d\Lambda_{t'} \tag{2.26}$$

With these definitions in mind, we can return to our vacuum expectations, which now become:

$$\begin{aligned}
&\langle B(t) - B(t_0) \rangle = 0 \\
&\langle (B(t) - B(t_0))^2 \rangle = \langle (B^\dagger(t) - B^\dagger(t_0))^2 \rangle = 0 \\
&\langle (B(t_1) - B(t_0))(B^\dagger(t) - B^\dagger(t_0)) \rangle = \min(|t_1 - t_0|, |t - t_0|)
\end{aligned}$$

Furthermore, we can return to our Schrödinger picture representation (2.19) from above, which we now properly denote by the following integral equation:

$$|\psi, t\rangle - |\psi, t_0\rangle = \int_{t_0}^{t} (L dB_{t'}^\dagger - L^\dagger dB_{t'}) |\psi, t'\rangle \tag{2.27}$$

Note the connection of the coupling terms L and $L^\dagger$ to the terms in Equation 2.17. This integral equation is what is known as a *quantum stochastic differential equation*,

and it is usually denoted by the following short hand:

$$d|\psi_t\rangle = (LdB_t^\dagger - L^\dagger dB_t)|\psi_t\rangle \tag{2.28}$$

Again, as in the classical case [52], we can now formulate two different notions of integration. In the Itô integral, we assume that the Riemann sum is taken with respect to the end point of the integrand, i.e.,

$$\int_{t_0}^{t} f(t')dB(t') = \lim_{n\to\infty} \sum_{i=0}^{n} f(t_i)[B(t_{i+1}) - B(t_i)] \tag{2.29}$$

Alternatively, in what is known as Stratanovich integration, we can evaluate the Riemann sum with respect to the mid-point of the integrand, i.e.

$$\int_{t_0}^{t} f(t')dB(t') = \lim_{n\to\infty} \sum_{i=0}^{n} \frac{(f(t_i) + f(t_{i+1}))}{2}[B(t_{i+1}) - B(t_i)] \tag{2.30}$$

Here the integrand $f(t)$ is assumed to be a a *non-anticipating* function, that is, one that is independent of the driving noise process $B(s)$ for $s > t$.[1]

Of course in ordinary calculus, the choice of Riemann sum is irrelevant as they both give rise to the same limit. However, this is not the case when integrating with respect to white noise. In particular, whereas in the Itô form, the integrand $f(t_i)$ and $[B(t_{i+1}) - B(t_i)]$ are independent of each other, in the Stratonovich from, $f(t_{i+1}) + f(t_i)$ and $[B(t_{i+1}) - B(t_i)]$ are not.

This difference is critical and is manifest in the corresponding algebraic rules for computing products of stochastic integrals. For example, notice that the Stratonovich integral follows the rules of conventional calculus. That is, the Leibniz rule (product

[1] In the mathematics literature, the requirement that $f(t)$ be non-anticipating is stated as the requirement that $f(t)$ be *adapted*, that is, it is measurable with respect to the filtration generated by the the random variables $B(s)$ for $S \leq t$. See for example [69, 7]

rule) is as we would expect:

$$d[B(t)B^\dagger(t)]_{\mathcal{S}} = dB(t)B^\dagger(t) + B(t)dB^\dagger(t) \tag{2.31}$$

However, as the integrand $f(i+1)$ does not commute with the increment $B(i+1) - B(i)$, we find that the following quantities are not equivalent:

$$\int_{t_0}^{t} f(t')dB(t') \neq \int_{t_0}^{t} dB(t')f(t') \tag{2.32}$$

On the other hand, while the Itô integral has the property that the increments are independent of and commute with the integrand, now the product rule must be appropriately modified. That is,

$$\begin{aligned} d[B(t)B^\dagger(t)]_{\mathcal{S}} &= dB(t)B^\dagger(t) + B(t)dB^\dagger + dB(t)dB^\dagger(t) & (2.33)\\ &= dB(t)B^\dagger(t) + B(t)dB^\dagger + dt & (2.34) \end{aligned}$$

So, for example, using the quantities we computed above, we arrive at the following quantities with integrals performed with respect to the Itô and Stratonovich forms of integration:

$$\left\langle \left\{ \int_0^t dB(t')B^\dagger(t') \right\}_{\mathcal{I}} \right\rangle = 0$$
$$\left\langle \left\{ \int_0^t dB(t')B^\dagger(t') \right\}_{\mathcal{S}} \right\rangle = \frac{1}{2}|t|$$

Note also that the mean value of an Itô integral is always zero. When we know the stochastic differential equation that a given integral equation satisfies, we can convert between the Itô and Stratonovich forms. Without the SDE, such a conversion would not be possible, as the Stratonovich integral depends on the value of the process at a future time, and this value can only be determined by the corresponding dynamical equation of motion. All of the QSDE's in this thesis will be of the Itô form, although, see, e.g. [44], for an example in quantum optics where conversion to the Stratonovich form is of some practical utility.

$dM_t^1 \setminus dM_t^2$	dA_t^{j*}	$d\Lambda_t^{jk}$	dA_t^j
dA_t^{l*}	0	0	0
$d\Lambda_t^{lm}$	$\delta_{mj} dA_t^{l*}$	$\delta_{mj}\, d\Lambda_t^{lk}$	0
dA_t^l	$\delta_{lj}\, dt$	$\delta_{lj}\, dA_t^k$	0

Table 2.1: Quantum Itô table for evaluating products of fundamental noise processes

Thus far, we have not incorporated internal Hamiltonian evolution of our system. This is easily accomplished by treating the Hamiltonian dynamics as a perturbation on top of the fast evolution at optical frequencies, and results in an Itô QSDE of the following form:

$$dU_t = \left(L dA_t^\dagger - L^\dagger dA_t - (iH + \frac{1}{2} L^\dagger L) dt \right) U_t \tag{2.35}$$

Typically, it is a QSDE of this form, describing the total system and bath dynamics, that is the starting point for analysis of open quantum system models.

2.2.3 Physical assumptions

The formalism for quantum stochastic calculus that we have derived can be applied to any Gaussian field-state that is initially unentangled with the system [20, 30, 53]. However, it is almost always the case (as it will be in this thesis) that we assume that the field is in a vacuum state, so that the global density matrix factors as $\rho = \rho_s \otimes \rho_{vac}$. Under this assumption, we can express the products of the fundamental noises in a simple table form (Table 2.1).

Of course, for the systems we are interested in, the bath is generally *not* in a vacuum state, but rather, is a coherent laser field driving the system. Recall, however, that a coherent state with amplitude α can be thought of as a displaced vacuum state, i.e.

$$|\alpha\rangle = e^{(\alpha a^\dagger - \alpha^* a)} |0\rangle = \mathcal{D}(\alpha)|0\rangle \tag{2.36}$$

In the language of the fundamental noise processes we have just derived, we can rewrite this expression, and take into account time dependence, as follows:

$$|\alpha, t\rangle = \exp\{\alpha \int_0^t dA_{t'}^\dagger - \alpha^\dagger \int_0^t dA_t\}|0\rangle \equiv W_t^\alpha |0\rangle \tag{2.37}$$

Here we have introduced a new operator, the *Weyl operator* W_t^α which is formally analogous to the traditional *displacement operator* $\mathcal{D}(\alpha)$ and which has the following differential form:

$$dW_t^\alpha = \left(\alpha dA_t^\dagger - \alpha^\dagger dA_t - \frac{1}{2}|\alpha|^2 dt\right) W_t^\alpha \tag{2.38}$$

Thus, as will become apparent in the subsequent sections, to model an open quantum system being driven by a coherent laser field, we treat the system as though it is coupled to a bath in the vacuum state and model the driving laser as an independent system whose output we feed into our initial system.

2.3 SLH Representation of QSDE's

While the physical derivation of quantum stochastic differential equations and the associated stochastic calculus assumed only a single mode, we can easily extend the formalism to account for multiple input and output fields. We can generalize the propagator for a system with multiple fields in the following way:

$$dU_t = \sum_{j,k} \left\{(S_{jk} - \delta_{jk}) d\Lambda_t^{jk} + L_j dB_t^{j\dagger} - L_j^\dagger S_{jk} dB_t^k - (iH + \frac{1}{2} L_j^\dagger L_j) dt\right\} U_t \tag{2.39}$$

Note that due to the presence of multiple fields, the gauge process now takes on a more general form, which allows for direct scattering between different field modes. In particular, if we let $a_i(t)$ and $a_j(t)$ denote quantum noise processes, then we can define the corresponding scattering process as:

$$\Lambda_t^{ij} = \int_0^t d\Lambda_t^{ij} \equiv \int_0^t dt a_i^\dagger(t) a_j(t) \tag{2.40}$$

In other words, while the gauge process in the single mode case corresponds to photon counting, with multiple fields present, it also allows for direct scattering between the different channels. Consequently, the generalized propagator above now includes the *scattering matrix* S, which is unitary, and may contain operators as elements.

We can also re-write the generalized propagator in the following way:

$$dU_t = \left\{ \mathrm{tr}[(\mathbf{S} - \mathbf{I})d\mathbf{\Lambda}] + d\mathbf{A}^\dagger \mathbf{L} - \mathbf{L}^\dagger \mathbf{S} d\mathbf{A} - \frac{1}{2}\mathbf{L}^\dagger \mathbf{L} dt - iH dt \right\} U_t \tag{2.41}$$

This form of the propagator makes explicit that the QSDE is completely specified once we know the scattering matrix $\mathbf{S}$, the coupling vector $\mathbf{L}$ and the Hamiltonian H. Consequently, it is convenient to represent an open quantum system, as described by the generalized propagator above, via its SLH representation, usually given as a triple $(\mathbf{S}, \mathbf{L}, H)$.

So, for example, the SLH representation of a beam-splitter, is given by:

$$BS_{SLH} = \left(\begin{bmatrix} \alpha & -\beta^\dagger \\ \beta & \alpha^\dagger \end{bmatrix}, \begin{bmatrix} 0 \\ 0 \end{bmatrix}, 0 \right) \tag{2.42}$$

Or, for a two-level atom in free space, we have:

$$TLA_{SLH} = (1, \sqrt{2\gamma_\perp}\sigma, \omega_e \sigma^\dagger \sigma) \tag{2.43}$$

And as I discussed earlier, a coherent drive, can be thought of as corresponding to the Weyl operator QSDE, which has the following simple SLH form:

$$W_t^\alpha = (1, \alpha, 0) \tag{2.44}$$

We will explore a full range of open system models in SLH form in Ch. 4, when we take a detailed look at coherent feedback networks for autonomous quantum memories.

2.4 Series and concatenation products for SLH models

The SLH representation of a quantum stochastic model is extremely compact– and hopefully less intimidating than the full propagator. But we've just scratched the surface of what can be done with this powerful representation. As we set out to do in the introduction, our primary aim has been to arrive at a simple set of algebraic rules for wiring up quantum systems, and ultimately, to arrive at a system for modeling quantum networks that parallels analogous approaches to circuit design in contemporary electrical engineering.

As it turns out, such rules do exist, and they conveniently operate directly at the SLH level. I will first give the definitions of the these two products, the *series product* for taking the output from one quantum system and feeding it into another, and the *concatenation product*, for stacking two quantum systems together, effectively treating them as a single system.

Given two systems $G_1 = (\mathbf{S}_1, \mathbf{L}_1, H_1)$ and $G_2 = (\mathbf{S}_2, \mathbf{L}_2, H_2)$, with the same number of field modes, the series product, denoted by $G_2 \lhd G_1$ is given by

$$G_2 \lhd G_1 = \left(\mathbf{S}_2\mathbf{S}_1, \mathbf{L}_2 + \mathbf{S}_2\mathbf{L}_1, H_1 + H_2 + \frac{1}{2i}(\mathbf{L}_2^\dagger \mathbf{S}_2 \mathbf{L}_1 - \mathbf{L}_1^\dagger \mathbf{S}_2^\dagger \mathbf{L}_2) \right) \tag{2.45}$$

The directionally of the series product is important. In the above example, the outputs from system G_1 are being fed into G_2. As would be expected, the series product is not commutative. Now, given two systems $G_1 = (\mathbf{S}_1, \mathbf{L}_1, H_1)$ and $G_2 = (\mathbf{S}_2, \mathbf{L}_2, H_2)$, not necessarily having the same number of modes, the concatenation product, denoted $G_2 \boxplus G_1$ is given by

$$G_2 \boxplus G_1 = \left(\begin{bmatrix} \mathbf{S}_1 & 0 \\ 0 & \mathbf{S}_2 \end{bmatrix}, \begin{bmatrix} \mathbf{L}_1 \\ \mathbf{L}_2 \end{bmatrix}, H_1 + H_2 \right) \tag{2.46}$$

Note that the concatenation product is *not* a parallel connection. The systems are

simply adjoined together formally, but without any exchange of the field modes. On the other hand, the series product more or less behaves the way a series connection from classical electronics does.

To provide some intuition, here is a heuristic derivation for the series product in the single mode case. Suppose we have two systems with propagators U_t^1 and U_t^2 and that we would like to feed the output of the first system G_1 into the second system G_2. As our systems are single mode, the scattering matrix (which is the identity) can be neglected, and the SLH model can be written in terms of the coupling terms and the Hamiltonian, $G_1 = (\mathbf{L}_1, H_1)$ and $G_2 = (\mathbf{L}_2, H_2)$.

In the Heisenberg picture, we can slice up our field into infinitesimal segments, and have each "piece" propagate through the system by evolving the unitaries $U^2_{[t+dt,t)}$ and then $U^1_{[t+dt,t)}$. The infinitesimal propagator is given by:

$$U^2_{dt}U^1_{dt} = (I + dU^2_0)(I + dU^1_0) \tag{2.47}$$

It is easy to verify that these operators do not commute, but physically, the reason is that the systems are coupled through the same bath mode. To compute the combined system unitary, we can apply the quantum Itô rule to obtain:

$$\begin{aligned} U^2_{dt}U^1_{dt} &= I + ((L_1 + L_2)dA_0^\dagger - (L_1 + L_2)^\dagger dA_0 - \\ &\quad (\frac{1}{2}(L_1^\dagger L_1 + L_2^\dagger L_2) + i(H_1 + H_2))dt - L_2^\dagger L_1 dt) \\ &= I + ((L_1 + L_2)dA_0^\dagger - (L_1 + L_2)^\dagger dA_0 - \\ &\quad (\frac{1}{2}(L_1 + L_2)^\dagger (L_1 + L_2) + i(H_1 + H_2 + \frac{1}{2i}(L_2^\dagger L_1 - L_1^\dagger L_2))dt) \end{aligned}$$

or in SLH form, $U^2_{dt}U^1_{dt} = \left(I, \mathbf{L}_2 + \mathbf{L}_1, H_1 + H_2 + \frac{1}{2i}(\mathbf{L}_2^\dagger \mathbf{L}_1 - \mathbf{L}_1^\dagger \mathbf{L}_2)\right)$. The series product $\triangleleft$ defined above is simply a multi-mode generalization of this joint infinitesimal propagator.

2.5 Adiabatic elimination

However disguised they may seem, all of the derivations we have carried out thus far fundamentally stem from Maxwell's equations and the Schrödinger equation. Of the two approximations that we have made– the rotating wave approximation and the Markov approximation– it is the latter which fundamentally leads to a dramatically simpler and more tractable model. Still, the resulting QSDE's are quite complex, and in the physics literature, it has long been known that in systems with widely separable time-scales, the fast dynamics can be *adiabatically eliminated* to produce a reduced order model describing only those quantities evolving on the longer time scales.

As has been a common theme in the last several years in the mathematical physics and quantum feedback control communities, the heuristic methods for performing adiabatic elimination (see for example, [18, 64]), have been made mathematically rigorous. In particular, the Bouten-van Handel-Silberfarb adiabatic elimination theory [10] provides an algorithm for computing an approximate propagator U_t^* to which the sequence of pre-limit propagators $U_t^{(k)*}$ converges, that is,

$$\lim_{k\to\infty} \sup_{0\geq t\geq T} ||U_t^{(k)*}|\psi\rangle - U_t^*|\psi\rangle|| = 0 \tag{2.48}$$

for all wave functions $|\psi\rangle$ which lie in the subspace of interest, i.e. the subspace where the slow dynamics take place.

Certain structural requirements need to be satisfied in order to apply this theory. Specifically, we begin with a *right* QSDE in the following form[2],

$$dU_t^{(k)} = U_t^{(k)} \left\{ \sum_{i,j=1}^{n} (N_{ij}^{(k)} - \delta_{ij}) d\Lambda_t^{ij} + \sum_{i=1}^{n} M_i^{(k)} dA_t^{i\dagger} + \sum_{i=1}^{n} L_i^{(k)} dA_t^i + K^{(k)} dt \right\} \tag{2.49}$$

[2]The reason for working with right QSDE's rather than left QSDE's is purely technical. See [10] for a mathematical justification.

where the operator coefficients satisfy the following scaling relationships with the parameter k:

$$K^{(k)} = -(iH + \frac{1}{2}\sum_l L_l^{(k)\dagger} L_l^{(k)})^\dagger = k^2 Y + kA + B \tag{2.50}$$

$$L_i^{(k)\dagger} = kF_i + G_i \tag{2.51}$$

$$N_{ij}^{(k)} = W_{ij} \tag{2.52}$$

Let P_0 be the projector onto the subspace of interest– the subspace where the slowly varying quantities live– and let P_1 denote the projector onto its orthogonal complement. Furthermore, the theory requires the existence of an operator $\tilde{Y}$ such that $\tilde{Y}Y = Y\tilde{Y} = P_1$. Then it follows that there exists an approximate propagator U_t, which satisfies the right QSDE,

$$dU_t = U_t \left\{ \sum_{i,j=1}^{n} (N_{ij} - \delta_{ij}) d\Lambda_t^{ij} + \sum_{i=1}^{n} M_i dA_t^{i\dagger} + \sum_{i=1}^{n} L_i dA_t^i + K dt \right\} \tag{2.53}$$

and which has the following operator coefficients when converted back to the usual *left* QSDE:

$$-(iH + \frac{1}{2} L_l^\dagger L_l)^\dagger = P_0(B - A\tilde{Y}A)P_0 \tag{2.54}$$

$$(S_{ji})^\dagger = \sum_l P_0 W_{il}(F_l^\dagger \tilde{Y} F_j + \delta_{ij}) P_0 \tag{2.55}$$

$$L_i^\dagger = P_0(G_i - A\tilde{Y}F_i)P_0 \tag{2.56}$$

$$(L_i^\dagger S_{ji})^\dagger = \sum_j P_0 W_{ij}(G_j^\dagger - F_j^\dagger \tilde{Y} A) P_0 \tag{2.57}$$

As would be expected, there are clear parallels between the form of the approximate QSDE given here and the heuristic methods utilized in the quantum optics literature ([18, 64]). This result will be essential in Chapter 4, when we examine networks of many quantum optical components forming autonomous quantum memories. For these systems, the limiting propagator provides a dramatic reduction in the size of the Hilbert space, while still preserving the essential dynamics.

2.5.1 Application for systems with displaced coherent inputs

The structural conditions of the adiabatic limit theorem are quite stringent, and occasionally situations will arise where they are not quite met. But as is often the case, we can find work arounds. In this section, I will describe a method, developed by Luc Bouten in [34], and which plays a critical role in computing reduced order equations of motion for the feedback network in the quantum memories analyzed in subsequent chapters.

Let (S^0, L^0, H^0) be a network with only vacuum inputs. Consider now the same network, but with coherent displaced inputs– we can of course compute this using the series product:

$$\begin{aligned} G^{(k)} &= (S^0, L^0, H^0) \lhd (I, d_k, 0) \\ &= (S^0, S^0 d_k + L^0, H^0 + \Im\{L^{0\dagger} S^0 d_k\}) = (S, L^{(k)}, H^{(k)}) \end{aligned} \tag{2.58}$$

Here, d_k is a vector with complex-valued entries, some of which are non-zero and which may or may not scale with k. We assume that the initial scattering matrix, $S = S^0$ has no scaling with k.

Clearly, this is a quite general condition, and unfortunately, it is precisely in situations such as this that the structural requirements above are no longer satisfied, in particular, because of the $S^0 d_k$ term in the coupling operators. We can, however, decompose the network in a manner that allows us to satisfy the conditions of the limit theorem. To begin with, we rewrite the network so that the scaled parameters are moved to the Hamiltonian of a new subcomponent:

$$\begin{aligned} G^{(k)} &= (S, 0, 0) \lhd (I, d_k, 0) \lhd (I, S^\dagger L^0, H^{(k)} - \Im\{d_k^\dagger S^{0\dagger} L^0\}) \\ &\equiv (S, 0, 0) \lhd (I, d_k, 0) \lhd \tilde{G}^{(k)} \end{aligned} \tag{2.59}$$

We can now apply the usual adiabatic elimination theorem to the subcomponent $\tilde{G}^{(k)}$,

so that $G^{(k)}$ is approximated by

$$\hat{G}^{(k)} = (S, 0, 0) \triangleleft (I, d_k, 0) \triangleleft \tilde{G} \tag{2.60}$$

as k tends to ∞.

2.6 The quantum optical master equation

Traditionally in quantum optics, the unconditional evolution of an open quantum system is described by the *Lindblad master equation*,

$$\dot{\rho} = -i[H, \rho] + \sum_i \left\{ L_i \rho L_i^\dagger - \frac{1}{2} L_i^\dagger L_i \rho - \frac{1}{2} \rho L_i^\dagger L_i \right\}, \tag{2.61}$$

When measurements are made, there are techniques for describing the *conditional evolution* of the system, but in this thesis, we are only interested in the unconditional evolution. Of course, the Lindblad master equation can be broken down into the part describing the coherent evolution of a system– the von Neumann equation– as well as a part describing the non-unitary evolution due to the system-bath interaction.

We can derive the Lindblad master equation from a QSDE representation of an open quantum system in the following manner. We begin with an open system model $M = (\mathbf{S}, \mathbf{L}, H)$, which, as we recall, corresponds to the following QSDE:

$$dU_t = \left\{ \mathrm{tr}[(\mathbf{S} - \mathbf{I}) d\mathbf{\Lambda}] + d\mathbf{A}^\dagger \mathbf{L} - L^\dagger \mathbf{S} d\mathbf{A} - \frac{1}{2} \mathbf{L}^\dagger \mathbf{L} dt - iH dt \right\} U_t \tag{2.62}$$

Suppose now that we want to compute the unconditional evolution of the expectation value of a system operator $\hat{O}$. In the Heisenberg picture, we can write this as $j_t(\hat{O}) = U_t^\dagger \hat{O} U_t$, and applying the quantum Itô rule, we have in differential form:

$$\begin{aligned} dj_t(\hat{O}) &= d(U_t^\dagger)\hat{O}U_t + U_t^\dagger \hat{O} d(U_t) + d(U_t^\dagger)\hat{O}d(U_t) && (2.63) \\ &= j_t(\mathcal{L}^\dagger \hat{O})dt + j_t([\mathcal{L}^\dagger, \hat{O}])dA_t + j_t([\hat{O}, L])dA_t^\dagger && (2.64) \end{aligned}$$

where the super-operator $\mathcal{L}$ is defined by its action:

$$\mathcal{L}^\dagger \hat{O} = i[H, \hat{O}] + L^\dagger \hat{O} L - \frac{1}{2}(L^\dagger L \hat{O} + \hat{O} L^\dagger L) \tag{2.65}$$

Now, to compute the expectation value of $\hat{O}$ as a function of time, we can simply evaluate the quantity $\langle j_t(\hat{O})\rangle = \mathrm{Tr}[\rho j_t(\hat{O})]$, where we take $\rho = \rho_s \otimes \rho_{vac}$, i.e. the global system state. Note that the differential form of this quantity, given above, can be simplified substantially with the assumption that the bath is in the vacuum state. As the expectation values of the noise processes with respect to the vacuum state vanish, we have:

$$d\langle j_t(\hat{O})\rangle = \langle j_t(\mathcal{L}^\dagger \hat{O})\rangle dt, \tag{2.66}$$

which is the usual quantum optical master equation that traditionally appears in the open system literature. From here, it is straightforward to recover the Lindblad master equation describing the unconditional evolution of the system in the Schrödinger picture:

$$d\rho = -i[H, \rho]dt + \sum_i \left\{ L_i \rho L_i^\dagger - \frac{1}{2} L_i^\dagger L_i \rho - \frac{1}{2} \rho L_i^\dagger L_i \right\} dt \tag{2.67}$$

as given above. Note that while the L and H terms of the Lindblad master equation are identical to those of a QSDE / SLH model, the scattering matrix does not appear. This is to be expected, as we have traced over the bath dynamics to arrive at the unconditional system evolution.

Chapter 3

Coherent feedback protocol for squeezed-light generation

Over the last decade, many experiments in quantum information protocols and precision metrology have utilized the optical Faraday rotation of light passing through spin polarized atomic samples. When I began graduate school, an experimental setup of particular interest was a proposal by Jacob Sherson and Klaus Mølmer, in which it is shown that polarization squeezed light can be achieved by sending a cw (continuous wave) beam or pulse of linearly polarized light through an atomic gas twice in different directions [61]. For a similar proposal in the context of atomic magnetometry, see [11].

The primary motivation behind our examining this result was less to understand the physics– Sherson and Mølmer had already analyzed the setup quite thoroughly from a physical perspective– but rather, to understand the mechanics of doing realistic physical modeling with quantum stochastic calculus and quantum stochastic differential equations. Of course, we already knew that the QSDE formalism was equivalent to the heuristic methods traditionally used in the literature, but at that time, no one had engaged in a practical project of a modeling nature with QSDE's, and so my objective was to see if I could reproduce the results of Sherson and Mølmer with these more modern tools.

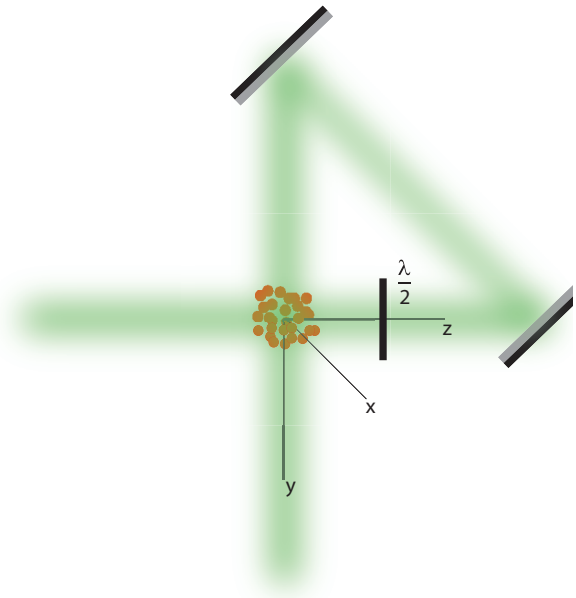

Figure 3.1: Sherson and Mølmer's setup for the generation of squeezed light. After passing through a gas of spin polarized atoms, the polarization of the cw beam or pulse of linearly polarized light is rotated with a half-wave plate, and it is then transmitted through the gas a second time from a different direction.

In the first section, I summarize the analysis of Sherson and Mølmer's derivation, using an input/output formalism derived from the work of Gardiner and Collet in the mid 1980's [19]. The specific calculation I've chosen to show here is from Jacob Sheron's thesis [60] (the paper [61] seems to not provide a particularly transparent analysis) and is illustrative of related analyses in their community for quantum teleportation and quantum memories in atomic gas systems– I present it here for comparison and will not use these techniques in the rest of this thesis. Then I give a QSDE-based analysis, showing where the correspondence lies between the input and output fields in both cases.

3.1 Analysis with Gardiner-Collett input/output formalism

3.1.1 Hamiltonian model for double-pass dynamics

As shown in Figure 3, we are interested in modeling a coherent drive which is double-passed through an atomic ensemble. As the interaction between the gas and the field is symmetric, we can characterize the atomic ground state by the collective spin vector $\hat{\vec{J}}$. Furthermore, assuming that the atoms are strongly spin polarized in the x direction, we can apply the Holstein-Primakoff approximation and introduce the dimensionless variables

$$(x_{at}, p_{at}) = (\hat{J}_y, \hat{J}_z)/\sqrt{J_x} \tag{3.1}$$

We start out with the double-pass Hamiltonian[1] for the combined atom-field system:

$$H(t) = g(t)p_{at}(t)p_L(t,t) + g(t)x_{at}(t)x_L(t-T_1,t)$$

In keeping with the notational conventions of [61], we index the light operators with two time arguments, the first of which denotes the time when an infinitesimal light segment arrives at the sample, and the second, describing time dependence. Eventually, we will replace the first index with input/output labels, i.e., we will use $x_L^{in}(t)$ and $x_L^{out}(t)$ in place of $x_L(0,t)$ and $x_L(t,t')$, where $t' > t+T_1$ denotes a time after the interaction is complete.

In the Heisenberg picture, the time evolution of an operator $\hat{O}(t)$ is given by:

$$\frac{d\hat{O}(t)}{dt} = \frac{i}{\hbar}[H, \hat{O}(t)] + \frac{\partial \hat{O}(t)}{\partial t}$$

[1] It is worth re-examining this Hamiltonian after studying the derivation of the double-pass QSDE in Section 3.2.2. In particular, note that the simultaneous passage mechanism is modeled in this formalism by adding a time delay to the xx interaction (the second term of the Hamiltonian), whereas in the QSDE-based treatment, we employ an interlacing procedure to derive the overall double-pass description from the constituent single-pass interactions.

In the subsequent analysis, we will neglect dynamics that take place on the time scale L/c, where L is the length of the sample– in other words, this is equivalent to the assumption of instantaneous propagation of light across the sample[2]. So in computing the Heisenberg equations of motion for the atomic and field observables, we will only include the contribution from the commutator of the given observable with the system Hamiltonian. For example, for the observable $x_{at}(t)$, we can compute:

$$\begin{aligned}
\frac{d}{dt}x_{at}(t) &= \frac{i}{\hbar}[H, x_{at}(t)] + \frac{\partial x_{at}(t)}{\partial t} \\
&\approx \frac{i}{\hbar}[H, x_{at}(t)] \\
&= \frac{i}{\hbar}[g(t)p_{at}(t)p_L(t,t), x_{at}(t)] \\
&= \frac{i}{\hbar}g(t)p_L(t,t)[p_{at}(t), x_{at}(t)] \\
&= g(t)p_L(t,t)
\end{aligned}$$

Proceeding in an analogous manner, we obtain the Heisenberg equations of motion for the position and momentum observables of the atomic gas and of the field:

$$\begin{aligned}
\frac{d}{dt}x_{at}(t) &= g(t)p_L(t,t) \\
\frac{d}{dt}p_{at}(t) &= -g(t)x_L(t-T_1,t) \\
\frac{d}{dt}x_L(\tau,t) &= g(t)p_{at}(t)\delta(\tau - t) \\
\frac{d}{dt}p_L(\tau,t) &= -g(t)x_{at}(t)\delta(\tau - t + T_1)
\end{aligned}$$

Solving the last two equations (keeping in mind the meaning of the two time indices), we obtain:

$$x_L(\tau,t) = x_L(\tau,0) + g(\tau)p_{at}(\tau)\Theta(t-\tau) \tag{3.2}$$

$$p_L(\tau,t) = p_L(\tau,0) - g(\tau)x_{at}(\tau+T_1)\Theta(t-\tau-T_1) \tag{3.3}$$

[2]Recall that this assumption is also implicit in the series product of Section 2.4

Notice that the Heavyside step function in these solutions ensures that the observable evolves only when the probe laser is in contact with the atomic sample. Substituting these solutions into the first two equations, we arrive at:

$$\begin{aligned}\frac{d}{dt}x_{at}(t) &= g(t)p_L(t,0)\\ \frac{d}{dt}p_{at}(t) &= -g(t)x_L(t-T_1,0) - g(t)g(t-T_1)p_{at}(t-T_1)\end{aligned}$$

Assuming that the atomic dynamics vary slowly on the time scale T_1, i.e. $p_{at}(t-T_1) \approx p_{at}(t)$, we can solve these equations to give:

$$\begin{aligned}x_{at}(t) &= x_{at}(0) + \int_0^t ds g(s)p_L(s,0)\\ p_{at}(t) &= p_{at}(0)e^{-\int_0^t ds[g(s)]^2} - \int_0^t ds e^{-\int_0^t du[g(u)]^2}x_L(s,0)\end{aligned}$$

These expressions can now be inserted into Eq. 3.2 to arrive at the time dependent output fields. At this point, we can now make the notational change we mentioned earlier and substitute $x_L^{in}(t)$ and $x_L^{out}(t)$ in place of $x_L(0,t)$ and $x_L(t,t')$. Furthermore, we will define collective light modes with, e.g., position operators $x_L = \int_0^T f(t)x_L(t)dt$. Assuming a symmetric mode with $f(t) = \frac{1}{\sqrt{T}}$, we obtain the following[3]:

$$\begin{aligned}x_L^{out} &= \frac{1}{\sqrt{T}}\int_0^T \left(x_L^{in}(t) + g(t)\left(p_{at}(0)e^{-\int_0^t ds[g(s)]^2} - \int_0^t ds e^{-\int_0^t du[g(u)]^2}x_L(s,0)\right)\right)dt\\ &= \frac{1}{\sqrt{T}}\int_0^T x_L^{in}(s)\left[1 - g(s)\int_s^T g(t)e^{-\int_s^t du[g(s)]^2 dt}\right] + \frac{p_{at}(0)}{\sqrt{T}}\int_0^T g(t)e^{-\int_0^t ds[g(s)]^2}dt\\ p_L^{out} &= \frac{1}{\sqrt{T}}\int_0^T \big(p_L^{in}(t) - g(t)\big(x_{at}(0) + \int_0^t ds g(s)p_L^{in}(s)\big)\big)dt\\ &= \frac{1}{\sqrt{T}}\int_0^T p_L^{in}(s)\big[1 - g(s)\int_s^T g(t)dt\big]ds - \frac{x_{at}(0)}{\sqrt{T}}\int_0^T g(t)dt\end{aligned}$$

[3]We will do an analogous rescaling of the light modes in the subsequent section before computing the final expectation values. See Section 3.2.3

3.1.2 Input/output relations for atom-field system

We want to derive input/output relations at constant interaction strength, i.e. making the substitution $g(t) \to g$:

$$\begin{aligned}
x_{at}(T) &= x_{at}(0) + g\sqrt{T}p^{in}L \\
p_{at}(T) &= p_{at}(0)e^{-g^2T} - g\int_0^T e^{-g^2(T-s)}x_L^{in}(s)ds \\
x_L^{out} &= \frac{1}{\sqrt{T}}\int_0^T e^{-g^2(T-s)}x_L^{in}(s)ds + \frac{p_{at}(0)(1-e^{-g^2T})}{g\sqrt{T}} \\
p_L^{out} &= \frac{1}{\sqrt{T}}\int_0^T p_L^{in}(s)[1-g^2(T-s)]ds - x_{at}(0)g\sqrt{T}
\end{aligned}$$

From these input/output relations, we can compute the corresponding variances. For example, using the autocorrelation function for the field variables $\langle x_L(t)x_L(t')\rangle = \langle p_L(t)p_L(t')\rangle = \frac{i}{2}\delta(t-t')$ we have:

$$\begin{aligned}
\langle x_L^2\rangle &= \left\langle \left(\frac{1}{\sqrt{T}}\int_0^T x_L(t')dt'\right)\left(\frac{1}{\sqrt{T}}\int_0^T x_L(t)dt\right)\right\rangle \\
&= \frac{1}{T}\int_0^T dt'\int_0^T \langle p_L(t)p_L(t')\rangle = \frac{1}{T}\int_0^T \frac{1}{2} = \frac{1}{2}
\end{aligned}$$

So, ultimately, computing the output variances for the atomic and field degrees of freedom, we arrive at:

$$\begin{aligned}
\mathrm{Var}(x_{at}(t)) &= \frac{1}{2}(1+g^2) \\
\mathrm{Var}(p_{at}(t) &= \frac{1}{2}\left(\frac{1+e^{-2g^2}}{2}\right) \\
\mathrm{Var}(x_L^{out}) &= \frac{1}{2}\frac{3+e^{-2g^2}-4e^{-g^2}}{2g^2} \\
\mathrm{Var}(p_L^{out}) &= \frac{1}{2}\left(1+\frac{g^4}{3}\right)
\end{aligned}$$

Thus we see that the complementary field quadratures, i.e. x_L^{out} and p_L^{out} correspond to squeezed and anti-squeezed modes respectively. In addition, from the variances

of the atomic-gas system, we see that this setup generates up to 3dB of atomic spin squeezing.

3.2 Analysis with quantum stochastic differential equations

Having examined this simple coherent feedback system in the input/output formalism used by Sherson and Mølmer, I now turn to re-producing the derivation using the quantum stochastic calculus formalism developed from first principles in the introduction. After a brief overview of the physical setup and the basic mathematical objects involved in the corresponding quantum stochastic model, I will give a derivation of the double pass QSDE using the heuristic infinitesimal generator method described in the introductory section on the series product (see Section 2.4). For comparison with the analysis given in the previous section, I then use the double-pass QSDE to derive the corresponding input/output relationships. Finally, I derive the joint-characteristic function for the atom-field system, from which the corresponding probability distributions of the atomic and field variables can be computed.

3.2.1 The model

We consider an atomic gas in interaction with the quantized electromagnetic field. As described in the previous section, since the interaction between the gas and the field is symmetric, we can characterize the atomic ground state by the collective spin vector $\hat{\vec{J}}$. Furthermore, assuming that the atoms are strongly spin polarized in the x direction, we can apply the Holstein-Primakoff approximation and introduce the dimensionless variables

$$(x_{at}, p_{at}) = (\hat{J}_y, \hat{J}_z)/\sqrt{J_x} \tag{3.4}$$

Setting $\hbar = 1$, these obey the canonical commutation relationship $[x_{at}, p_{at}] = i$.

The atomic gas is described by the Hilbert space of quadratically integrable functions

$L^2(\mathbb{R})$ and the electromagnetic field by the *symmetric Fock space* $\mathcal{F}$ over $L^2(\mathbb{R})$ (space of one-photon wave functions), i.e.

$$\mathcal{F} := \mathbb{C} \oplus \bigoplus_{k=1}^{\infty} L^2(\mathbb{R})^{\otimes_s k}.$$

With the Fock space $\mathcal{F}$ we can describe superpositions of field-states with different numbers of photons. The joint system of the gas and field together is described by the Hilbert space $L^2(\mathbb{R}) \otimes \mathcal{F}$.

As described in first chapter, we examine the interaction between the gas and the electromagnetic field in the weak coupling limit [24, 23, 1] so that in the interaction picture, the unitary dynamics of the gas and the field together is given by a quantum stochastic differential equation (QSDE) in the sense of Hudson and Parthasarathy [30]:

$$dU_t = \{-L^* dA_t + L dA_t^* - \frac{1}{2} L^* L dt - iH dt\} U_t, \tag{3.5}$$

with $L = \frac{\alpha(p-ix)}{\sqrt{2}}$, $H = \frac{1}{4}\alpha^2(px + xp)$, and $U_0 = I$. We will formally derive this QSDE in the following section. Here, the operators L^* and L are proportional to the the raising and lowering operators on the atomic gas system and A_t and A_t^* denote the field annihilation and creation processes.

Note that the evolution U_t acts nontrivially on the combined system $L^2(\mathbb{R}) \otimes \mathcal{F}$. That is, L and A_t are understood to designate the single system-operators $L \otimes I$ and $I \otimes A_t$ respectively. As described in the introductory sections on quantum stochastic calculus, recall that Equation (3.5) should be understood as a shorthand for the integral equation

$$\begin{aligned} U_t = I &- \int_0^t L^* U_\tau dA_\tau + \int_0^t L U_\tau dA_\tau^* - \frac{1}{2}\int_0^t L^* L U_\tau d\tau \\ &- i\int_0^t H U_\tau d\tau, \end{aligned}$$

where the integrals on the right-hand side are stochastic integrals, and where the stochastic increments satisfy the standard Itô table (see 2.1).

As a notational convenience, we adopt the following convention when applying the quantum Itô rule: Let $\{Z_i\}_{i=1,\ldots,p}$ be stochastic integrals. Then we write

$$d(Z_1 Z_2 \ldots Z_p) = \sum_{\substack{\nu \subset \{1,\ldots,p\} \\ \nu \neq \emptyset}} \{\nu\},$$

where the sum runs over all *non-empty* subsets of $\{1, \ldots, p\}$. For any $\nu = \{i_1, \ldots, i_k\}$, the term $\{\nu\}$ is the contribution to $d(Z_1 Z_2 \ldots Z_p)$ coming from differentiating only the terms with indices in the set $\{i_1, \ldots, i_k\}$ and preserving the order of the factors in the product. The differential $d(Z_1 Z_2 Z_3)$, for example, contains terms of type $\{1\}$, $\{2\}$, $\{3\}$, $\{12\}$, $\{13\}$, $\{23\}$ and $\{123\}$. We have $\{2\} = Z_1(dZ_2)Z_3$, $\{13\} = (dZ_1)Z_2(dZ_3)$, $\{123\} = (dZ_1)(dZ_2)(dZ_3)$, etc.

3.2.2 Derivation of the double-pass QSDE

I will now briefly review the derivation of the single pass QSDE's as given in [8]. From these, it is fairly straightforward to construct the overall QSDE for the double-pass system. Recall that the Faraday interaction Hamiltonian for a laser and spin polarized atomic gas is given by:

$$H dt = 2\theta F_z S_z dt = \theta F_z (d\Lambda_t^{++} - d\Lambda_t^{--}) \tag{3.6}$$

Then the time evolution of the combined system is given by the unitary propagator $U_t^0 = \exp\left(i \int_0^t (d\Lambda_s^{++} - d\Lambda_s^{--}) ds\right)$. Applying the Itô rule, we arrive at the following QSDE:

$$dU_t^0 \left\{ \left(e^{i\theta F_z} - 1\right) d\Lambda_t^{++} + \left(e^{-i\theta F_z} - 1\right) d\Lambda_t^{--} \right\} U_t^0 \tag{3.7}$$

In other words, we see that the collective spin of the atomic gas is rotated by an angle $\pm\theta$ along the z-axis, depending on circularity of the light. In the linearly polarized

basis, we can re-express this QSDE in the following form:

$$dU_t = \{(\cos(\theta F_z) - 1)\,(d\Lambda_t^{xx} + d\Lambda_t^{yy}) - \sin(\theta F_z)\,(d\Lambda_t^{xy} - d\Lambda_t^{yx})\}\,U_t \tag{3.8}$$

Anticipating the use of SLH notation in subsequent chapters, note that the above QSDE is equivalent to the following SLH model:

$$F_{SLH} = \left(\begin{bmatrix} \cos(\theta F_z) - 1 & -\sin(\theta F_z) \\ \sin(\theta F_z) & \cos(\theta F_z) - 1 \end{bmatrix}, \begin{bmatrix} 0 \\ 0 \end{bmatrix}, 0\right) \tag{3.9}$$

Note that this model describes an atomic gas which mediates scattering between two bosonic channels. To ultimately arrive at a model with a single channel which couples $x(p)$ of the atomic gas with $x(p)$ of the field, we need to examine the dynamics in the strong driving, weak coupling limit. Assuming a driving laser with coherent amplitude α, and fixed measurement strength $M = \theta^2\alpha^2$, as α increases and $\theta = \sqrt{M}/\alpha$ decreases, we can expect for the x channel to remain in a coherent state, as the relative effect of the atoms on the x-polarized channel will decrease.

Under this assumption on the x-channel (the y-channel is still in the vacuum state), the time evolution for the combined system is given by Eq. 3.7. For $\beta, \gamma \in \{x, y\}$

$$d\Lambda_t^{\beta\gamma} = a_t^{\beta *} a_t^{\gamma} dt, \qquad dA_t^{\beta} = a_t^{\beta} dt, \qquad dA_t^{\beta *} = a_t^{\beta *} dt,$$

Again, invoking the assumption that the x-channel is approximately in a coherent state, we can replace a_t^x by $\alpha e^{i\phi_t}$ and a_t^{x*} by $\alpha e^{-i\phi_t}$. Then for large α and small θ, we obtain:

$$\begin{aligned} dU_t^0 = \Big\{ \big(\cos(\theta F_z) - 1\big)\big(\alpha^2 dt + d\Lambda_t^{yy}\big) \; - \\ \sin(\theta F_z)\alpha\big(e^{-i\phi_t} dA_t^y - e^{i\phi_t} dA_t^{y*}\big)\Big\} U_t^0. \end{aligned}$$

Replacing, θ by $\sqrt{M}/\alpha$ and taking the limit α to infinity, the time evolution of the

global system now satisfies the following QSDE:

$$d\overline{U}_t = \left\{ \sqrt{M} F_z \left(e^{-i\phi_t} dA_t^y - e^{i\phi_t} dA_t^{y*} \right) - \frac{M}{2} F_z^2 dt \right\} \overline{U}_t.$$

If we now make the Holstein-Primakoff approximation and introduce the dimensionless variables $(x_{at}, p_{at}) = (\hat{J}_y, \hat{J}_z)/\sqrt{J_x}$, we arrive at the following single channel QSDE's for each pass of the combined setup:

$$dU_t^1 = \left\{ -i\alpha p \frac{dA_t - dA_t^*}{i\sqrt{2}} - \tfrac{1}{4}\alpha^2 p^2 dt \right\} U_t^1 \tag{3.10}$$

$$dU_t^2 = \left\{ -i\alpha x \frac{dA_t^* + dA_t}{\sqrt{2}} - \tfrac{1}{4}\alpha^2 x^2 dt \right\} U_t^2 \tag{3.11}$$

To derive the QSDE for the double pass system, we first divide up the light into pulses at discrete time intervals and have each "piece" make multiple passes. Consider the following:

$$\begin{aligned} U_{t+dt}^i &= U_t^i + dU_t^i = M_t^i U_t^i \\ &= M_t^i M_{t-\Delta t}^i ... M_0^i U_0^i = M_t^i M_{t-\Delta t}^i ... M_0^i \end{aligned}$$

where $i = 1, 2$; $M_t^1 = \{I - i\alpha p(\frac{dA_t^* - dA_t}{i\sqrt{2}}) - \frac{1}{4}\alpha^2 p^2 dt\}$, and $M_t^2 = \{I - i\alpha x(\frac{dA_t^* + dA_t}{\sqrt{2}}) - \frac{1}{4}\alpha^2 x^2 dt\}$. The last two equalities follow by recursively applying the first and the fact that $U_0^1 = U_0^2 = I$. This expression is equivalent to the series product in [73, 72] and [26]. We can now write the QSDE for the combined system as follows:

$$\begin{aligned} U_{t+dt}^{21} &= (M_t^2 M_t^1)(M_{t-\Delta t}^2 M_{t-\Delta t}^1) ... (M_0^2 M_0^1) \\ &= (M_t^2 M_t^1) U_t^{21} \\ \Rightarrow dU_t^{21} &= (M_t^2 M_t^1) U_t^{21} - U_t^{21} \end{aligned}$$

Expanding the above product using the Itô table and dropping the superscripts, we arrive at the double pass QSDE:

$$dU_t = \{ -L^* dA_t + L dA_t^* - \frac{1}{2} L^* L dt - iH dt \} U_t, \tag{3.12}$$

with $L = \frac{\alpha(p-ix)}{\sqrt{2}}$, $H = \frac{1}{4}\alpha^2(px + xp)$, and $U_0 = I$ as before.

Of course, as we would expect, we can simply use the series product to arrive at the same expression in SLH form:

$$\begin{aligned} P_1 \lhd P_2 &= (1, \frac{\alpha}{\sqrt{2}}p, 0) \lhd (1, \frac{-i\alpha}{\sqrt{2}}x, 0) \\ &= \left(1, \frac{\alpha}{\sqrt{2}}p + \frac{-i\alpha}{\sqrt{2}}x, \Im[(\frac{\alpha}{\sqrt{2}}p)^\dagger \frac{-i\alpha}{\sqrt{2}}x]\right) \\ &= \left(1, \frac{\alpha}{\sqrt{2}}(p - ix), \frac{1}{4}|\alpha|^2(xp + px)\right), \end{aligned}$$

which is equivalent to the QSDE given above.

3.2.3 Correspondence with input/output formalism

Although we will not be using the input-output formalism [19], we present it here for comparison with [61]:

$$\begin{aligned} x_{at}^{in} &= \hat{J}_y/\sqrt{J_x} & x_{ph}^{in}dt &= \frac{dA_t + dA_t^*}{\sqrt{2}} \\ x_{at}^{out} &= U_t^* x_{at}^{in} U_t & x_{ph}^{out}dt &= \frac{d\left[U_t^*(A_t + A_t^*)U_t\right]}{\sqrt{2}} \end{aligned}$$

$$\begin{aligned} p_{at}^{in} &= \hat{J}_z/\sqrt{J_x} & p_{ph}^{in}dt &= \frac{dA_t - dA_t^*}{i\sqrt{2}} \\ p_{at}^{out} &= U_t^* p_{at}^{in} U_t & p_{ph}^{out}dt &= \frac{d\left[U_t^*(A_t - A_t^*)U_t\right]}{i\sqrt{2}} \end{aligned}$$

For the sake of simplicity in later computations, we have defined x_{ph}^{out} and p_{ph}^{out} in such a way that $[x_{ph}^{out}, p_{ph}^{out}] = it$. As will be apparent later, once we have calculated the variances for these operators, we rescale by a factor of $1/t$ to obtain the actual variances for the modes that we are interested in (i.e. the squeezed and anti-squeezed modes). Applying the Itô rule, and evaluating the products of stochastic integrals using the Itô table, we can express the above input-output relations in the language

of [61] (see also Section 3.1):

$$
\begin{aligned}
x_{ph}^{out}(t) &= x_{ph}^{in}(t) + \alpha p_{at}^{out}(t) && (3.13)\\
p_{ph}^{out}(t) &= p_{ph}^{in}(t) - \alpha x_{at}^{out}(t) && (3.14)\\
\frac{dx_{at}^{out}(t)}{dt} &= \alpha p_{ph}^{in}(t) && (3.15)\\
\frac{dp_{at}^{out}(t)}{dt} &= -\alpha(x_{ph}^{in}(t) + \alpha p_{at}^{out}(t)) && (3.16)
\end{aligned}
$$

As an example, we derive the expression for $x_{ph}^{out}(t)$:

$$
\begin{aligned}
x_{ph}^{out}dt &= \frac{d\left[U_t^*(A_t + A_t^*)U_t\right]}{\sqrt{2}}\\
&= \{1\} + \{2\} + \{3\} + \{12\} + \{23\} + \{13\} + \{123\}
\end{aligned}
$$

A simple calculation shows that the terms $\{1\}$, $\{3\}$, and $\{13\}$ sum to zero, and from the Itô table we see that third powers of increments (i.e. $\{123\}$) vanish, leaving us with $\{2\}$, $\{12\}$ and $\{23\}$ to calculate:

$$
\begin{aligned}
\{2\} &= \frac{dA_t + dA_t^*}{\sqrt{2}}\\
\{12\} &= dU_t^*\frac{dA_t + dA_t^*}{\sqrt{2}}U_t = U_t^*\frac{L^*}{\sqrt{2}}U_t dt\\
\{23\} &= \{12\}^* = U_t^*\frac{L}{\sqrt{2}}U_t dt
\end{aligned}
$$

Summing the preceding terms, and substituting for x_{ph}^{in}, we obtain:

$$
\begin{aligned}
\{2\} + \{12\} + \{23\} &= \frac{dA_t + dA_t^*}{\sqrt{2}} + U_t^*\frac{(L^* + L)}{\sqrt{2}}U_t dt\\
&= x_{ph}^{in}dt + U_t^*\alpha p_{at}^{in}U_t dt\\
\Rightarrow x_{ph}^{out}(t) &= x_{ph}^{in}(t) + \alpha p_{at}^{out}(t)
\end{aligned}
$$

For comparison with the results in [61], α should be equated with θ, and as we have ignored damping, τ should be set to 1.

3.2.4 Derivation of the joint characteristic functions

We now derive the joint characteristic functions for the combined atom-field system. Define $F[t,k,l]$ and $G[t,k,l]$ as follows (see for instance, [6]):

$$F[t,k,l] := \langle v\otimes\Phi \mid U_t^*(e^{ilp}\otimes e^{ik\frac{(A_t+A_t^*)}{\sqrt{2}}})U_t \mid v\otimes\Phi\rangle \tag{3.17}$$

$$G[t,k,l] := \langle v\otimes\Phi \mid U_t^*(e^{ilx}\otimes e^{k\frac{(A_t-A_t^*)}{\sqrt{2}}})U_t \mid v\otimes\Phi\rangle \tag{3.18}$$

In this notation, F denotes the joint characteristic function for $\frac{A_t+A_t^*}{\sqrt{2}}$ and p, while G denotes the joint characteristic function for $\frac{A_t-A_t^*}{i\sqrt{2}}$ and x. While in general, we would need to calculate the joint characteristic function for all 4 variables, in the particular system we are studying, the function decouples into two independent components. Here, F and G are expectation values taken with respect to an x-polarized spin state of the atoms and the vacuum state of the field, as described in the previous section. Since we are interested in obtaining joint characteristic functions, and not individual moments, the atomic and field operators are given by complex exponentials of the respective observables.

We can calculate $F[t,k,l]$ and $G[t,k,l]$ by solving partial differential equations given by the following lemma:

Lemma:

$$\frac{\partial F}{\partial t} = -\tfrac{1}{4}(\alpha l-k)^2F - \alpha(\alpha l-k)\tfrac{\partial F}{\partial l} \tag{3.19}$$

$$\frac{\partial G}{\partial t} = -\tfrac{1}{4}(\alpha l+k)^2G - \alpha k\tfrac{\partial G}{\partial l} \tag{3.20}$$

where $F[0,k,l] = G[0,k,l] = e^{-\frac{l^2}{4}}$.

Proof: Let $F(Z) := \langle v\otimes\Phi \mid U_t^*(Z\otimes e^{ik\frac{(A_t+A_t^*)}{\sqrt{2}}})U_t \mid v\otimes\Phi\rangle$ so that $F[e^{ilp}] = F[t,k,l]$. Using the notation introduced previously, we have the expression $dF[e^{ilp}] = \langle v\otimes\Phi \mid \{1\}+\{2\}+\{3\}+\{12\}+\{23\}+\{13\}+\{123\} \mid v\otimes\Phi\rangle$. Applying the Itô rule and noting

that the third powers of increments vanish, we are left with the following differentials to calculate:

$$\begin{aligned}
\{1\} &= dU_t^*(e^{ilp} \otimes e^{ik\frac{(A_t+A_t^*)}{\sqrt{2}}})U_t \\
\{2\} &= U_t^*\big(e^{ilp} \otimes (\tfrac{ik(dA_t+dA_t^*)}{\sqrt{2}} - \tfrac{1}{4}k^2dt)e^{ik\frac{(A_t+A_t^*)}{\sqrt{2}}}\big)U_t \\
\{3\} &= U_t^*(e^{ilp} \otimes e^{ik\frac{(A_t+A_t^*)}{\sqrt{2}}})dU_t
\end{aligned}$$

$$\begin{aligned}
\{12\} &= dU_t^*\big(e^{ilp} \otimes (\tfrac{ik(dA_t+dA_t^*)}{\sqrt{2}} - \tfrac{1}{4}k^2dt)e^{ik\frac{(A_t+A_t^*)}{\sqrt{2}}}\big)U_t \\
\{23\} &= U_t^*\big(e^{ilp} \otimes (\tfrac{ik(dA_t+dA_t^*)}{\sqrt{2}} - \tfrac{1}{4}k^2dt)e^{ik\frac{(A_t+A_t^*)}{\sqrt{2}}}\big)dU_t \\
\{13\} &= dU_t^*(e^{ilp} \otimes e^{ik\frac{(A_t+A_t^*)}{\sqrt{2}}})dU_t
\end{aligned}$$

In the above expressions, dU_t and dU_t^* are given by equation (3.5). The terms dA_t and dA_t^* vanish with respect to the vacuum expectation (see, for instance [53]) and we find that $\{1\}, \{3\}$, and $\{13\}$ give the following:

$$\begin{aligned}
&\langle v \otimes \Phi \mid \{1\} + \{3\} + \{13\} \mid v \otimes \Phi\rangle \\
&\qquad = -\frac{1}{2}F[L^*Le^{ilp} + iHe^{ilp}]dt \\
&\qquad - \frac{1}{2}F[e^{ilp}L^*L + ie^{ilp}H]dt + F[L^*e^{ilp}L] \\
&\qquad = F[\mathcal{L}(e^{ilp})]dt,
\end{aligned}$$

where $\mathcal{L}(e^{ilp})$ is the Lindblad operator given by

$$\mathcal{L}(e^{ilp}) = -\frac{1}{2}\{L^*L, e^{ilp}\} + i[H, e^{ilp}] + L^*e^{ilp}L$$

Recalling that $L = \frac{\alpha(p-ix)}{\sqrt{2}}$, $L^* = \frac{\alpha(p+ix)}{\sqrt{2}}$, and $H = \frac{1}{4}\alpha^2(px + xp)$, we can expand the Lindblad term as follows:

$$\begin{aligned} F[\mathcal{L}(e^{ilp})]dt &= F[-\frac{1}{2}\{L^*L, e^{ilp}\} + i[H, e^{ilp}] + Le^{ilp}L^*]dt \\ &= -\tfrac{1}{4}\alpha^2 l^2 F[e^{ilp}]dt - i\alpha^2 l F[pe^{ilp}]dt \\ &= -\tfrac{1}{4}\alpha^2 l^2 F[t,l,k]dt - \alpha^2 l\tfrac{\partial F[t,l,k]}{\partial l}dt \end{aligned}$$

In the last step, we used that the term $F[pe^{ilp}]$ can be written as the partial derivative $-i\frac{\partial F[t,l,k]}{\partial l}$. Summing the remaining terms, we have:

$$\begin{aligned} &\langle v \otimes \Phi \mid \{2\} + \{12\} + \{23\} \mid v \otimes \Phi\rangle \\ &\quad = -\tfrac{1}{4}k^2 F[e^{ilp}] - \tfrac{ik}{\sqrt{2}}F[L^*e^{ilp} + e^{ilp}L] \\ &\quad = -\tfrac{1}{4}k^2 F[e^{ilp}] - \tfrac{ik}{\sqrt{2}}F[\tfrac{\alpha(p+ix)}{\sqrt{2}}e^{ilp} + e^{ilp}\tfrac{\alpha(p-ix)}{\sqrt{2}}] \\ &\quad = -\tfrac{1}{4}k^2 F[e^{ilp}] + \tfrac{\alpha kl}{2}F[t,k,l] + \alpha k\tfrac{\partial F[t,l,k]}{\partial l} \end{aligned}$$

Collecting like terms, we arrive at the expression stated in the lemma. The initial condition is obtained by noting that the atoms begin in a $\hat{J}_x$ eigenstate and that at time $t = 0$, $A_t = A_t^* = 0$ and $U_t = U_t^* = I$. As we have applied the Holstein-Primakoff approximation, introducing the variables $(x_{at}, p_{at}) = (\hat{J}_y, \hat{J}_z)/\sqrt{J_x}$, we then see that the initial state is a Gaussian with variance $\frac{1}{2}$. The derivation for $G[t,k,l]$ proceeds analogously. ■

We then arrive at the following solutions for the joint characteristic functions:

$$F[t,k,l] = e^{-\frac{1}{2}\left[\sigma^2_{p_{at}} l^2 + 2\sigma^2_{p_{at},x_{ph}} kl + \sigma^2_{x_f} k^2\right]} \tag{3.21}$$

$$G[t,k,l] = e^{-\frac{1}{2}\left[\sigma^2_{x_{at}} l^2 + 2\sigma^2_{x_{at},p_{ph}} kl + \sigma^2_{p_f} k^2\right]} \tag{3.22}$$

where

$$\sigma^2_{p_{at}} = \tfrac{1}{4}(1+e^{-2\alpha^2 t}) \tag{3.23}$$
$$\sigma^2_{p_{at},x_{ph}} = -\tfrac{1}{4\alpha}(1+e^{-2\alpha^2 t}-2e^{-t\alpha^2}) \tag{3.24}$$
$$\sigma^2_{x_f} = \tfrac{1}{4\alpha^2}(3+e^{-2\alpha^2 t}-4e^{-\alpha^2 t}) \tag{3.25}$$

and

$$\sigma^2_{x_{at}} = \frac{1}{2}(1+\alpha^2 t) \tag{3.26}$$
$$\sigma^2_{x_{at},p_{ph}} = -\tfrac{1}{4}\alpha^3 t^2 \tag{3.27}$$
$$\sigma^2_{p_f} = \frac{1}{2}t + \tfrac{1}{6}\alpha^4 t^3 \tag{3.28}$$

The expressions σ^2 denote the variances and covariances of the respective quantities. From equations (3.23), (3.25), (3.26), and (3.28), we see that this setup generates arbitrary amounts of polarization squeezing and at most 3 dB of atomic spin squeezing. Although it is to be expected that for a linear system an initial Gaussian state remains Gaussian, the derivation of the joint characteristic function makes this fact explicit.

3.3 Summary

The physical mechanism identified by Sherson and Mølmer is certainly of interest in its own right. But from the perspective of coherent feedback control and the more general goal of realistic physical modeling with QSDE's, this was a small step in a much more ambitious direction. In particular, as we will examine in the subsequent chapter on autonomous quantum memories, the simple heuristic derivation of the series product that we use here becomes much more powerful when used in in the more general form as proposed by Gough and James. This allows us to not only tackle more complicated linear and non-linear systems by hand, but ultimately, to implement these algebraic rules in a computer algebra system that enables us to scale up the synthesis of quantum networks effectively to arbitrary levels of complexity,

limited only, of course, by our ability to simulate the resulting systems.

Chapter 4

Coherent feedback networks for quantum error correction

I will now examine a class of quantum memory models which synthesize and build upon the intuition developed in the previous chapters. Perhaps it's also worth noting that the pedagogical progression that organizes this thesis is fairly accurate historically as a chronological record of events. When I was first examining the polarization squeezing setup described in the previous chapter, the series product did not exist– hence the heuristic derivation of the double-pass QSDE. Of course, the intuition is entirely present in this work, pointing the way to the substantially more general approach to quantum network synthesis that the Gough-James series and concatenation products allow for. The models I analyze in this chapter– initially developed by Kerckhoff, Nurdin, Pavlichin, and Mabuchi in [35]– are the first examples of photonic networks synthesized within the Gough-James framework. And as I will show in the latter half of the chapter, with the aid of computer algebra, we can essentially conceive of and design networks of arbitrary complexity, a feat which would simply be impossible with a heuristic input/output formalism.

4.1 Overview of nanophotonic quantum memory design

Quantum feedback control provides a systems engineering perspective on the analysis and design of quantum memories, complementing alternative ideas extending from theoretical physics. Whereas the latter approach has emphasized the connections of quantum error correction and quantum computation to many body physics [37, 14], the quantum control community has viewed decoherence suppression as a problem that should ideally be formulated as a non-commutative generalization of classical stochastic and hybrid control theory. In a sense, we can view this research program as a 1950's/60's-era agenda translated forward a half century. That is, given the novel resources of photonics, quantum electronics, and spintronics, we can ask ourselves what the basic constituent components might be of a post-classical information processing machine, and how the exchange of signals among such components could be used to realize desired functionality [2, 9, 46].

Within this setting we have recently investigated nanophotonic circuit models for quantum memories that autonomously implement well-known stabilizer codes. In these models, each physical qubit is strongly coupled to an optical or microwave resonator, and the resonators are coupled by waveguides to form a coherent feedback network (photonic circuit). When the circuit is powered by appropriate stationary laser inputs, the resulting continuous-time dynamics effect error detection and correction without any additional external clocking or control signals. In such models, the classical signal processing apparatus assumed in standard treatments of quantum error correction is replaced by a small number of controller qubits, making it possible to derive a master equation for the closed-loop behavior that can be modified straightforwardly to incorporate a wide range of realistic decoherence mechanisms [35, 36, 56] (see also 4.3.2 in this thesis).

The operational principles of these quantum memory models, as well as the methods used to derive their equations of motion, exemplify a quantum-optical generalization

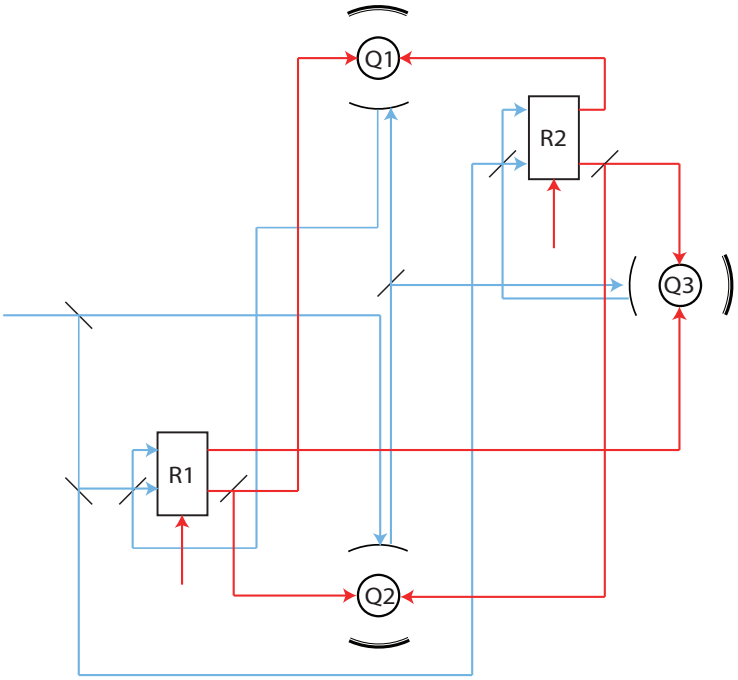

Figure 4.1: Photonic network implementing 3-qubit bit-flip/phase-flip code

of conventional electric circuit theory in which guided electromagnetic fields play the role of signals and qubit-resonators serve as input/output devices that process them coherently.

The models we examine in this chapter are class of quantum photonic circuits that autonomously implement a form of quantum error correction (QEC) based on stabilizer coding, continuous syndrome measurement and restorative feedback. No external control or clocking signals are required; once fabricated according to specification the circuit should continuously implement the QEC protocol by virtue of the fixed Hamiltonian couplings among its cavity QED-based components and optical waveguides. The circuit is powered by coherent laser inputs, whose frequencies should be accurately stabilized but whose amplitudes need only respect a certain parameter

hierarchy– note the relationship of this hierarchy to the adiabatic elimination theorem used to derive the reduced order equations of motion [10] (see also Section 2.5). Such QEC models present a useful set of elementary examples for quantum circuit theory incorporating features such as coherent optical signals, component-component entanglement and feedback loops.

The physical intuition of the network dynamics can be thought of in the following manner. At one level of abstraction, each photonic circuit consists of a one-to-one correspondence with a given stabilizer code. If our stabilizer code has N qubits, then the corresponding network has N register qubits implemented in cavity-QED based components. The "control signals" are the error syndromes which are extracted by measuring stabilizer generators. To process each of these control signals, we presume additional qubits, the cavity-QED controllers, or relays, again in one-to-one correspondence with the stabilizer generators.

The fundamental physical mechanism which enables these designs is the QND measurement of the error syndrome, i.e. the stabilizer generator measurement. In a bad cavity limit ($\kappa \to \infty$), a probe beam resonant with the cavity will enter and exit 'immediately' when the atom is in the uncoupled state. In this case, the input and output beams will be in phase– i.e. the probe beam gains no additional phase shift. However, when we are in a regime called the "small volume limit" ($g_c, \kappa \to \infty$, with g_c/κ constant), the probe will be reflected from the off-resonant, atom-cavity system, and pick up an additional π phase shift. That is, when the system is constructed so that the cavity decay rate and coupling constant obey a certain parameter hierarchy, the combined system acts as a static, state-dependent phase-shifter. In the subsequent sections when we derive the corresponding SLH models, this will be manifest as a triple with only a scattering matrix, but no coupling or Hamiltonian terms.

The remaining sections are organized as follows. Following the exposition in [35], I will give a detailed derivation of the SLH component models necessary for constructing autonomous quantum memories implementing stabilizer error correcting codes, and

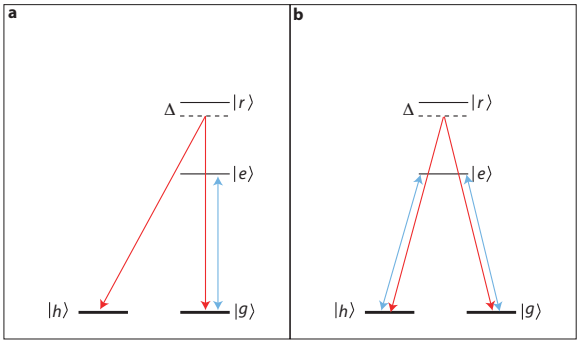

Figure 4.2: Atomic level diagrams for Z-probe/feedback and X-probe/feedback interactions

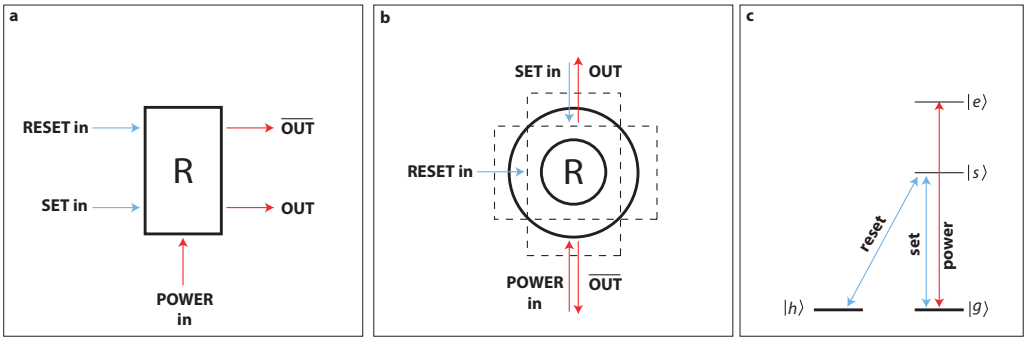

Figure 4.3: Input/output diagrams and atomic level structure for cavity-QED relay

construct the Gough-James circuit model and master equation for the bit-flip/phase-flip code. I will then demonstrate how the basic network synthesis framework implicit in the Gough-James circuit algebra can be systematically implemented in a computer algebra system to enable what we might call "photonic design automation" that allows for the synthesis of quantum circuits of arbitrary complexity. I then describe a related workflow for transforming photonic circuit models, and as an example, derive reduced order equations of motion for the 3-qubit and 9-qubit Bacon-Shor codes which also incorporate the effects of propagation losses. Finally, I extend the analyses conducted thus far for the 3 and 9-qubit code to arbitrary stabilizer codes by deriving a class of phenomenological master equations which capture the high-level

principles of coherent-feedback quantum memories.

4.2 Network components for quantum memory circuits

In this section, I give a detailed derivation of the component models used for the bit-flip/phase-flip code. The exposition is directly adapted from the appendices of [35], so those readers who are intimately familiar with that work may safely skip this over, although I have tried to expand on and highlight several salient features of the analysis at various points. Furthermore, the motivation for the work in the subsequent section on the QHDL paradigm for photonic network synthesis was inspired by the notion that we could automate laborious calculations such as these, so for the reader exposed to this material for the first time, it should be of some value to see precisely what symbolic operations need to be algorithmically implemented to achieve a high degree of automation with the QSDE and Gough-James frameworks.

4.2.1 Probe model for syndrome extraction

I first present the model for sequentially interrogating the qubits and extracting the error syndrome– the physical mechanism described here was first proposed by Duan and Kimble in [15], which formed the physical basis for the continuous-time two-qubit parity measurement setup described in [34]. See also [49] for a dispersive model with smaller phase shifts.

Pre-limit model

The probe interaction consists of a three level atomic system in a λ-configuration in conjunction with a quantized mode of a single-sided cavity. For the Z probe, the $|g\rangle \leftrightarrow |e\rangle$ transition is strongly coupled and on resonance with the cavity mode, while the $|h\rangle$ state is fully uncoupled. In the case of the X probe, both $|g\rangle \leftrightarrow |e\rangle$ and $|h\rangle \leftrightarrow |e\rangle$ transitions are simultaneously coupled and on resonance with the

cavity mode. In a rotating frame and under the rotating wave approximation, the Hamiltonian for both systems is given by the familiar Jaynes-Cummings model:

$$H = ig_c(\sigma^* a - \sigma a^*) \tag{4.1}$$

where a is the cavity mode annihilation operator and σ is the atomic lowering operator. In the case of the bit-flip code, $\sigma = |g\rangle\langle e|$ on the atomic states, whereas in the phase-flip code $\sigma = \frac{1}{\sqrt{2}}(|g\rangle + |h\rangle)\langle e|$. The coupling rate g_c is assumed to be real in all of the networks presented here.

Our atom-cavity system is not closed– photons in the cavity can decay into the environment and when excited, the atom will spontaneously emit photons into a mode transverse to the cavity mode. As described in the introduction, the interaction of a system with the environment can be incorporated into the quantum stochastic differential equation framework with the following terms as part of the coupling vector:

$$L_1 = \sqrt{2\kappa}a; \;\; L_2 = \sqrt{2\gamma_\perp}\sigma \tag{4.2}$$

Here, κ and $\gamma_\perp$ are the cavity field and atomic dipole decay rates, respectively. Note that there is no direct coupling between the cavity and atomic decay channels. Hence, the scattering matrix S is simply the identity. In SLH form, the right QSDE describing the dynamics for the Z and X systems is given by the following triple:

$$Q = \left(I, \begin{bmatrix} \sqrt{2\kappa}a \\ \sqrt{2\gamma_\perp}\sigma \end{bmatrix}, ig_c(\sigma^* a - \sigma a^*) \right). \tag{4.3}$$

Adiabatic elimination

Having established the pre-limit model, we can now apply the adiabatic elimination theorem to Q to obtain a simple, scattering-matrix model which we will use to construct the final network master equation.

As prescribed in [10] (see Section 2.5), we define a sequence of parameter-dependent

QSDE's with a scaling parameter k:

$$dQ_t^{(k)} = Q_t^{(k)}\Big\{ -k\sqrt{2\kappa}a dA_t^{1*} + k\sqrt{2\kappa}a^* dA_t^1 - \sqrt{2\gamma_\perp}\sigma dA_t^{2*} + \sqrt{2\gamma_\perp}\sigma^* dA_t^2 - k^2\kappa a^* a dt - \gamma_\perp \sigma^*\sigma dt - k^2 g_c(\sigma^* a - \sigma a^*)dt\Big\}.$$

The operator coefficients of the above left QSDE are

$$K^{(k)} = -k^2\kappa a^* a - \gamma_\perp \sigma^*\sigma - k^2 g_c\left(a^*\sigma - a\sigma^*\right) \tag{4.4}$$

$$L^{(k)} = \begin{pmatrix} k\sqrt{2\kappa}a^* \\ \sqrt{2\gamma_\perp}\sigma^* \end{pmatrix} \tag{4.5}$$

$$N^{(k)} = I. \tag{4.6}$$

As described in the introductory section on adiabatic elimination, we can now derive a limiting propagator Q_t that will be used in the network model in place of the physical cQED model. To satisfy the structural conditions 2.5 we use:

$$Y = -\kappa a^* a - g_c\left(a^*\sigma - a\sigma^*\right), \quad A = 0, \quad B = -\gamma_\perp \sigma^*\sigma,$$
$$F = \begin{pmatrix} \sqrt{2\kappa}a^* \\ 0 \end{pmatrix}, \quad G = \begin{pmatrix} 0 \\ \sqrt{2\gamma_\perp}\sigma^* \end{pmatrix}, \quad W = I. \tag{4.7}$$

For the Z probe, we choose $H_0 = \mathsf{span}\left\{|\, g, 0\rangle, |\, h, 0\rangle\right\}$ and define

$$\begin{aligned}
\tilde{Y}\ \{|\, g\, 0\rangle, |\, h\, 0\rangle\} &= 0, \\
\tilde{Y}\ |\, h\, n\rangle &= -\frac{1}{\kappa n}|\, h\, n\rangle, \quad n \geq 1; \\
\tilde{Y}\ |\, e\ (n-1)\rangle &= -\frac{g_c\sqrt{n}}{\kappa^2 n\,(n-1) + g_c^2 n}|\, g\, n\rangle - \frac{\kappa n}{\kappa^2 n\,(n-1) + g_c^2 n}|\, e\ (n-1)\rangle, \quad n \geq 1; \\
\tilde{Y}\ |\, g\, n\rangle &= -\frac{\kappa\,(n-1)}{\kappa^2 n\,(n-1) + g_c^2 n}|\, g\, n\rangle + \frac{g_c\sqrt{n}}{\kappa^2 n\,(n-1) + g_c^2 n}|\, e\ (n-1)\rangle, \quad n \geq 1.
\end{aligned} \tag{4.8}$$

This gives us the condition $Y\tilde{Y} = \tilde{Y}Y = P_1$. The limiting operator coefficients are,

$$K = 0, \quad L_1 = L_2 = 0, \quad M_1 = M_2 = 0, \tag{4.9}$$

and (with $\Pi_{in} = |i, n\rangle\langle i, n|$)

$$\begin{aligned} N_{11} &= P_0 W_{11} \left(F_1^* \tilde{Y} F_1 + \delta_{11} \right) P_0 = P_0 + 2\kappa P_0 a \tilde{Y} a^* \left(\Pi_{g0} + \Pi_{h0} \right) \\ &= P_0 + 2\kappa P_0 a \tilde{Y} \left(|\, g\, 1\rangle \langle g\, 0| + |\, h1\rangle \langle h\, 0| \right) \\ &= P_0 + 2\kappa P_0 a \left(\frac{1}{g_c} |\, e\, 0\rangle \langle g\, 0| - \frac{1}{\kappa} |\, h\, 1\rangle \langle h\, 0| \right) \\ &= P_0 - 2\, |\, h\, 0\rangle \langle h\, 0| \\ &= \Pi_{g0} - \Pi_{h0} \equiv Z, \end{aligned}$$

And for the remaining matrix elements:

$$\begin{aligned} N_{12} &= P_0 W_{11} \left(F_1^* \tilde{Y} F_2 + \delta_{12} \right) P_0 = 0 \\ N_{21} &= P_0 W_{22} \left(F_2^* \tilde{Y} F_1 + \delta_{21} \right) P_0 = 0 \\ N_{22} &= P_0 W_{22} \left(F_2^* \tilde{Y} F_2 + \delta_{22} \right) P_0 = 1 \end{aligned} \tag{4.10}$$

Thus we see that the limiting system has the following SLH form:

$$Q = \left(\begin{bmatrix} \mathrm{Z} & 0 \\ 0 & \mathrm{I} \end{bmatrix}, \begin{bmatrix} 0 \\ 0 \end{bmatrix}, 0 \right), \tag{4.11}$$

Although the probe model is strictly speaking a 2-port device, as it can be decomposed into the concatenation $Q = (Z, 0, 0) \boxplus (1, 0, 0)$ we will frequently use the short-hand notation $Q = (Z, 0, 0)$ to denote the limiting SLH model. For the X probe case in the phase-flip network, an analogous derivation will give rise to the SLH model $Q = (X, 0, 0)$.

4.2.2 Feedback model for error correction

In the previous section, we saw how the coupled atom-cavity system allows for a physical implementation of syndrome extraction for the stabilizer generators in the bit-flip/phase-flip code. I now describe an analogous mechanism– the Raman interaction model– that allows errors to be corrected in the coherent feedback loop. Note that the probe and feedback networks are effectively independent entities, so that in addition to continuous interrogation by the probe networks, the qubit cavities are also illuminated by (possibly) two free field modes that drive atomic Raman transitions between the ground states of the qubit subspace.

Pre-limit model

For the feedback model, we assume an additional atomic excited state $|r\rangle$, distinct and far detuned from $|e\rangle$. The ground states are coupled to $|r\rangle$ via interactions with transverse free fields. When two of these field modes, far detuned by frequency Δ from the $\{|h\rangle, |g\rangle\} \leftrightarrow |r\rangle$ transition simultaneously illuminate the qubit, Raman resonance conditions are satisfied, inducing coherent Rabi oscillations between the two ground states. For the bit-flip network, these interactions are modeled in a QSDE by the following Hamiltonian and coupling operators:

$$\begin{aligned} H^{(k)} &= k^2\Delta|r\rangle\langle r| \equiv k^2\Delta\Pi_r \\ L_1^{(k)} &= \sqrt{\gamma}|h\rangle\langle r| \equiv \sqrt{\gamma}\sigma_{hr} \\ L_2^{(k)} &= \sqrt{\gamma}|g\rangle\langle r| \equiv \sqrt{\gamma}\sigma_{gr}. \end{aligned} \tag{4.12}$$

Here, we have scaled the detuning Δ with k, in anticipation of the adiabatic elimination procedure that follows. For the phase-flip network, the above coupling operators are modified with $\sigma_{hr} \to \frac{1}{\sqrt{2}}(\sigma_{hr} + \sigma_{gr})$ and $\sigma_{gr} \to \frac{1}{\sqrt{2}}(\sigma_{hr} - \sigma_{gr})$. We incorporate two additional coupling terms to model the interactions of the $\{|h\rangle, |g\rangle\} \leftrightarrow |r\rangle$ transitions

with all other free modes (assuming the limit $\gamma \ll \gamma_{\parallel}$):

$$\begin{aligned} L_3^{(k)} &= \sqrt{\gamma_{\parallel}}\sigma_{hr} \\ L_4^{(k)} &= \sqrt{\gamma_{\parallel}}\sigma_{gr} \end{aligned} \tag{4.13}$$

Adiabatic elimination

Application of the adiabatic elimination theorem [10] to the above (using the modified technique discussed in section 2.5.1) results in an approximate Hamiltonian interaction

$$H = -\frac{\gamma}{\Delta}\left(|\beta_1|^2\Pi_h + |\beta_2|^2\Pi_g + \beta_1\beta_2^*\sigma_{gh} + \beta_1^*\beta_2\sigma_{gh}^*\right) \tag{4.14}$$

and all atomic operators drop out of the field coupling operators (eliminating all spontaneous emission dynamics). Thus, coherent transitions between the two ground states may be driven by the last two terms in H when both Raman modes are in large-amplitude coherent states. Note, however, that the ground state energy shifts represented by the first two terms correspond to AC Stark shifts which are detrimental to the performance of the memory. For a discussion of compensatory mechanisms, see Appendix A.

4.2.3 List of network components for bit-flip/phase-flip code

In this section, I simply list out all of the individual components necessary to construct the 3-qubit bit-flip/phase-flip code.

Qubit cavities:

The qubit cavities in the network can all be decomposed into a concatenation product of subcomponents. Because of the asymmetry in the stabilizer generators, that is, since qubit $Q2$ is contained in both syndrome measurements, $Q2$ will consist of a decomposition into 4 cavities (2 probe and 2 feedback), whereas the remaining qubits are decomposed into 3 cavities (1 probe and 2 feedback). That is, $Q_2 = Q_{21} \boxplus Q_{22} \boxplus Q_{23} \boxplus Q_{24}$, where Q_{21} and Q_{24} are the subcomponents affiliated to the probe lasers, while Q_{22} and Q_{23} correspond to each leg of the Raman transition. $Q1$

and $Q3$ are single sided cavities which decompose as $Q_j = Q_{j1} \boxplus Q_{j2} \boxplus Q_{j3}$ $(j = 1, 3)$. Q_{j2} is the subcomponent affiliated to the probe laser coupling. Q_{j1} and Q_{j3} again correspond to the two legs of the Raman transition.

Probe interactions:

As we derived above (see Section 4.2.1), the cavity subcomponents corresponding to the Z-probe interaction have the following SLH models in the small-volume limit:

$$Q_{12} = \left(Z^{Q1}, 0, 0\right), \; Q_{21} = \left(Z^{Q2}, 0, 0\right), \; Q_{24} = \left(Z^{Q2}, 0, 0\right), \; Q_{32} = \left(Z^{Q3}, 0, 0\right). \quad (4.15)$$

For the phase-flip network, the X-probe interaction can be formed by making the substitution $Z^{Qi} \to X^{Qi}$.

Raman transitions:

For the bit-flip feedback network, we have the following set of SLH models for the Raman interaction:

$$\begin{aligned} Q_{11} &= \left(1, \sqrt{\gamma}\sigma_{gr}^{Q1}, \frac{1}{2}\Delta\Pi_r^{Q1}\right), \quad Q_{13} = \left(1, \sqrt{\gamma}\sigma_{hr}^{Q1}, \frac{1}{2}\Delta\Pi_r^{Q1}\right), \\ Q_{22} &= \left(1, \sqrt{\gamma}\sigma_{hr}^{Q2}, \frac{1}{2}\Delta\Pi_r^{Q2}\right), \quad Q_{23} = \left(1, \sqrt{\gamma}\sigma_{gr}^{Q2}, \frac{1}{2}\Delta\Pi_r^{Q2}\right), \\ Q_{31} &= \left(1, \sqrt{\gamma}\sigma_{gr}^{Q3}, \frac{1}{2}\Delta\Pi_r^{Q3}\right), \quad Q_{33} = \left(1, \sqrt{\gamma}\sigma_{hr}^{Q3}, \frac{1}{2}\Delta\Pi_r^{Q3}\right), \end{aligned} \quad (4.16)$$

Again, for the corresponding phase-flip network, the SLH models can be formed by making the substitutions $\sigma_{hr} \to \frac{1}{\sqrt{2}}(\sigma_{hr}+\sigma_{gr})$ and $\sigma_{gr} \to \frac{1}{\sqrt{2}}(\sigma_{hr}-\sigma_{gr})$. The particular choice of coupling operators in theses models is motivated by the need to attenuate the effects of feedback-induced AC Stark shifts– see Appendix A for a detailed discussion.

Coherent displacements:

As described in Section 2.2.3, in the SLH formalism, a laser can be modeled via the QSDE for the Weyl operator. There are two types of lasers in this network, one set at the probe frequency and the other at the Raman frequency. Each has the following

SLH model (with $d = \alpha$ for the probe network and $d = \beta$ for the feedback network):

$$W_d = (I, d, 0)\,;. \tag{4.17}$$

Beamsplitters:

As shown in the introduction, a beamsplitter has the following SLH model:

$$B(\alpha, \beta) = \left(\begin{bmatrix} \alpha & -\beta^\dagger \\ \beta & \alpha^\dagger \end{bmatrix}, \begin{bmatrix} 0 \\ 0 \end{bmatrix}, 0 \right) \tag{4.18}$$

In the current QEC networks, all beamsplitters are 50/50:

$$B = \left(\begin{bmatrix} \frac{1}{\sqrt{2}} & \frac{1}{\sqrt{2}} \\ -\frac{1}{\sqrt{2}} & \frac{1}{\sqrt{2}} \end{bmatrix}, 0, 0 \right). \tag{4.19}$$

Relays:

The fundamental "computation unit" in the networks are the cavity-QED relays described in [45]. The relays are what allow the network to decide when to issue restorative feedback based on the error syndrome measurements. Each of the two relays, R_1 and R_2, is a 4-port device with the concatenation decomposition $R_k = R_{k1} \boxplus R_{k2}$. The field inputs to R_{k2} control the state of the relay, which in turn controls the routing of the field inputs to R_{k1}. The relays have the following SLH form:

$$\begin{aligned} R_{k1} &= \left(\begin{bmatrix} \Pi_g^{Rk} & -\Pi_h^{Rk} \\ -\Pi_h^{Rk} & \Pi_g^{Rk} \end{bmatrix}, 0, 0 \right), \\ R_{k2} &= \left(\begin{bmatrix} \Pi_g^{Rk} & -\sigma_{hg}^{Rk} \\ -\sigma_{gh}^{Rk} & \Pi_h^{Rk} \end{bmatrix}, 0, 0 \right), \end{aligned} \tag{4.20}$$

for $k = 1, 2$, where the superscripts keep track of operators on different component states.

Bit-/phase-flip errors:

To model errors in the system, we can concatenate "error component models" onto the final QEC network. The errors correspond to SLH models that couple the system to either Pauli-X errors (for the bit-flip code)

$$E_X^{Qi} = \left(I, \sqrt{\Gamma} X^{Qi}, 0\right) \tag{4.21}$$

or Pauli-Z errors (for the phase-flip code)

$$E_Z^{Qi} = \left(I, \sqrt{\Gamma} Z^{Qi}, 0\right) \tag{4.22}$$

The mean rate of errors is Γ and, of course, equivalently, we could simply add the corresponding Lindblad terms to the final master equation rather than concatenating the SLH models to the network (see Section 2.6).

4.2.4 Network calculations with Gough-James circuit algebra

A schematic diagram of the overall quantum network is shown in Fig. 4.4. Our aim is to use the Gough-James circuit algebra to compute the full SLH model for the network $G \boxplus G'$, with the subnets G and G' defined as the following decomposition into probe and feedback components:

$$\begin{aligned} G_p &= R_{12} \lhd B \lhd ((Q_{12} \lhd Q_{21}) \boxplus (I,0,0)) \lhd B \lhd \left(W_{\sqrt{2}\alpha} \boxplus (I,0,0)\right), \\ G_f &= (Q_{11} \boxplus Q_{31} \boxplus Q_{22}) \lhd (B \boxplus_2 (I,0,0)) \lhd (R_{11} \boxplus (I,0,0)) \lhd (W_\beta \boxplus (I_2,0,0)), \end{aligned} \tag{4.23}$$

The network G' is formed by permuting the component indices in the following manner:

$$R_{22} \leftrightarrow R_{12},\ R_{21} \leftrightarrow R_{11},\ Q_{23} \leftrightarrow Q_{11},\ Q_{33} \leftrightarrow Q_{22},\ Q_{13} \leftrightarrow Q_{31},\ Q_{24} \leftrightarrow Q_{21},\ Q_{32} \leftrightarrow Q_{12}. \tag{4.24}$$

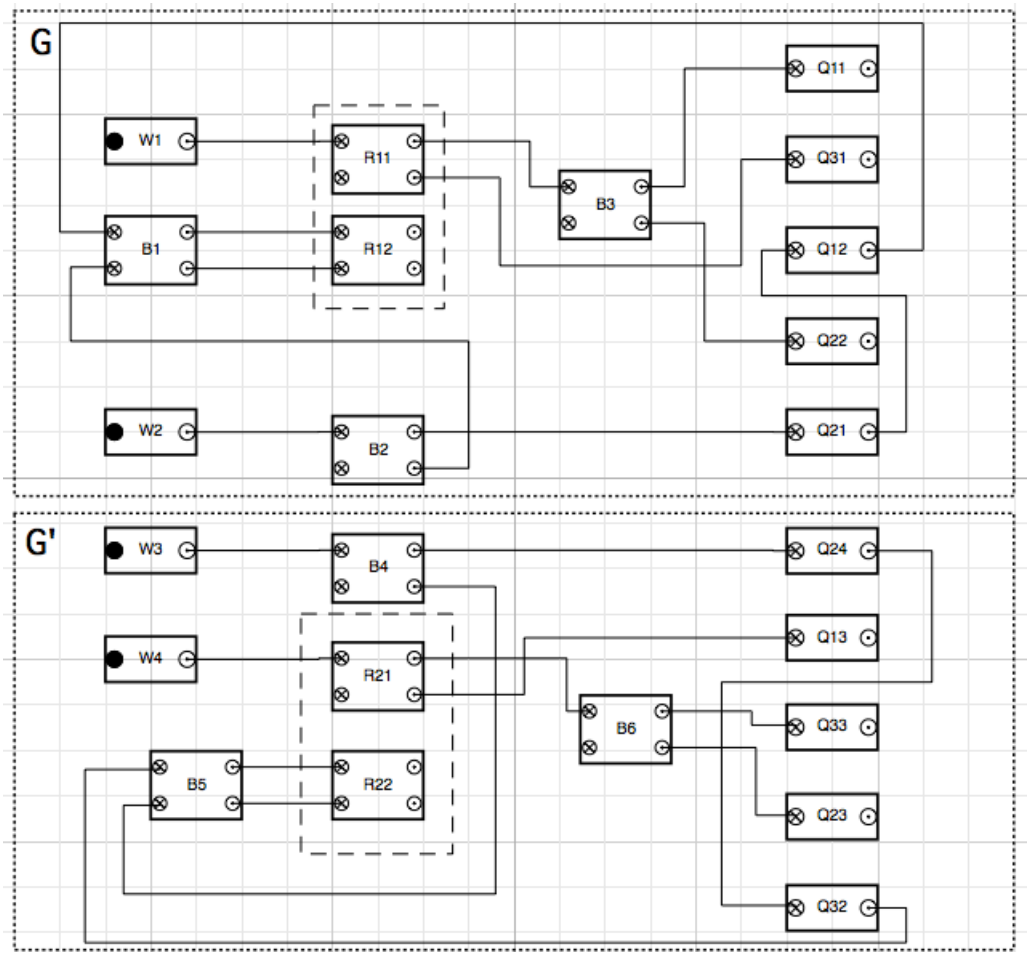

Figure 4.4: Diagrammatic representation of quantum correction network. Note that the Gough-James network expression can essentially be read off from a schematic representation of this form.

Thus, the overall network takes the following SLH form:

$$N = \left(\mathrm{diag}(\mathrm{S}^{(\mathrm{p})}, \mathrm{S}'^{(\mathrm{p})}, \mathrm{S}^{(\mathrm{f})}, \mathrm{S}'^{(\mathrm{f})}), \begin{bmatrix} L^{(p)} \\ L'^{(p)} \\ L^{(f)} \\ L'^{(f)} \end{bmatrix}, \mathrm{H}^{(\mathrm{p})} + \mathrm{H}'^{(\mathrm{p})} + \mathrm{H}^{(\mathrm{f})} + \mathrm{H}'^{(\mathrm{f})} \right) \quad (4.25)$$

As stated earlier, note that the bit-flip/phase-flip errors can essentially be thought of as separate "circuit components" $E^{Qi}_{X,Z}$, which are concatenated to N prior to deriving

the Lindblad master equation– these "error components" are not shown in the circuit diagram of Figure 4.4.

Probe network

Substituting the component models into the Gough-James expression for the probe network, we have for the G_p, the following SLH model:

$$\begin{aligned}
\mathbf{S}_{G_p} &= \frac{1}{2}\begin{bmatrix} O^{(12)}\Pi_g^{R1} + E^{(12)}\sigma_{hg}^{R1} & E^{(12)}\Pi_g^{R1} + O^{(12)}\sigma_{hg}^{R1} \\ -E^{(12)}\Pi_h^{R1} - O^{(12)}\sigma_{gh}^{R1} & -O^{(12)}\Pi_h^{R1} - E^{(12)}\sigma_{gh}^{R1} \end{bmatrix} \\
\mathbf{L}_{G_p} &= \frac{\alpha}{\sqrt{2}}\begin{bmatrix} \Pi_g^{R1}O^{(12)} + \sigma_{hg}^{R1}E^{(12)} \\ -\sigma_{gh}^{R1}O^{(12)} - \Pi_h^{R1}E^{(12)} \end{bmatrix} \\
H_{G_p} &= 0
\end{aligned} \tag{4.26}$$

And analogously for G_p':

$$\begin{aligned}
\mathbf{S}_{G_p'} &= \frac{1}{2}\begin{bmatrix} O^{(32)}\Pi_g^{R2} + E^{(32)}\sigma_{hg}^{R2} & E^{(32)}\Pi_g^{R2} + O^{(32)}\sigma_{hg}^{R2} \\ -E^{(32)}\Pi_h^{R2} - O^{(32)}\sigma_{gh}^{R2} & -O^{(32)}\Pi_h^{R2} - E^{(32)}\sigma_{gh}^{R2} \end{bmatrix} \\
\mathbf{L}_{G_p'} &= \frac{\alpha}{\sqrt{2}}\begin{bmatrix} \Pi_g^{R2}O^{(32)} + \sigma_{hg}^{R2}E^{(32)} \\ -\sigma_{gh}^{R2}O^{(32)} - \Pi_h^{R2}E^{(32)} \end{bmatrix} \\
H_{G_p'} &= 0
\end{aligned} \tag{4.27}$$

For the bit-flip correcting network, $E^{(ij)} = Z^{Qi}Z^{Qj} + 1$ and $O^{(ij)} = Z^{Qi}Z^{Qj} - 1$ are proportional to two-qubit parity projectors. For the phase flip network, $E^{(ij)} = X^{Qi}X^{Qj} + 1$ and $O^{(ij)} = X^{Qi}X^{Qj} - 1$.

Feedback network

Substituting the component models into the Gough-James expression for the feedback network, we have for G_f, the following SLH model:

$$\begin{aligned}
\mathbf{S}_{G_f} &= \frac{1}{\sqrt{2}}\begin{bmatrix} \Pi_g^{R1} & -\Pi_h^{R1} & 1 \\ -\sqrt{2}\Pi_h^{R1} & \sqrt{2}\Pi_g^{R1} & 0 \\ -\Pi_g^{R1} & \Pi_h^{R1} & 1 \end{bmatrix} \\
\mathbf{L}_{G_f} &= \begin{bmatrix} \sqrt{\gamma}\sigma_{gr}^{Q1} + \frac{1}{\sqrt{2}}\beta\Pi_g^{R1} \\ \sqrt{\gamma}\sigma_{gr}^{Q3} - \beta\Pi_h^{R1} \\ \sqrt{\gamma}\sigma_{hr}^{Q2} - \frac{1}{\sqrt{2}}\beta\Pi_g^{R1} \end{bmatrix} \\
H_{G_f} &= \frac{\Delta}{2}\sum_{i=1}^{3}\Pi_r^{Qi} + \mathrm{Im}\left\{\sqrt{\frac{\gamma}{2}}\beta(\sigma_{gr}^{Q1*}\Pi_g^{R1} - \sigma_{hr}^{Q2*}\Pi_g^{R1} - \sqrt{2}\sigma_{gr}^{Q3*}\Pi_h^{R1})\right\}
\end{aligned} \tag{4.28}$$

And analogously for G_f':

$$\begin{aligned}
\mathbf{S}_{G_{f'}} &= \frac{1}{\sqrt{2}}\begin{bmatrix} \Pi_g^{R2} & -\Pi_h^{R2} & 1 \\ -\sqrt{2}\Pi_h^{R2} & \sqrt{2}\Pi_g^{R2} & 0 \\ -\Pi_g^{R2} & \Pi_h^{R2} & 1 \end{bmatrix} \\
\mathbf{L}_{G_{f'}} &= \begin{bmatrix} \sqrt{\gamma}\sigma_{gr}^{Q1} + \frac{1}{\sqrt{2}}\beta\Pi_g^{R1} \\ \sqrt{\gamma}\sigma_{gr}^{Q3} - \beta\Pi_h^{R1} \\ \sqrt{\gamma}\sigma_{hr}^{Q2} - \frac{1}{\sqrt{2}}\beta\Pi_g^{R1} \end{bmatrix} \\
H_{G_{f'}} &= \frac{\Delta}{2}\sum_{i=1}^{3}\Pi_r^{Qi} + \mathrm{Im}\left\{\sqrt{\frac{\gamma}{2}}\beta(\sigma_{gr}^{Q1*}\Pi_g^{R1} - \sigma_{hr}^{Q2*}\Pi_g^{R1} - \sqrt{2}\sigma_{gr}^{Q3*}\Pi_h^{R1})\right\}
\end{aligned} \tag{4.29}$$

4.2.5 Second adiabatic elimination

The adiabatic elimination procedure that we performed previously was taken in the "small volume limit," and produced the simplified scattering model for the probe network and the Raman transition model for the feedback network. However, there is another separation of time-scales that we can exploit to produce yet another reduction in model complexity– that is, we can eliminate the Raman state in the qubit model

to produce a further simplified model which restricts the dynamics to the ground state transitions. Here, so as to scale both the input coherent amplitude and excited state detuning, we utilize the modified adiabatic elimination method described in the introduction (see Section 2.5.1). Redefining $\beta \to k\beta$, $\Delta \to k^2\Delta$, and $G_f \boxplus G'_f \to G_f^{(k)} \boxplus G_f^{(k)\prime}$ with scaling parameter k, we have the following sequence of pre-limit SLH models for G_f:

$$\begin{aligned}
\mathbf{S}_{\tilde{G}_f^{(k)}} &= I \\
\mathbf{L}_{\tilde{G}_f^{(k)}} &= \sqrt{\frac{\gamma}{2}} \begin{bmatrix} \sigma_{gr}^{Q1}\Pi_g^{R1} - \sqrt{2}\sigma_{gr}^{Q3}\Pi_h^{R1} - \sigma_{hr}^{Q2}\Pi_g^{R1} \\ -\sigma_{gr}^{Q1}\Pi_h^{R1} + \sqrt{2}\sigma_{gr}^{Q3}\Pi_g^{R1} + \sigma_{hr}^{Q2}\Pi_h^{R1} \\ \sigma_{gr}^{Q1} + \sigma_{hr}^{Q2} \end{bmatrix} \\
H_{\tilde{G}_f^{(k)}} &= k^2\frac{\Delta}{2}\sum_{i=1}^{3}\Pi_r^{Qi} + 2\,\mathrm{Im}\left\{\sqrt{\frac{\gamma}{2}}k\beta(\sigma_{gr}^{Q1*}\Pi_g^{R1} - \sigma_{hr}^{Q2*}\Pi_g^{R1} - \sqrt{2}\sigma_{gr}^{Q3*}\Pi_h^{R1})\right\}
\end{aligned} \tag{4.30}$$

And analogously for G'_f:

$$\begin{aligned}
\mathbf{S}_{\tilde{G}_f^{(k')}} &= I \\
\mathbf{L}_{\tilde{G}_f^{(k')}} &= \sqrt{\frac{\gamma}{2}} \begin{bmatrix} \sigma_{gr}^{Q2}\Pi_g^{R2} - \sqrt{2}\sigma_{hr}^{Q1}\Pi_h^{R2} - \sigma_{hr}^{Q3}\Pi_g^{R2} \\ -\sigma_{gr}^{Q2}\Pi_h^{R2} + \sqrt{2}\sigma_{hr}^{Q1}\Pi_g^{R2} + \sigma_{hr}^{Q3}\Pi_h^{R2} \\ \sigma_{gr}^{Q2} + \sigma_{hr}^{Q3} \end{bmatrix} \\
H_{\tilde{G}_f^{(k')}} &= k^2\frac{\Delta}{2}\sum_{i=1}^{3}\Pi_r^{Qi} + 2\,\mathrm{Im}\left\{\sqrt{\frac{\gamma}{2}}k\beta(-\sqrt{2}\sigma_{hr}^{Q1*}\Pi_h^{R2} + \sigma_{gr}^{Q2*}\Pi_g^{R2} - \sigma_{hr}^{Q3*}\Pi_g^{R2})\right\}
\end{aligned} \tag{4.31}$$

Applying the limit theorem to the concatenated network $\tilde{G}_F^{(k)} = \tilde{G}_f^{(k)} \boxplus \tilde{G}_f^{(k)\prime}$ yields the limiting system $\tilde{G}_F = (\mathbf{S}, \mathbf{L}, H)$ with $\mathbf{S} = I, \mathbf{L} = 0$ and:

$$\begin{aligned}
H = \Omega\Big(&\sqrt{2}X^{Q1}\Pi_g^{R1}\Pi_h^{R2} + X^{Q2}\Pi_g^{R1}\Pi_g^{R2} - \sqrt{2}X^{Q3}\Pi_h^{R1}\Pi_g^{R2} - \\
&\Pi_g^{R1}(\Pi_g^{Q1} + \Pi_h^{Q2}) - 2\Pi_h^{R1}\Pi_g^{Q3} - \Pi_g^{R2}(\Pi_g^{Q2} + \Pi_h^{Q3}) - 2\Pi_h^{R2}\Pi_h^{Q1}\Big)
\end{aligned} \tag{4.32}$$

where the Raman interaction strength is now set by $\Omega = \gamma|\beta|^2/2\Delta$.

Displacement vector from asymptotic approximation

Recall that to apply the adiabatic elimination theorem on the full network, we were confronted with a situation where our network inputs were coherent displaced inputs and not vacuum inputs. For the procedure described in Section 2.5.1, we construct the network $G_F^{(k)}$, which is an asymptotic approximation of $G_f^{(k)} \boxplus G_f^{(k)\prime}$, with the following SLH model:

$$\mathbf{S}_{G_F^{(k)}} = \mathrm{diag}\left\{S^{(f)}, S'^{(f)}\right\} \tag{4.33}$$

$$\mathbf{L}_{G_F^{(k)}} = \begin{bmatrix} \frac{1}{\sqrt{2}}k\beta\Pi_g^{R1} \\ -k\beta\Pi_h^{R1} \\ -\frac{1}{\sqrt{2}}k\beta\Pi_g^{R1} \\ \frac{1}{\sqrt{2}}k\beta\Pi_g^{R2} \\ -k\beta\Pi_h^{R2} \\ -\frac{1}{\sqrt{2}}k\beta\Pi_g^{R2} \end{bmatrix} \tag{4.34}$$

$$H_{G_F^{(k)}} = \Omega\Big(\sqrt{2}X^{Q1}\Pi_g^{R1}\Pi_h^{R2} + X^{Q2}\Pi_g^{R1}\Pi_g^{R2} - \sqrt{2}X^{Q3}\Pi_h^{R1}\Pi_g^{R2} - \Pi_g^{R1}(\Pi_g^{Q1} + \Pi_h^{Q2}) - 2\Pi_h^{R1}\Pi_g^{Q3} - \Pi_g^{R2}(\Pi_g^{Q2} + \Pi_h^{Q3}) - 2\Pi_h^{R2}\Pi_h^{Q1}\Big) \tag{4.35}$$

As usual, for the phase-flip network, we simply make the replacements X^{Qi} with Z^{Qi} and $2\Pi_{\substack{h\\g}}^{Qi} \to I \pm X^{Qi}$ in the Hamiltonian above.

In the following section when we construct the master equation, however, we will leave out the coupling terms that arise from this asymptotic approximation, as their physical effect is to simply decohere the relay ground states. When the network is properly initialized so that the relays are in the ground states, these terms will have no effect.

4.2.6 Network master equation

Now that we have the SLH model for the full network, it is straightforward to obtain the Lindblad master equation from the Hamiltonian and coupling terms (see Section 2.6):

$$\frac{d\rho_t}{dt} = -i\left[H, \rho_t\right] + \sum_{j=1}^{n}\left\{L_j\rho_t L_j^* - \frac{1}{2}L_j^* L_j\rho_t - \frac{1}{2}\rho_t L_j^* L_j\right\}; \tag{4.36}$$

$$\begin{aligned}
H &= \Omega\Big(\sqrt{2}X^{Q1}\Pi_g^{R1}\Pi_h^{R2} + X^{Q2}\Pi_g^{R1}\Pi_g^{R2} - \sqrt{2}X^{Q3}\Pi_h^{R1}\Pi_g^{R2} - \\
&\qquad \Pi_g^{R1}(\Pi_g^{Q1} + \Pi_h^{Q2}) - 2\Pi_h^{R1}\Pi_g^{Q3} - \Pi_g^{R2}(\Pi_g^{Q2} + \Pi_h^{Q3}) - 2\Pi_h^{R2}\Pi_h^{Q1}\Big), \\
L_1 &= \frac{\alpha}{\sqrt{2}}\left(\Pi_g^{R1}O^{(12)} + \sigma_{hg}^{R1}E^{(12)}\right), \\
L_2 &= \frac{\alpha}{\sqrt{2}}\left(-\sigma_{gh}^{R1}O^{(12)} - \Pi_h^{R1}E^{(12)}\right), \\
L_3 &= \frac{\alpha}{\sqrt{2}}\left(\Pi_g^{R2}O^{(32)} + \sigma_{hg}^{R2}E^{(32)}\right), \\
L_4 &= \frac{\alpha}{\sqrt{2}}\left(-\sigma_{gh}^{R2}O^{(32)} - \Pi_h^{R2}E^{(32)}\right), \\
L_5 &= \sqrt{\Gamma}X^{Q1}, \quad L_6 = \sqrt{\Gamma}X^{Q2}, \quad L_7 = \sqrt{\Gamma}X^{Q3}.
\end{aligned} \tag{4.37}$$

As in the derivations carried out above, to form the master equation for the corresponding 3-qubit phase-flip network, we simply make the substitutions $X^{Qi} \leftrightarrow Z^{Qi}$ and $2\Pi_{\substack{h\\g}}^{Qi} \rightarrow I \pm X^{Qi}$. The coupling terms and the Hamiltonian terms in this master equation transparently correspond to the probe and feedback components of the photonic network– the coupling terms L_1 and L_2 measure the joint parity of Q1 and Q2 and modify the state of $R1$ accordingly, and L_3 and L_4 measure the joint parity of Q3 and Q2, driving the state of $R2$. Depending on the state of the relays, the Hamiltonian terms then correspond to the Raman interaction which mediates corrective feedback. The remaining terms in the Hamiltonian correspond to AC Stark shifts which are a consequence of the Raman interaction mechanism (see Appendix A for additional discussion).

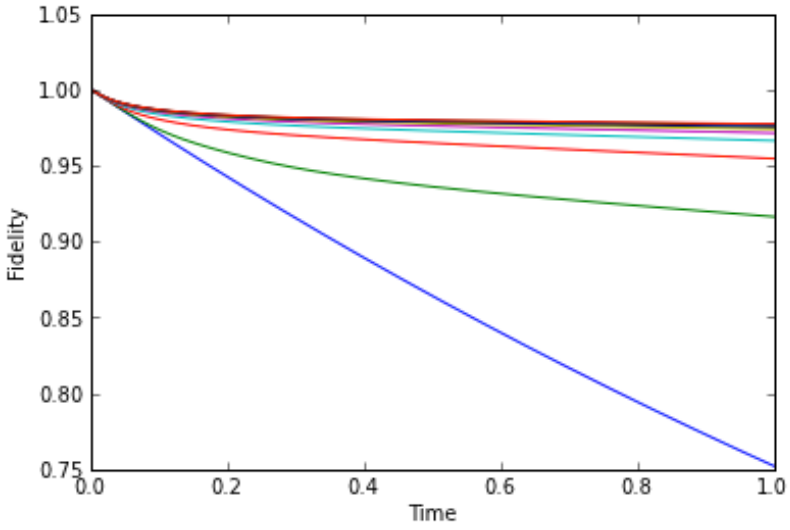

Figure 4.5: Decay of fidelity $\langle\Psi_0|\rho_t|\Psi_0\rangle$ for 3-qubit bit-flip code with varying values for the feedback strength $\Omega = \frac{|\beta|^2\gamma}{2\Delta}$ taking values in the range 0 to 200 in increments of 10. The probe strength is set to $\alpha = \frac{\Omega}{8}$.

Fig. 4.5 shows the performance of the photonic network in the bit-flip configuration, quantified by numerical integration of the above mater equation.

4.3 QHDL paradigm for photonic design automation

The coherent feedback circuit for the bit-flip code that I have just described demonstrates a powerful set of principles: a fully autonomous quantum memory in which both the register and the controller qubits are described by quantum mechanical equations of motion; an application of the adiabatic elimination theory of Bouten, van Handel, and Silberfarb [10] (see also Section 2.5), which results in a substantial reduction in the complexity of the resulting model; and finally, a proof-of-principle application of the Gough-James circuit algebra for modeling quantum networks.

More broadly, the work I have described thus far in this chapter can be situated in the context of a range of current research projects in photonics and quantum electronics which are devoted to the development of transducers, logic gates, and related components based on quantum-mechanical device physics [31, 51]. And as I have argued, in order to realize the long-term vision of advanced technology based on complex networks of interconnected quantum devices, equal attention will need to be paid to developing the quantum theory of autonomous (embedded) photonic, optomechanical and optoelectronic circuits [65]. This should be true not only for the most ambitious paradigm of true quantum computing and communication, but also for engineering approaches that seek to leverage coherent photonic, electronic or spintronic resources for quantitative improvements in the speed and/or energy efficiency of classical sensing [67], information processing [47] and communication [28].

Regardless of the chosen implementation paradigm or domain of application, one foreseeable future bottleneck is to construct time-domain Heisenberg equations of motion for circuits of arbitrary complexity. The quantum memory model that I have described in the preceding sections suggests that the Gough-James circuit algebra can in principle be used for exactly this purpose. However, in examining the calculations presented above, it is quite clear that there is a limit to what one can compute by hand. Despite the strictly algorithmic nature of the series and concatenation product based calculations, there quickly becomes an explosion in the complexity of the equations themselves as we add more components to a network.

At this point, there is a natural analogy to draw between the synthesis of quantum networks and standard workflows for circuit design in the engineering world. Anyone who has taken an elementary course in electricity and magnetism or laboratory electronics, is familiar with the basic equations that describe the operation of resistors, capacitors, and inductors, or the "golden rules" for operational amplifiers. And although one can work out the behavior of simple circuits using these rules, for significantly larger networks, software systems are generally used in what is called "electronic design automation" or EDA. With the Gough-James circuit algebra, we

can imagine an analogous role for what we might call "photonic design automation," in other words, a system in which quantum networks are constructed at the schematic level, and in which the underlying equations of motion are computed in an automated fashion via algorithmic implementation of the synthesis rules for QSDE's.

In traditional electrical engineering, the port connection topology of a collection of components is usually called a netlist. Several widely-used conventions exist for text-based specification of the netlist of a circuit according to some formal grammar. For example, VHSIC Hardware Description Language (VHDL) [54] and Verliog [66] are formats intended mainly for use in digital electronics, while Modelica [17] is a more recent format designed to accommodate multiple physical domains. Any of these text-based netlist formats can be used to specify the port connection topology of a photonic, optomechanical or optoelectronic circuit, with the practical advantage that such formats can be generated and read by graphical-user-interface circuit design software such as `gschem` or OpenModelica. It is natural to consider the task of computer-automated 'parsing' of a text-based netlist specification to produce a Gough-James circuit expression, which can then be reduced algebraically to a time-domain model for the quantum stochastic circuit dynamics. We have previously demonstrated in our research group [65] such a schematic capture workflow, based on VHDL, for the construction of quantum circuit models. In this section, I give a brief overview of the QHDL workflow, and then move on to consider the *transformation* of quantum photonic circuit models as a fundamental methodology for verification and robustness analysis, working with Modelica rather than VHDL as a netlist specification format because of its simplified grammar and its integration with *Mathematica* [70], which will be used as a computational engine for symbolic manipulation.

An outline of our current circuit analysis approach is presented in Fig. 4.6. An initial netlist description of the circuit is produced using schematic capture or coded by hand; an important goal for future work in this field will be the algorithmic synthesis of circuit topologies implementing a desired function. Some circuit transformations

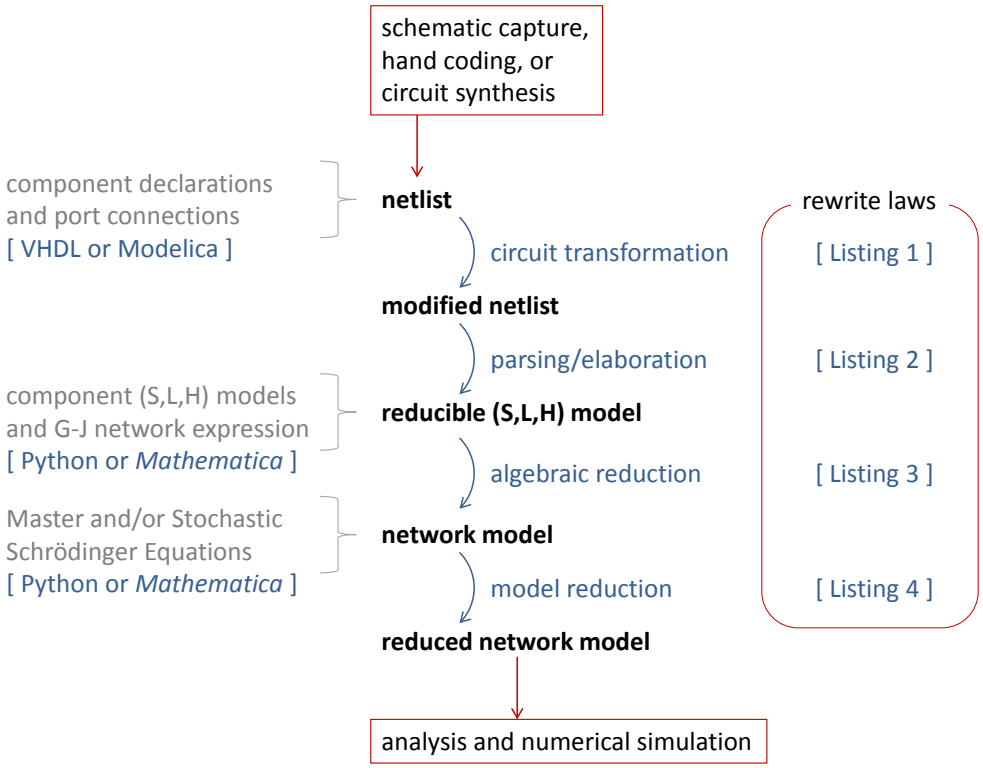

Figure 4.6: Quantum photonic circuit analysis workflow, viewed as a series of transformations of a circuit model. While some rewrites are most naturally applied at the level of the netlist term algebra, others must be done in the algebra of Hilbert-space operators. The Gough-James algebra provides a natural intermediate representation of the circuit model. Listings 1-4 can be found in the Supplementary Data for [56].

will most naturally be applied at the netlist level of description—below I will consider the addition of optical propagation losses as an example. The initial or modified netlist can then be rewritten into the Gough-James algebra of series and concatenation products of (S, L, H) component models, and the Gough-James circuit model can in turn be reduced to an overall (S, L, H) model for the entire circuit. Further transformations of the circuit model, such as adiabatic elimination of fast dynamics, are then implemented via manipulations of the Hilbert-space operators appearing in the circuit scattering matrix, coupling vector and Hamiltonian. Final equations of motion can then be extracted for symbolic analysis and/or numerical simulation.

4.3.1 Circuit model transformations via term-rewriting

It is interesting to note that all the above circuit model transformations can be regarded as applications of compact sets of rewrite laws in a term rewriting system (TRS) [68]. As noted above, we have chosen to implement such rewrite laws within *Mathematica*. The study of TRSs provides a common framework for abstract algebra, the theory of computation, and formal verification methods and is an active area of research in contemporary engineering. As it appears that photonic circuit models of the type we consider here can be treated on equal footing, it seems reasonable to hope that sophisticated TRS-based tools being developed for classical synthesis and verification [48] could be adapted for use in quantum engineering as well.

An elementary question to ask about these quantum memory circuits is how their performance would be degraded by propagation losses in the waveguides. While it is straightforward in principle to perform this type of robustness analysis via numerical simulation of modified quantum circuit models, the complexity of even the ideal (lossless) models is such that adding loss terms by hand would be prohibitively tedious. In order to obtain a valid quantum optical model for the circuit with propagation losses, each port-to-port connection in the lossless model should be replaced by a compound connection in which the original upstream port is connected to one input port of a beam-splitter and the corresponding beam-splitter output port is then connected to the original downstream port. The reflection coefficient of the beam-splitter sets the effective propagation loss of the connection, and each such addition of an unconnected output port (corresponding to the beam-splitter reflection) to the circuit model increases the number of Lindblad terms in the overall Master Equation.

In order to illustrate how this type of transformation can be performed automatically in our circuit analysis workflow, we first display a segment of Modelica code specifying the netlist for a simple sub-circuit that implements a continuous two-qubit parity

measurement [34]:

```
model TwoQubitParity
  Photonics.Components.CoherentField W(Amplitude=alpha);
  Photonics.Components.SingleCavity Q1(CavityType=Zprobe, HilbertSpace=Q1);
  Photonics.Components.SingleCavity Q2(CavityType=Zprobe, HilbertSpace=Q2);
equation
  connect(W.output1,Q1.input1);
  connect(Q1.output1,Q2.input1);
end TwoQubitParity;
```

The code specifying the `TwoQubitParity` sub-circuit begins with a set of declarations (the three lines prior to the **`equation`** keyword) of the three components it contains: a coherent field input `W` and qubit-cavity components `Q1` and `Q2`. The two lines after the **`equation`** keyword specify the architecture via simple statements of which output ports are connected to which input ports. In order to insert a propagation loss between `Q1` and `Q2`, it suffices simply to rewrite the netlist specification by adding the line `Photonics.Components.Loss L(LossParam=theta);` to the declaration block and substituting the line `connect(Q1.output,Q2.input1);` in the architecture block with the lines `connect(Q1.output1,L.input1);` and `connect(L.output1,Q2.input1);`. Clearly, such manipulations of the netlist specification code can be implemented straightforwardly using pattern matching and string replacement. We provide example *Mathematica* code for this purpose in Listing 1 of the Supplementary Data for reference [56].

A larger-scale example of the propagation loss transformation is depicted in Fig. 4.7. The upper panel presents a screen capture (from the Modelica system designer) of a graphical representation of half the photonic circuit for an autonomous quantum memory based on the bit-flip/phase-flip code, without propagation losses (see also Figure 4.4). The lower panel shows the same sub-circuit after a transformation inserting beam-splitters into every port connection to enable rigorous modeling of propagation losses. It should be emphasized that although this type of loss-insertion transformation is quite simply accomplished via rewriting of the netlist specification, it would be far more complicated to implement at the subsequent levels of model representation

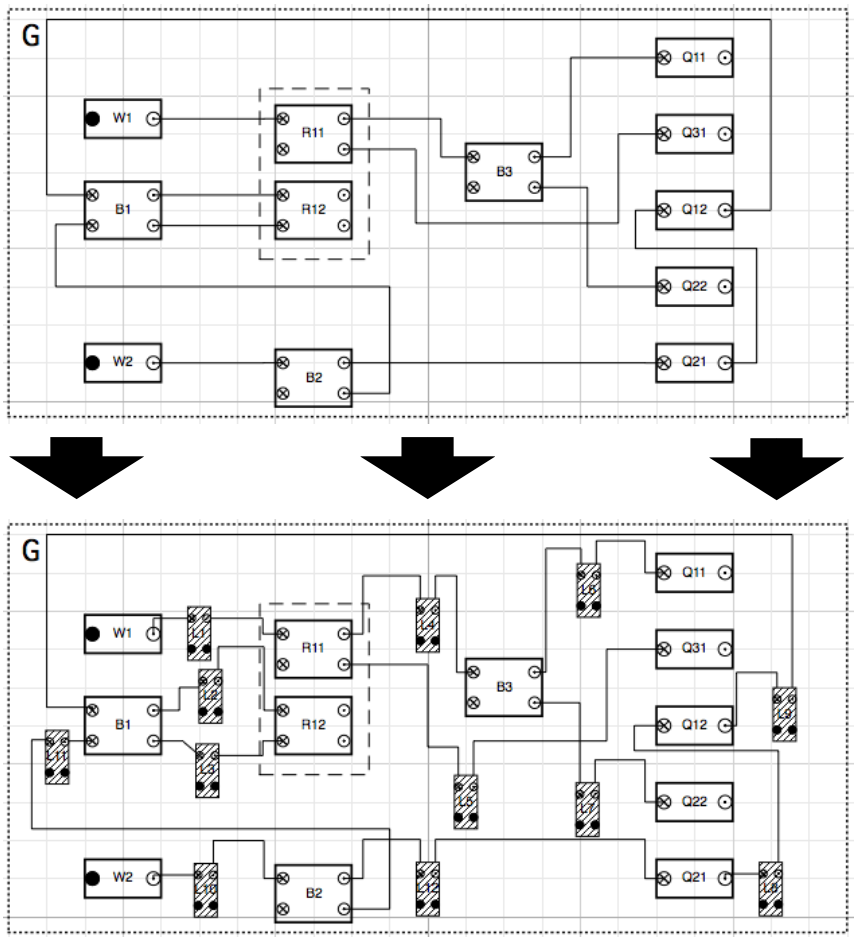

Figure 4.7: TOP: Screen capture from the Modelica system designer of a graphical representation of half the photonic circuit for a quantum memory based on the bit-flip/phase-flip code. This diagram is analogous to the schematic in Appendix C of [35] and also Figure 4.4. BOTTOM: Corresponding circuit representation including propagation losses.

as a Gough-James circuit expression or overall (S, L, H) triple.

Proceeding to the next stage of the circuit analysis workflow, we utilize a *Mathematica* script to rewrite the final connectivity model from the netlist term algebra to the Gough-James algebra. Terms in the Gough-James algebra are constructed from constants representing the components, and operators indicating the connections among components. Infix notation is used with parentheses for clarity. The elementary operators for connecting components are the series product (denoted $\lhd$), with $B \lhd A$ indicating that all output ports of component A are connected to corresponding input ports of component B, and the concatenation product (denoted $\boxplus$), with $D \boxplus C$ indicating that components D and C coexist in the circuit but have no connections. The result of a series or concatenation product can be treated as a new component. The input/output ports of $B \lhd A$ are the input ports of A and the output ports of B; $D \boxplus C$ has the input and output ports of both C and D. In practice it is useful to add a permutation (crossover) operator that reorders the output ports of a component, as well as a feedback operator $[M]_{i \to j}$ that connects output port i of a component M to its own input port j. It is generally also necessary to utilize ancillary n-line 'pass-through' components I_n to construct a complete circuit expression. For example, if A has two output ports and B has four input ports, a connection of the outputs of A to the first two inputs of B without any other connections would be written $B \lhd (A \boxplus I_2)$.

The minimal task in this stage of the analysis is thus to replace the list of port-to-port connections in the Modelica architecture block with component-to-component connections, inserting ancillary pass-through or permutation blocks as necessary. This is not a one-to-one mapping—many distinct Gough-James circuit expressions can faithfully represent a given netlist. All such expressions are equivalent in that the application of algebraic reduction rules (see below) will bring any such equivalent circuit expression to a unique normal form, the overall (S, L, H) triple for the circuit. It is useful however to consider strategies for obtaining relatively compact Gough-James circuit expressions, for ease of inspection and also to minimize the complexity of the subsequent algebraic reduction. The algorithm we use is based on the idea

of trying to group together components that are the most connected [1]. For example, if two 2-port components are connected by `connect(A.output1,B.input1);` and `connect(A.output2,B.input2);` we can bring them cleanly into the Gough-James circuit expression as $(B \triangleleft A)$. The algorithm assigns a score to each pair of connected components according to how fully connected the two circuit elements are. The higher the score, the more certain the algorithm is that grouping the two elements together will lead to a compact circuit expression. The parsing algorithm then finds the highest-scoring connector joining the two elements, replacing them with either a series or feedback product (padding with pass-through components as necessary), and repeating the process over and over until we have accounted for all of the netlist connections in a single Gough-James expression (using $\boxplus$ to join together any disconnected sub-nets).

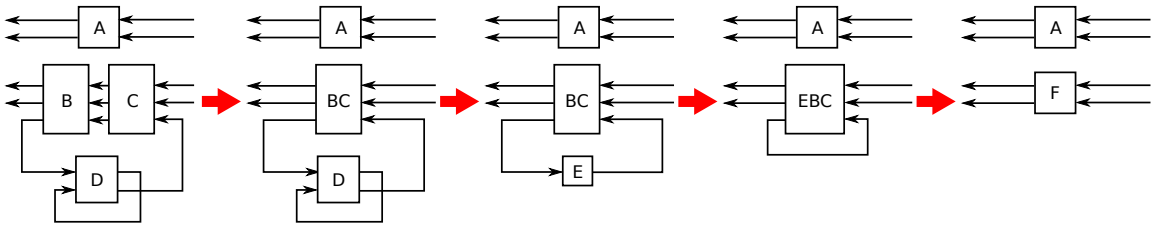

Figure 4.8: Steps the circuit parser takes to convert a simple netlist into a Gough-James circuit expression.

As an example, consider the circuit diagram at the left of Fig. 4.8. In the first step, the parser replaces B and C with $BC = B \triangleleft C$ (the pair has a 'score' of 1.0 because all of the C outputs match inputs in B). The remaining steps are analogous:

Step	Replacement	Score
1	$BC = B \triangleleft C$	1.00
2	$E = [D]_{1\to 2}$	1.00
3	$EBC = (I_2 \boxplus E) \triangleleft BC$	0.33
4	$F = [EBC]_{3\to 3}$	1.00

[1] I wanted to acknowledge Ryan Hamerly for devising and implementing this incredibly clever algorithm

The final circuit expression, $A \boxplus F$, can be read off from the substitutions in the table above. It is:

$$A \boxplus \left[(I_2 \boxplus [D]_{1\to 2}) \lhd B \lhd C \right]_{3\to 3} \tag{4.38}$$

Mathematica code for implementing this algorithm is included in Listing 2 of the Supplementary Data of [56].

Algebraic reduction of a Gough-James circuit expression is performed by applying normal quantum-mechanical operator algebra plus the following rewrite rules [26]:

$$B \lhd A \;\rightarrow\; \left(S_B S_A, L_B + S_B L_A, H_B + H_A + \mathrm{Im}\{L_B^\dagger S_B L_A\} \right), \tag{4.39}$$

$$B \boxplus A \;\rightarrow\; (S_B \oplus S_A, L_B \oplus L_A, H_B + H_A)\,. \tag{4.40}$$

Here $\oplus$ denotes the usual direct sum of matrices or vectors. An analogous rule for the feedback operation $[A]_{i\to j}$ is described in [65]. Here (S_B, L_B, H_B) is the parameter triple for component B and (S_A, L_A, H_A) is the triple for component A. We assume that the software can obtain component parameter triples in symbolic form from a library. We include a *Mathematica* script that implements the above rewrite rules in Listing 3 of the Supplementary Data in reference [56]. When these rules have been applied to completion, the original Gough-James expression is replaced by a single (S, L, H) triplet that represents the entire circuit. In general the circuit (S, L, H) expression can be rather unwieldy and may not be amenable to intuitive interpretation—its parameters summarize the coupled quantum dynamics of all the components in the circuit in a way that makes it straightforward to extract overall evolution equations for numerical simulation, but analytic verification of the circuit behavior will generally require further model reduction steps.

We are now in a position to elaborate on an earlier comment regarding the advantage of considering circuit model transformations very early in the analysis workflow. The top-left and top-center diagrams in Fig. 4.9 depict a simple beamsplitter and a compound beamsplitter that can be formed by a Mach-Zehnder type connection topology [65]. The corresponding Gough-James expressions and scattering matrices

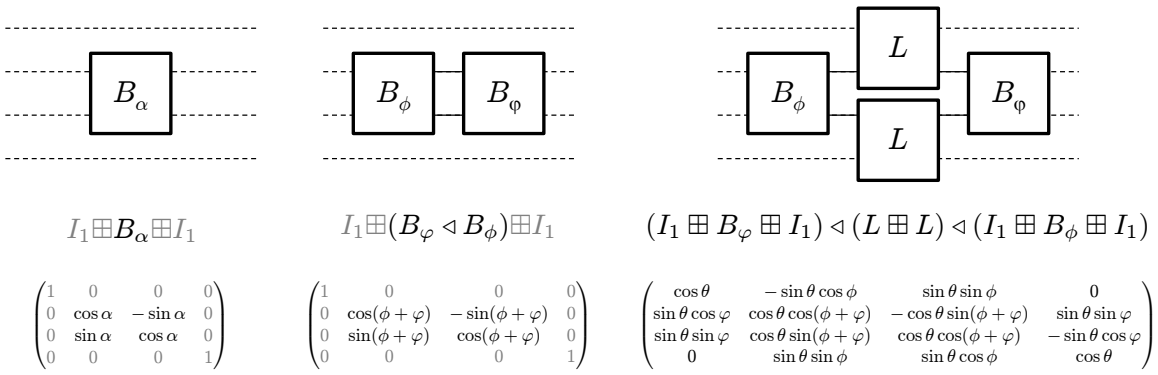

Figure 4.9: Example of equivalent circuit (S, L, H) models (left and center columns) corresponding to distinct netlists that transform differently under addition of propagation losses. The top row shows circuit diagrams, the middle row shows the corresponding Gough-James expressions, and the bottom row shows the overall scattering matrices S for each circuit.

(which are the only non-zero components of the (S, L, H) triples for such simple circuits) are shown in the middle and bottom rows of Fig. 4.9. If $\phi + \varphi = \alpha$ the simple and compound beam-splitters are equivalent photonic circuits (in the instantaneous-coupling limit, without propagation losses). The single beamsplitter circuit does not change under a transformation rule that adds losses to internal port-to-port connections only, while the compound beamsplitter circuit is transformed to the circuit described in the right column of Fig. 4.9. Here θ is a loss parameter and $L = B_\theta$; note that we recover the lossless scattering matrix as $\theta \to 0$. This example clearly illustrates that some information about internal port-to-port connections is lost by the time the circuit model has been reduced to an overall (S, L, H) parameter triple, implying that some important types of circuit transformations (such as the addition of propagation losses) cannot be implemented directly on the final (S, L, H) model but rather must be implemented at an earlier stage of the rewrite chain.

Once an overall circuit (S, L, H) model has been obtained, a final class of transformations (which could not have been performed at the netlist or Gough-James levels of representation) may be applied via rewrites in the operator algebra. For example,

our analyses of the quantum memory circuits proposed in [35, 36] have relied on a limit theorem for QSDEs [27, 10] (see also Section 2.5) to produce reduced models for the overall network that are amenable to behavior verification and tractable for numerical simulation. Practically, application of the limit theorem requires that certain operator products be computed which correspond to the coefficients of a limit QSDE for the slow degrees of freedom in an open quantum system (see Section 2.2 of [10] for general results and [35] for specific application to our QEC circuit models). Once the limiting subspace has been defined and the corresponding structural requirements have been verified, computation of the limit QSDE requires a straightforward but potentially cumbersome series of algebraic manipulations that can easily be automated using pattern matching and string replacement; a sample *Mathematica* script for this purpose is provided in Listing 4 of the Supplementary Data of reference [56].

M_{12}	M_{23}	X_1	X_2	X_3
0	0	0	0	0
1	0	1	0	0
0	1	0	0	1
1	1	0	1	0

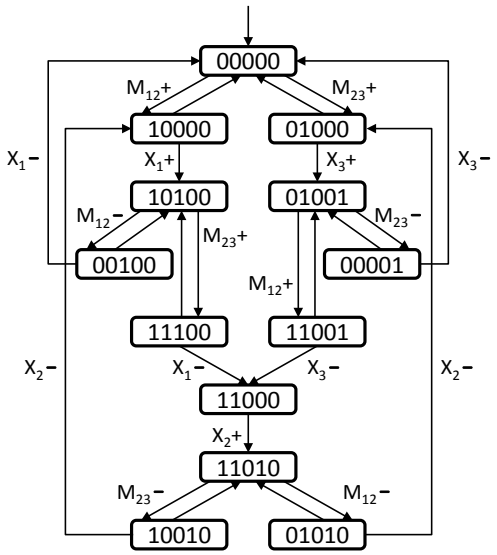

Figure 4.10: LEFT: Table of possible input/syndrome signal values (M_{12}, M_{23}) and desired output/correction (X_1, X_2, X_3) signal values for the desired bit-flip QEC controller [35]. RIGHT: Asynchronous Transition System [71, 13] specifying the desired controller behavior.

The left table of Fig. 4.10 shows the well-known control scheme for the bit-flip QEC protocol. Here M_{ij} is a measurement signal taking values in $\{0, 1\}$ that indicates the

presence of an odd parity condition between qubits i and j in the quantum register. For the three-qubit bit-flip code, two such syndrome measurements are sufficient to localize an error. Whereas M_{12} and M_{23} are input signals to the controller, we use X_1, X_2 and X_3 to indicate the values of controller output signals that drive corrective bit-flip actions on qubits 1,, 2 and 3, respectively. Each row of the table indicates the required configuration of the controller output signals X_k when the input signals are as indicated in the first two columns. The diagram on the right side of Fig. 4.10 presents a Transition System (TS) [71, 13] as a full (asynchronous) specification of the desired behavior of the controller. In the TS diagram, which has the form of a graph with labeled directed edges, each node represents a state of the controller, the directed edges indicate possible transitions between states, and the label on any given edge indicates a corresponding signal transition. The binary string specifying each controller state corresponds to the values of the signals M_{12}, M_{23}, X_1, X_2 and X_3 in order. The state and transition labels are thus redundant and the latter have been omitted in a few places to avoid cluttering the diagram.

After transformation via the QSDE limit theorem mentioned above, the (S, L, H) model (without propagation losses) for our bit-flip QEC circuit [35] contains the following Lindblad operators and Hamiltonian terms pertaining to the behavior of the controller:

$$
\begin{aligned}
L_{s1} &= \alpha\left(\sigma_+^{R1} M_{12} - \Pi_0^{R1}(1 - M_{12})\right), && (4.41)\\
L_{r1} &= \alpha\left(-\Pi_1^{R1} M_{12} + \sigma_-^{R1}(1 - M_{12})\right), && (4.42)\\
L_{s2} &= \alpha\left(\sigma_+^{R2} M_{23} - \Pi_0^{R2}(1 - M_{23})\right), && (4.43)\\
L_{r2} &= \alpha\left(-\Pi_1^{R2} M_{23} + \sigma_-^{R2}(1 - M_{23})\right), && (4.44)\\
H_c &= \Omega\left(\sqrt{2} X^{Q1} \Pi_1^{R1} \Pi_0^{R2} + X^{Q2} \Pi_1^{R1} \Pi_1^{R2} - \sqrt{2} X^{Q3} \Pi_0^{R1} \Pi_1^{R2}\right). && (4.45)
\end{aligned}
$$

Here $|\alpha|^2$ represents the strength (photons per unit time) of a probe optical field used to monitor the syndromes of the quantum register and Ω is a parameter for the feedback strength [35]. Our QEC controller circuit utilizes a pair of set-reset relay components [45] R_1 and R_2 driven by the syndrome inputs M_{12} and M_{23} to

switch the output signals X_1, X_2 and X_3. In the above expressions Π_m^{Rn} denotes a projection operator into state m for R_n, $\sigma_{+(-)}^{Rn}$ is a raising (lowering) operator for R_n, and X^{Qn} is a Pauli σ_x operator for register qubit n. The Lindblad terms above implement the responses of the relay states to the syndrome inputs. For example, in a Master Equation or Stochastic Schrödinger Equation for the QEC circuit, L_{s1} and L_{r1} will contribute dynamical terms that cause R_1 to decay exponentially (with rate $|\alpha|^2$) to state 0 when $M_{12} = 0$ and to state 1 when $M_{12} = 1$. The remaining Lindblad terms will do the same for R_2 and M_{23}. The three terms in the control Hamiltonian H_c implement corrective feedback on the register qubits whenever the states of the relays are not both 0, following precisely the scheme given in the table of Fig. 4.10. We thus see that the behavior of our bit-flip QEC circuit can be verified by inspection relative to a conventional asynchronous controller specification such as the TS diagram of Fig. 4.10. We wish to emphasize, however, that this type of transparent correspondence between the (S, L, H) terms and desired TS behavior emerges only after the QSDE limit transformation in the analysis of our QEC circuits.

4.3.2 Performance of 3-qubit/9-qubit codes with losses

If the analysis workflow is repeated for our QEC circuit models with a propagation-loss transformation inserted at the netlist level, new Lindblad operators are generated such as

$$L_{pl} = \alpha\theta Z^{Q2}, \tag{4.46}$$

for the bit-flip case, and

$$L_{pl} = \alpha\theta Z^{Q2} Z^{Q5} Z^{Q8}, \tag{4.47}$$

for the nine-qubit code. Here θ is a propagation loss parameter and Z^{Qj} is the Pauli σ_z operator for qubit j in the quantum register. In both cases we see that nonzero optical propagation loss causes the appearance of new error processes that are not corrected by the original QEC code—a phase error in the bit-flip circuit, and a three-qubit correlated phase error in the nine-qubit circuit. This is of course not a pathology of our photonic QEC implementation, but rather an intrinsic property of the codes

used—analogous error terms arise in a conventional approach as a consequence of ancilla decoherence while syndrome observables are being accumulated by a sequence of two-qubit gates. Additional loss-induced modifications of the QEC circuit dynamics are computed automatically by the model rewriting workflow.

To assess the quantitative impact of propagation losses we can numerically integrate the Master Equation corresponding to the (reduced) circuit (S, L, H) [65]. As shown in Fig. 4.11 and Fig. 4.12, the fidelity of the encoded qubit decays more rapidly as the propagation loss parameter θ is increased. For simplicity, we here have assigned the same loss parameter to each port-to-port connection in the initial netlist. We wish to emphasize that this level of quantitative analysis for the nine-qubit code would be practically intractable without the automated circuit analysis workflow that we have outlined in this section– the unsimplified lossy Hamiltonian contains thousands of terms. An excerpt of the netlist and corresponding Gough-James circuit expression are included in the Supplementary Data for [56], together with the coupling vector and Hamiltonian operator from the overall circuit (S, L, H) for the reduced model.

To conclude this section, we have described a model transformation workflow for analyzing complex quantum photonic circuits and have illustrated key concepts using examples related to prior work on autonomous quantum error correction. Code listings are provided in the Supplementary Data for reference [56] to demonstrate how the model transformations can be implemented via compact sets of rewrite rules. A practical approach to analyzing the functional robustness of a photonic circuit to propagation losses in its internal waveguide connections has been presented with numerical results for bit-flip and nine-qubit QEC models. And finally, we have introduced the possibility of formal verification via (S, L, H) analysis of quantum photonic circuit behavior relative to conventional (in contemporary electrical engineering) specification formats for asynchronous controllers.

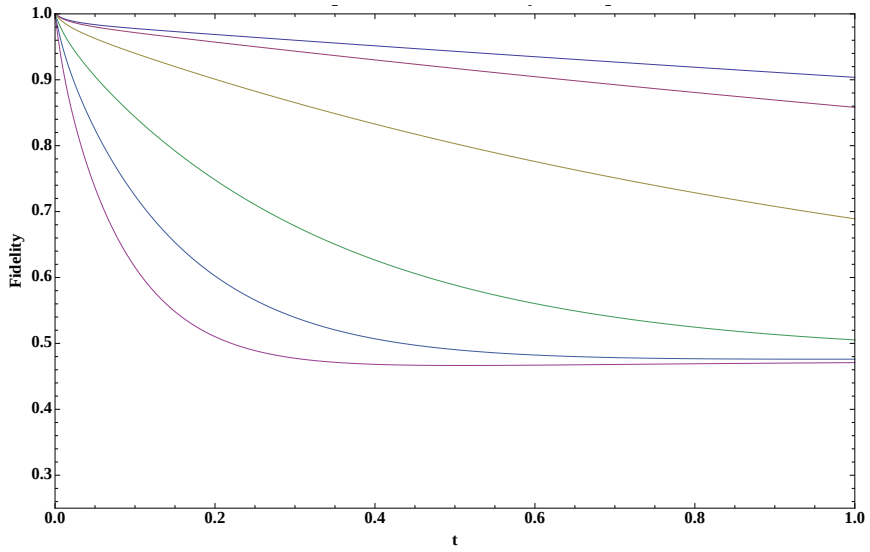

Figure 4.11: Decay of fidelity $\langle\Psi_0|\rho_t|\Psi_0\rangle$ for 3-qubit bit-flip code with loss parameters $\theta = \{0, 1, 2.5, 5, 7.5, 10\}\pi/1000$ (top to bottom curves) for a bit-flip QEC circuit. For consistency with [35], the feedback strength $\Omega = \frac{|\beta|^2\gamma}{2\Delta}$ is set to a constant value of 210.

4.4 Robustness of autonomous quantum memories

In the previous sections, I have shown how the the Gough-James quantum network algebra [25, 26, 27] can be utilized together with a recent limit theorem for quantum stochastic differential equations (QSDEs) [10] to facilitate the derivation of an intuitive master equation for a given quantum memory model from an explicit construction of the underlying nanophotonic circuit, in a manner inspired by schematic capture methods of contemporary electrical engineering [56, 65] (see the previous section 4.3). In this section, in order to focus on higher architectural principles, I will skip over such details and jump directly to considering a class of master equations that arises from the general approach of embedding continuous-time relaxations of stabilizer quantum error correcting codes in the autonomous dynamics of a coherent feedback network.

As in the previous examples, we model an autonomous quantum memory using a

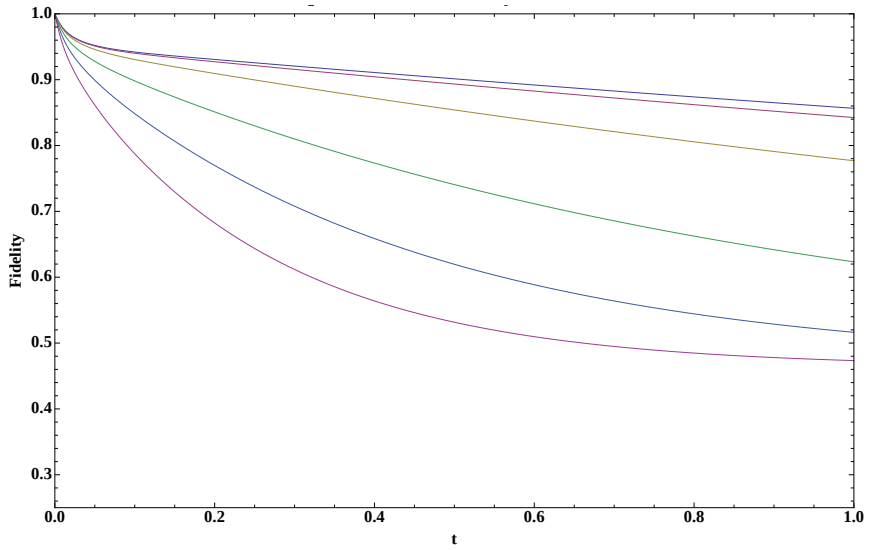

Figure 4.12: Decay of fidelity $\langle\Psi_0|\rho_t|\Psi_0\rangle$ for 9-qubit Bacon-Shor code with loss parameters $\theta = \{0, 1, 2.5, 5, 7.5, 10\}\pi/1000$ (top to bottom curves) for a nine-qubit QEC circuit. For consistency with [36], the feedback strength $\Omega = \frac{|\beta|^2\gamma}{2\Delta}$ is set to a constant value of 200 for each of these runs.

Markovian master equation [21],

$$\dot{\rho} = -i[H, \rho] + \sum_i \left\{ L_i \rho L_i^\dagger - \frac{1}{2} L_i^\dagger L_i \rho - \frac{1}{2} \rho L_i^\dagger L_i \right\}, \tag{4.48}$$

where H is a Hamiltonian for the internal dynamics of the memory and controller qubits, and the Lindblad operators L_i describe couplings to reservoir modes that mediate decoherence (including memory errors) and entropy removal (via spontaneous emission-type processes). At this level of description, the dynamics of the electromagnetic field modes within the waveguides and resonators of the photonic circuit have been adiabatically eliminated (Section 4.1). Here in considering arbitrary stabilizer codes we assume that the register qubit model described in 4.2.2 [34] can be generalized to incorporate atomic level structures whose Raman resonance conditions effectively implement an **AND** operation on as many feedback signals as the code requires. We assume a feedback controller construction based on nanophotonic relays [45] as in prior work.

4.4.1 Canonical master equation for stabilizer codes

Consider a stabilizer quantum error correcting code [22, 50] that encodes one qubit of information in Q register qubits with N stabilizer generators. We refer to the complete set of stabilizer generators as $\mathcal{S} = \{M_n\}_{n=1}^{N}$. Recall that a stabilizer code redundantly encodes information in the joint state of the register qubits, that each stabilizer generator is a joint observable of the register qubits with eigenvalues ± 1, and that a measurement of the full set of stabilizer generators values (the error *syndrome*) suffices to localize any correctable error but yields no information on the encoded qubit. To explicitly construct the master equation for an autonomous quantum memory based on $\mathcal{S}$ we use the following procedure. For each stabilizer generator M_n include two Lindblad operators of the form

$$L_{2n-1} = \alpha \left(\sigma_{+}^{R_n} (I + M_n) - \Pi_{g}^{R_n} (I - M_n) \right), \tag{4.49}$$

$$L_{2n} = \alpha \left(\sigma_{-}^{R_n} (I - M_n) + \Pi_{h}^{R_n} (I + M_n) \right), \tag{4.50}$$

where $\sigma_{\pm}^{R_n}$, $\Pi_{g}^{R_n}$ and $\Pi_{h}^{R_n}$ are (qubit-like) raising/lowering operators and projectors onto g and h basis states for the n^{th} relay of the feedback controller, and α parameterizes the amplitudes of the electromagnetic probe fields, which in turn determines the syndrome measurement rate. If the code is *separable*, in the sense that disjoint sets of stabilizer generators mediate X and Z error syndrome extraction, the quantum memory Hamiltonian can be written in the form

$$H = \sum_{n=1}^{Q} \Omega \left(X_n \cdot \mathcal{F}_{\mathcal{S}_X} [X_n] + Z_n \cdot \mathcal{F}_{\mathcal{S}_Z} [Z_n] \right). \tag{4.51}$$

If the code is not separable then

$$H = \sum_{n=1}^{Q} \Omega \left(X_n \cdot \mathcal{F}_{\mathcal{S}} [X_n] + Y_n \cdot \mathcal{F}_{\mathcal{S}} [Y_n] + Z_n \cdot \mathcal{F}_{\mathcal{S}} [Z_n] \right), \tag{4.52}$$

where the function $\mathcal{F}_{\mathcal{S}} [E_n]$ maps a single-qubit error to a projector onto a state of the controller relays. The action of $\mathcal{F}$ straightforwardly represents the lookup table

of correctable errors and corresponding syndromes. For example, suppose there are six stabilizer generators and that they take the values 1 -1 -1 1 -1 1 for a register state with a bit-flip error on the fourth qubit. Then $\mathcal{F}_{\mathcal{S}}\left[X_4\right] = \Pi_h^{R_1}\Pi_g^{R_2}\Pi_g^{R_3}\Pi_h^{R_4}\Pi_g^{R_5}\Pi_h^{R_6}$ (the h state of relay n is associated with the $+1$ value of M_n, and the g state with value -1). When the code is separable, we use $\mathcal{S}_X$ and $\mathcal{S}_Z$ to denote disjoint subsets of $\mathcal{S}$. In both of the above Hamiltonian expressions, Ω parameterizes the strength of the feedback fields.

4.4.2 Master equation for 7-qubit code

To illustrate our construction we first consider the seven-qubit code [22, 50], which is separable. The following lookup table gives the corresponding error syndromes for single-qubit X, Z, and Y errors with ■ corresponding to a $+1$ value for a given stabilizer generator and ◯ to -1:

Error syndromes for 7-qubit code

Error	M1	M2	M3	M4	M5	M6
X1	■	■	■	○	○	○
X2	■	■	■	○	○	■
X3	■	■	■	○	■	○
X4	■	■	■	○	■	■
X5	■	■	■	■	○	○
X6	■	■	■	■	○	■
X7	■	■	■	■	■	○
Z1	○	○	○	■	■	■
Z2	○	○	■	■	■	■
Z3	○	■	○	■	■	■
Z4	○	■	■	■	■	■
Z5	■	○	○	■	■	■
Z6	■	○	■	■	■	■
Z7	■	■	○	■	■	■
Y1	○	○	○	○	○	○
Y2	○	○	■	○	○	■
Y3	○	■	○	○	■	○
Y4	○	■	■	○	■	■
Y5	■	○	○	■	○	○
Y6	■	○	■	■	○	■
Y7	■	■	○	■	■	○

It is easily seen that the error syndrome for Y_n is simply the logical **OR** of the syndromes for X_n and Z_n, which combined with the algebraic relation $Y_n \propto X_n Z_n$ makes it possible to design a feedback network that independently detects and corrects X and Z errors—when a Y_n error occurs it can be diagnosed and treated as the occurrence of both an X_n and a Z_n error.

Applying the construction described above for the separable case, we arrive at the following master equation for a coherent feedback implementation of the seven-qubit

code:

$$\begin{aligned} H = \ \Omega\Big(& X_1\Pi_g^{R_4}\Pi_g^{R_5}\Pi_g^{R_6} + X_2\Pi_g^{R_4}\Pi_g^{R_5}\Pi_h^{R_6} + X_3\Pi_g^{R_4}\Pi_h^{R_5}\Pi_g^{R_6} + \\ & X_4\Pi_g^{R_4}\Pi_h^{R_5}\Pi_h^{R_6} + X_5\Pi_h^{R_4}\Pi_g^{R_5}\Pi_g^{R_6} + X_6\Pi_h^{R_4}\Pi_g^{R_5}\Pi_h^{R_6} + \\ & X_7\Pi_h^{R_4}\Pi_h^{R_5}\Pi_g^{R_6} + Z_1\Pi_g^{R_1}\Pi_g^{R_2}\Pi_g^{R_3} + Z_2\Pi_g^{R_1}\Pi_g^{R_2}\Pi_h^{R_3} + \\ & Z_3\Pi_g^{R_1}\Pi_h^{R_2}\Pi_g^{R_3} + Z_4\Pi_g^{R_1}\Pi_h^{R_2}\Pi_h^{R_3} + Z_5\Pi_h^{R_1}\Pi_g^{R_2}\Pi_g^{R_3} + \\ & Z_6\Pi_h^{R_1}\Pi_g^{R_2}\Pi_h^{R_3} + Z_7\Pi_h^{R_1}\Pi_h^{R_2}\Pi_g^{R_3}\Big), \end{aligned} \tag{4.53}$$

$$\begin{aligned} L_1 &= \alpha\left(\sigma_+^{R_1}(I + X_1X_2X_3X_4) - \Pi_g^{R_1}(I - X_1X_2X_3X_4)\right), \\ L_2 &= \alpha\left(\sigma_-^{R_1}(I - X_1X_2X_3X_4) + \Pi_h^{R_1}(I + X_1X_2X_3X_4)\right), \\ L_3 &= \alpha\left(\sigma_+^{R_2}(I + X_1X_2X_5X_6) - \Pi_g^{R_2}(I - X_1X_2X_5X_6)\right), \\ L_4 &= \alpha\left(\sigma_-^{R_2}(I - X_1X_2X_5X_6) + \Pi_h^{R_2}(I + X_1X_2X_5X_6)\right), \\ L_5 &= \alpha\left(\sigma_+^{R_3}(I + X_1X_3X_5X_7) - \Pi_g^{R_3}(I - X_1X_3X_5X_7)\right), \\ L_6 &= \alpha\left(\sigma_-^{R_3}(I - X_1X_3X_5X_7) + \Pi_h^{R_3}(I + X_1X_3X_5X_7)\right), \\ L_7 &= \alpha\left(\sigma_+^{R_4}(I + Z_1Z_2Z_3Z_4) - \Pi_g^{R_4}(I - Z_1Z_2Z_3Z_4)\right), \\ L_8 &= \alpha\left(\sigma_-^{R_4}(I - Z_1Z_2Z_3Z_4) + \Pi_h^{R_4}(I + Z_1Z_2Z_3Z_4)\right), \\ L_9 &= \alpha\left(\sigma_+^{R_5}(I + Z_1Z_2Z_5Z_6) - \Pi_g^{R_5}(I - Z_1Z_2Z_5Z_6)\right), \\ L_{10} &= \alpha\left(\sigma_-^{R_5}(I - Z_1Z_2Z_5Z_6) + \Pi_h^{R_5}(I + Z_1Z_2Z_5Z_6)\right), \\ L_{11} &= \alpha\left(\sigma_+^{R_6}(I + Z_1Z_3Z_5Z_7) - \Pi_g^{R_6}(I - Z_1Z_3Z_5Z_7)\right), \\ L_{12} &= \alpha\left(\sigma_-^{R_6}(I - Z_1Z_3Z_5Z_7) + \Pi_h^{R_6}(I + Z_1Z_3Z_5Z_7)\right). \end{aligned} \tag{4.54}$$

Any desired Markovian error model can be incorporated via additional Lindblad terms, *e.g.*, for bit-flip errors,

$$L_{12+n} = \sqrt{\Gamma}X_n, \quad n \in 1 \ldots Q, \tag{4.55}$$

or for spontaneous emission-type decoherence,

$$L_{12+n} = \sqrt{\Gamma}(X_n - iY_n), \quad n \in 1 \ldots Q. \tag{4.56}$$

In either case, the parameter Γ adjusts the decoherence rate. Noise processes acting on the controller degrees of freedom can be included in the analogous fashion.

4.4.3 Master equation for 5-qubit code

If we next consider the five-qubit code, the smallest quantum error correcting code capable of protecting a single encoded qubit against arbitrary single-qubit errors [22, 50], the following lookup table gives the error syndromes for X, Z and Y errors acting on the register qubits:

Error syndromes for 5-qubit code

Error	M1	M2	M3	M4
X1	■	○	■	■
X2	○	■	○	■
X3	■	○	■	○
X4	■	■	○	■
X5	○	■	■	○
Z1	■	■	○	■
Z2	■	■	○	○
Z3	○	■	■	■
Z4	○	○	■	■
Z5	■	○	○	■
Y1	■	○	○	○
Y2	○	■	○	○
Y3	○	○	■	○
Y4	○	○	○	■
Y5	○	○	○	○

It appears by inspection that the syndromes of X_n, Z_n and Y_n are not simply related, so evidently we must implement a feedback controller with sufficient logic to react

conditionally to each of the fifteen four-bit syndromes. For the separable seven-qubit code we have seen that only two independent sets of seven three-bit syndromes need to be interpreted, suggesting that the feedback control sub-circuit in an autonomous quantum memory based on the seven-qubit code could be substantially simpler than for the five-qubit code, *even though it involves two additional stabilizer generators.* Given that we have in mind a homogeneous implementation paradigm, in which the quantum error-correcting controller is constructed from components that are very similar in nature to those of the codeword register [35], this comparison suggests a general advantage of separable codes in terms of implementation circuit complexity and concomitant physical resource requirements.

Applying the construction described above for a non-separable code, we arrive at the following master equation for a coherent feedback implementation of the five-qubit code:

$$\begin{aligned} H = \; \Omega\Big(& X_1\Pi_h^{R_1}\Pi_g^{R_2}\Pi_h^{R_3}\Pi_h^{R_4} + X_2\Pi_g^{R_1}\Pi_h^{R_2}\Pi_g^{R_3}\Pi_h^{R_4} + X_3\Pi_h^{R_1}\Pi_g^{R_2}\Pi_h^{R_3}\Pi_g^{R_4} + \\ & X_4\Pi_h^{R_1}\Pi_h^{R_2}\Pi_g^{R_3}\Pi_h^{R_4} + X_5\Pi_g^{R_1}\Pi_h^{R_2}\Pi_h^{R_3}\Pi_g^{R_4} + \\ & Z_1\Pi_h^{R_1}\Pi_h^{R_2}\Pi_g^{R_3}\Pi_g^{R_4} + Z_2\Pi_h^{R_1}\Pi_h^{R_2}\Pi_h^{R_3}\Pi_g^{R_4} + Z_3\Pi_g^{R_1}\Pi_h^{R_2}\Pi_h^{R_3}\Pi_h^{R_4} + \\ & Z_4\Pi_g^{R_1}\Pi_g^{R_2}\Pi_h^{R_3}\Pi_h^{R_4} + Z_5\Pi_h^{R_1}\Pi_g^{R_2}\Pi_g^{R_3}\Pi_h^{R_4} + \\ & Y_1\Pi_h^{R_1}\Pi_g^{R_2}\Pi_g^{R_3}\Pi_g^{R_4} + Y_2\Pi_g^{R_1}\Pi_h^{R_2}\Pi_g^{R_3}\Pi_g^{R_4} + Y_3\Pi_g^{R_1}\Pi_g^{R_2}\Pi_h^{R_3}\Pi_g^{R_4} + \\ & Y_4\Pi_g^{R_1}\Pi_g^{R_2}\Pi_g^{R_3}\Pi_h^{R_4} + Y_5\Pi_g^{R_1}\Pi_g^{R_2}\Pi_g^{R_3}\Pi_g^{R_4}), \end{aligned} \tag{4.57}$$

$$
\begin{aligned}
L_1 &= \alpha\left(\sigma_+^{R_1}(I + Z_2X_3X_4Z_5) - \Pi_g^{R_1}(I - Z_2X_3X_4Z_5)\right), \\
L_2 &= \alpha\left(\sigma_-^{R_1}(I - Z_2X_3X_4Z_5) + \Pi_h^{R_1}(I + Z_2X_3X_4Z_5)\right), \\
L_3 &= \alpha\left(\sigma_+^{R_2}(I + Z_1Z_3X_4X_5) - \Pi_g^{R_2}(I - Z_1Z_3X_4X_5)\right), \\
L_4 &= \alpha\left(\sigma_-^{R_2}(I - Z_1Z_3X_4X_5) + \Pi_h^{R_2}(I + Z_1Z_3X_4X_5)\right), \\
L_5 &= \alpha\left(\sigma_+^{R_3}(I + X_1Z_2Z_4X_5) - \Pi_g^{R_3}(I - X_1Z_2Z_4X_5)\right), \\
L_6 &= \alpha\left(\sigma_-^{R_3}(I - X_1Z_2Z_4X_5) + \Pi_h^{R_3}(I + X_1Z_2Z_4X_5)\right), \\
L_7 &= \alpha\left(\sigma_+^{R_4}(I + X_1X_2Z_3Z_5) - \Pi_g^{R_4}(I - X_1X_2Z_3Z_5)\right), \\
L_8 &= \alpha\left(\sigma_-^{R_4}(I - X_1X_2Z_3Z_5) + \Pi_h^{R_4}(I + X_1X_2Z_3Z_5)\right). \qquad (4.58)
\end{aligned}
$$

Again, decoherence processes acting on the register qubits and/or the controller degrees of freedom can be incorporated using additional Lindblad terms.

The modeling approach that I have described also admits a straightforward extension to incorporate the effects of optical propagation losses in the waveguides that connect components within the nanophotonic circuit [56], which lead to important considerations of loss-tolerant circuit layout that will be discussed below. As an illustrative example we first consider the probe subnetwork that extracts the error syndrome for the first stabilizer generator in the five-qubit code, $Z_2X_3X_4Z_5$. This measurement is implemented by sequentially interrogating the second, third, fourth and fifth register qubit-resonator components with a coherent laser field. In an idealized model with no optical propagation losses for the probe field, the net effect of these couplings is represented completely by the pair of coupling terms L_1 and L_2 given in the above section. In a more realistic model that accounts for optical waveguide losses, however, information leaks out into the environment as the probe field propagates between components in the photonic circuit. In the previous section (4.3.2), we saw that the resulting decoherence processes are described by additional coupling terms which amount to errors, some of which are correlated errors of multiple qubits that

the five-bit code is not designed to correct:

$$L_n = \alpha\theta Z_5, \qquad L_{n+1} = \alpha\theta X_4 Z_5,$$
$$L_{n+2} = \alpha\theta X_3 X_4 Z_5, \qquad L_{n+3} = \alpha\theta Z_2 X_3 X_4 Z_5. \tag{4.59}$$

Here θ parameterizes the probe field loss per waveguide segment. Similar sets of additional errors would arise from losses along the probe field paths associated with each of the other three stabilizer generators.

4.4.4 Connection to discrete-time, measurement based models

While our analysis leading to Eqs. (4.59) has been grounded in the specialized modeling framework of autonomous nanophotonic circuits, these findings generally parallel known results from discrete-time, measurement-based implementation scenarios. We obtained correlated error processes by considering probe field propagation losses in a coherent feedback network, but analogous difficulties would result from any syndrome extraction mechanism in which the ancillary qubits used to accumulate the stabilizer generator values are subject to decoherence. For example, an idealized continuous-time measurement of the parity of a pair of register qubits Q_1, Q_2 in our framework [34, 35] can be thought of as corresponding to the standard quantum computational circuit diagram on the left, below:

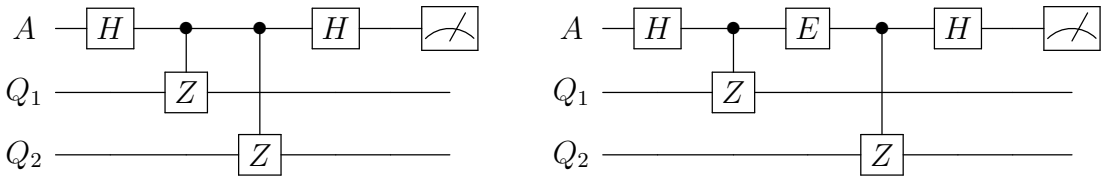

The propagation losses we have considered essentially correspond to an error process acting on the ancillary qubit A, which takes place between the controlled-Z gates as indicated by the E gate in the above-right diagram. Of course, ancilla decoherence in quantum error correction has been treated in detail in the literature on fault-tolerant

computing, as described for example in [55, 32]. In our context it is natural to assume that the dominant type of error process acting on the syndrome probe fields is optical loss, and in what follows I will show that it is possible to improve the robustness of the type of autonomous quantum memory we consider simply by optimizing the circuit layout.

4.4.5 Gauge subsystems and circuit layout optimization

There turns out to be an interesting connection between circuit layout and robustness to propagation losses in our approach, for autonomous quantum memories based on subsystem codes. Also known as operator quantum error correcting codes, subsystem codes are generalizations of decoherence free subspaces, noiseless subsystems, and quantum error correcting codes, which have gained popularity in recent years because of the large class of encoded logical operators these codes induce, which allows for simplified error recovery [4, 43]. In [36] we considered a nanophotonic circuit for implementing a continuous-time version of the Bacon-Shor code, and noted that it is possible to reduce the circuit complexity by taking advantage of the subsystem flexibility in choosing register-qubit operations for corrective feedback. Here we further note that the subsystem structure also presents key advantages for syndrome extraction, as (following a fundamental insight discussed by Aliferis and Cross [3]) we can route the probe fields along paths that push the extra errors induced by optical propagation losses onto the unimportant gauge qubit degrees of freedom. Consequently, the correlated errors described above for the five-qubit code and in [56] for the nine-qubit code (4.3.2) are no longer present and the storage fidelity of the encoded qubit is substantially increased (confirming a prediction presented originally in [36]). We will quantify the performance improvement using numerical simulations, below.

To illustrate the robust routing strategy, we consider the Bacon-Shor six-body stabilizer generator $Z_8 Z_7 Z_5 Z_4 Z_2 Z_1$, which is one of two such Z-string operators for the bit-flip subnetwork [36, 56, 3] (see also 4.3.2). In our nanophotonic circuit model, optical propagation losses experienced by the probe field used to monitor this stabilizer

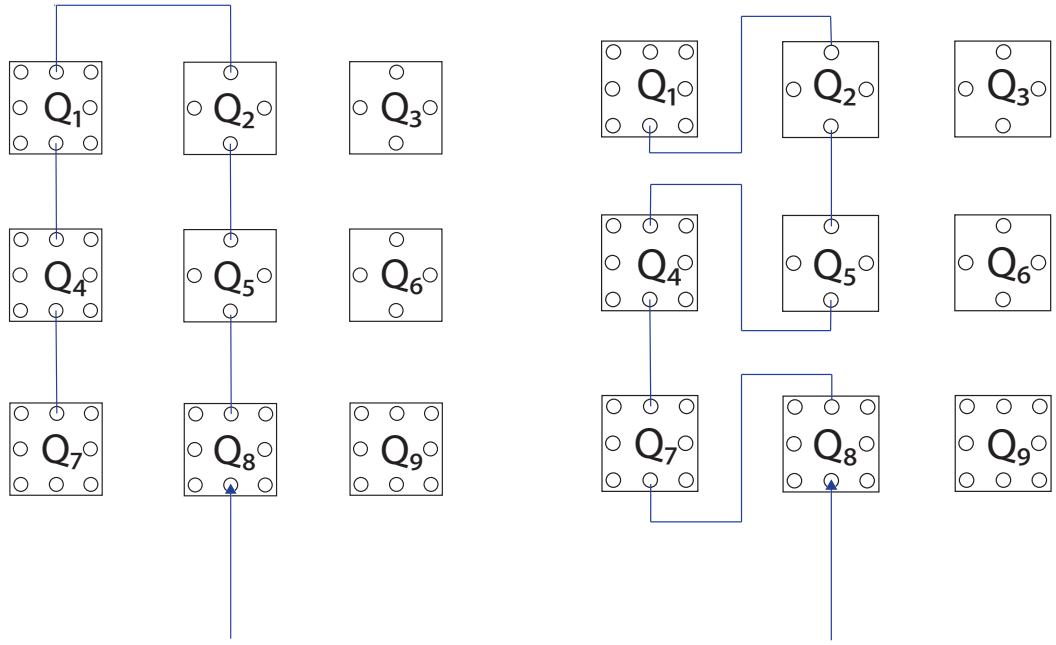

Figure 4.13: Left: Standard probe network for Bacon-Shor nine-qubit code. Right: Subsystem routing for loss protection.

generator will give rise to the following coupling terms, four of which are network-induced errors that the code is not designed to correct (while L_n is a correctable error and L_{n+5} merely dephases the stabilizer generator eigenstates, which does not compromise the quantum memory):

$$\begin{aligned} L_n &= \alpha\theta Z_8, & L_{n+1} &= \alpha\theta Z_5 Z_8, \\ L_{n+2} &= \alpha\theta Z_2 Z_5 Z_8, & L_{n+3} &= \alpha\theta Z_1 Z_2 Z_5 Z_8, \\ L_{n+4} &= \alpha\theta Z_4 Z_1 Z_2 Z_5 Z_8, & L_{n+5} &= \alpha\theta Z_7 Z_4 Z_1 Z_2 Z_5 Z_8. \end{aligned} \tag{4.60}$$

In deriving the above set of coupling terms we have assumed a geometrically simple routing of the probe beam, assuming the register qubit-resonator components are arranged in a 3×3 grid (which allows us to simplify the feedback signal routing as discussed in [36]), as shown in the left-hand schematic of Fig. 4.13. The scattering order is $Z_8 \to Z_5 \to Z_2 \to Z_1 \to Z_4 \to Z_7$, which bears a clear relation to the

correlated error terms shown in Eqs. (4.60). However, we can measure the same stabilizer generator by routing the probe beam to the components in a different order as shown in the right-hand schematic of Fig. 4.13, $Z_8 \rightarrow Z_7 \rightarrow Z_4 \rightarrow Z_5 \rightarrow Z_2 \rightarrow Z_1$. In an idealized model with no propagation losses the scattering order should make no difference since the single-qubit Pauli operators commute. However, with propagation losses the second routing scheme leads to the following coupling terms in place of those of Eqs. (4.60):

$$\begin{aligned} L_{n+1} &= \alpha\theta Z_8, & L_{n+2} &= \alpha\theta Z_7 Z_8, \\ L_{n+3} &= \alpha\theta Z_4 Z_7 Z_8, & L_{n+4} &= \alpha\theta Z_5 Z_4 Z_7 Z_8, \\ L_{n+5} &= \alpha\theta Z_2 Z_5 Z_4 Z_7 Z_8, & L_{n+6} &= \alpha\theta Z_1 Z_2 Z_5 Z_4 Z_7 Z_8. \end{aligned} \tag{4.61}$$

In the subsystem structure of the Bacon-Shor code, the operators $Z_1 Z_2$, $Z_2 Z_3$, $Z_4 Z_5$, $Z_5 Z_6$, $Z_7 Z_8$, and $Z_8 Z_9$ are all logical operators on the unimportant gauge-qubit degrees of freedom. Consequently, each of the coupling terms in Eqs. (4.61) corresponds to either a single logical qubit error or the product of a logical qubit error and one or more gauge qubit errors. Since the single qubit errors taking place on the logical space are protected by the network, this implementation of the probe mechanism is substantially more tolerant of propagation losses, as we illustrate using numerical simulations in Fig. 4.14.

In Fig. 4.14 we display the average fidelity decay $F(t) \equiv \langle \Psi_0 | \rho_t | \Psi_0 \rangle$ over 10^4 simulated quantum trajectories (each) for lossy quantum memories implementing the five-, six-, seven- and nine-qubit codes [22, 59, 4], which may be compared directly with analogous results from our prior work on other codes [35, 36, 56] (see also 4.3.2). In Fig. 4.15 we display the average decay (again over 10^4 quantum trajectory simulations for each code) of an alternative performance measure,

$$F^*_\tau(t) = \max_{t^* \in [t, t+\tau]} F(t^*).$$

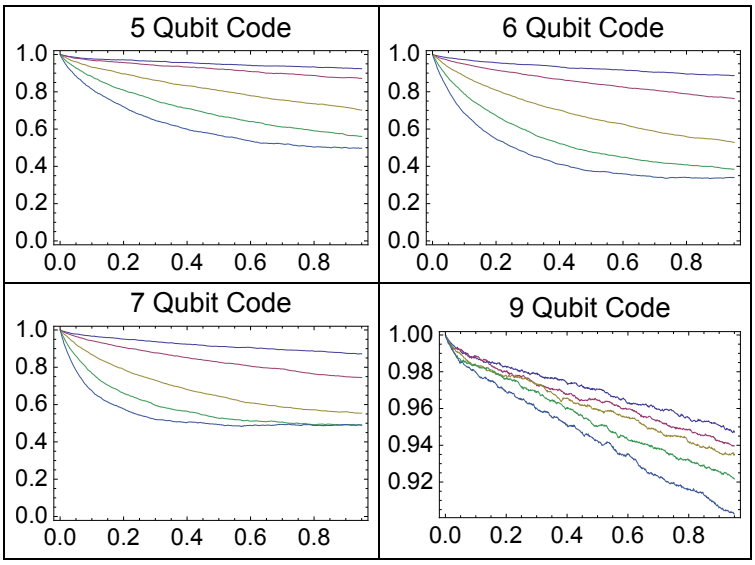

Figure 4.14: Decay of fidelity $\langle\Psi_0|\rho_t|\Psi_0\rangle$ for the five-, six-, seven- and nine-qubit quantum error correcting codes with loss parameters $\theta = \{0, 1, 2.5, 5, 7.5, 10\}\pi/1000$ (top to bottom curves). For consistency with [35] the feedback strength $\Omega = \frac{|\beta|^2\gamma}{2\Delta}$ is set to a constant value of 200 in each case. Note the substantial difference in the scale of the Y-axis for the bottom right corner plot—this is for the nine-qubit Bacon-Shor code with the loss-tolerant probe network.

The quantity F^* represents an easily computable, convenient statistic which we believe is a more meaningful measure of performance of a realistic quantum memory than the canonical fidelity measure. Our definition of F^* is motivated by the observation that, in any realistic quantum memory, there must be a finite latency of error correction. This behavior is clearly illustrated for our class of models by the individual quantum trajectory simulations of fidelity versus time shown in Fig. 4.16. Because of the (random) time delay required for an error-correcting controller with finite-strength measurement and feedback to restore the register state after a decoherence event, fidelity does not decay monotonically along individual quantum trajectories [46]. This behavior has a pronounced effect on the appearance of a simple plot of average $F(t)$ at small t as some trajectories in the ensemble will experience errors at very early times without recovering immediately; this sub-ensemble induces the steep initial decay transient seen for example for $t \lesssim 0.05$ in the nine-qubit panel

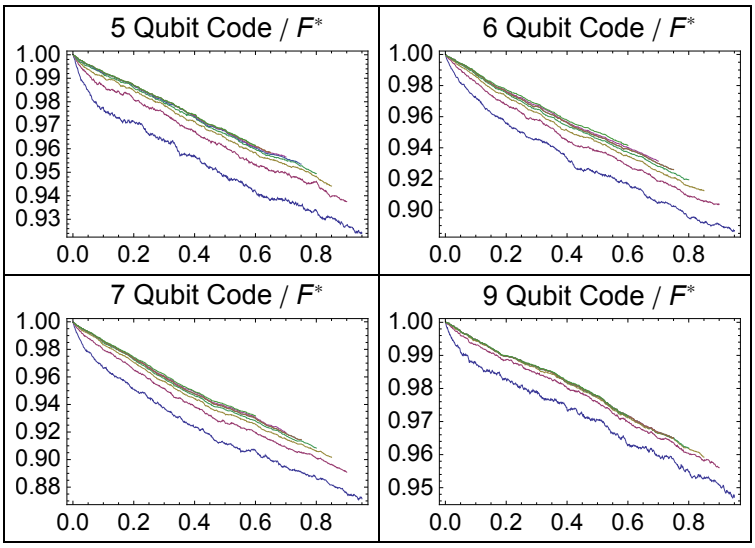

Figure 4.15: Averaged finite time-horizon fidelity for 10^4 quantum trajectories (each) of lossy five-, six-, seven-, and nine-qubit codes with loss parameter $\theta = \frac{\pi}{1000}$ and $\tau = 0.05, 0.1, 0.15, 0.2, 0.25, 0.3, 0.35$ and 0.4 (bottom to top traces in each sub-panel).

of Fig. 4.14. If we recognize that many (even most) of these trajectories will in fact regain $F \sim 1$ after a finite delay, as seen in the examples of Fig. 4.16, it seems intuitive to adopt a performance measure such as $F^*(t)$ that looks ahead over a window of time in each trajectory to check for such a recovery. Of course if an additional error should occur within a given trajectory before the feedback network has had time to correct the initial one, the encoded information can be lost and $F^*(t) \to 0$ accordingly.

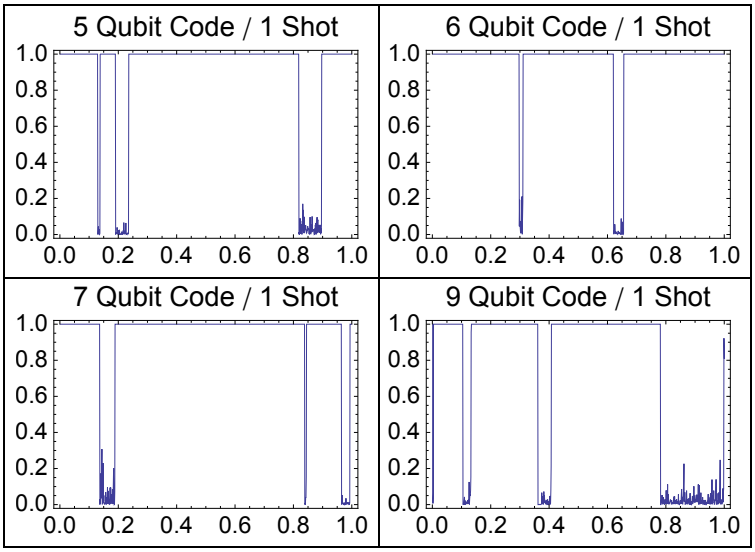

Figure 4.16: Fidelity trace for single-shot quantum trajectory simulations of five-, six-, seven-, and nine-qubit codes.

Chapter 5

Conclusion

The work I've described in this thesis represents a focused case study of several systems in which feedback control of quantum dynamics is accomplished via field-mediated, all-optical signal processing. In the introductory sections, I reviewed some recently developed quantum optics theory for modeling open quantum systems and described how these tools, and in particular, the Gough-James circuit algebra, can be used in a context which suggests a photonics analogue of classical electrical circuit theory. This theory is remarkably flexible in its application and I've given a few representative examples of the kinds of systems that can be modeled, such as the squeezed-light setup described in the second chapter, and the autonomous quantum memories which were the focal point of the thesis.

Let me close with a few brief remarks about quantum error correction and coherent feedback control. In the introduction, I suggested that coherent feedback control can be thought of as an engineering analogue to quantum information theory. That is, rather than starting with a quantum algorithm and trying to work backwards to engineer a system tailored to that particular algorithm's performance requirements, the viewpoint that I've advocated in this work is to see if we can develop an understanding of quantum mechanical performance advantages from an engineering perspective by starting with the basic principles of feedback control and working from the bottom up. So while this perspective motivates the work I've presented here, the autonomous

quantum memories I've analyzed in the second half of this thesis do not quite qualify as being "true" coherent feedback systems. That is, notice that the cavity-QED relays are effectively classical devices. Despite being described by quantum mechanical equations of motion, we can determine which of the two states the switch is in by monitoring the power of the output ports. Consequently, it is perhaps more appropriate to call these devices "semi-coherent" feedback systems, whereas the squeezed light setup described in the second chapter is a fully coherent feedback device.

To design fully coherent quantum memories, it seems as though we would need to move beyond the stabilizer framework. Stabilizer codes are fundamentally classical codes in that the localization of the error subspace is determined by bit strings of classical information– see for example, the intuitive picture of stabilizer codes presented in Appendix B. It would seem that truly coherent quantum memories might gain a performance advantage over semi-coherent devices by taking advantage of the complementary modes of an optical probe field [29] to reduce the number of error operators that are measured or decrease the feedback latency. However, as these field operators do not commute, the stabilizer framework, which takes as its starting point, an Abelian subgroup of an error group, would not be adequate. Unfortunately, the theory of non-stabilizer codes [40, 38, 41, 42, 39] is not nearly as developed and it is not entirely straightforward to imagine extending coherent controllers in the linear setting to the non-linear setting of quantum error correction. This is certainly a deep and interesting topic for future research.

As one final point for future investigation, let me mention a connection between the work I've presented here and quantum computing via adiabatic evolution [16]. Part of the interest in the adiabatic approach to quantum computing (AQC) has come from the fact that there appears to be an inherent resistance to errors due to the energy gap between the qubit ground and excited states. Still, it does seem that for reliable large scale computation, some kind of active error correction would be needed, and in [33, 74], the authors have shown that the stabilizer formalism can be adapted to the setting of continuous, adiabatic evolution. These models do not involve active

error correction, but rather, they use stabilizer codes to create an energy gap between the code-space and the error space. The observation that the "always on" nature of adiabatic evolution is compatible with stabilizer codes suggests an immediate connection with the models I have presented here. In particular, recall the canonical master equation of chapter 4 for autonomous quantum memories. Although this Hamiltonian is time-independent, it is straightforward to simulate an analogous time-dependent Hamiltonian in which adiabatic evolution of the form described in [16] is "superimposed" on top of the quantum memory. Of course, this is a purely phenomenological model, and future work on this topic might involve designing realistic physical models for incorporating quantum error correction via coherent feedback along side the continuous time evolution of the adiabatic interpolation Hamiltonian.

Practically, it seems as though the master equation corresponding to an adiabatic quantum computer + error correction with coherent feedback should look like the following:

Hamiltonian: if the code is separable:

$$H = \frac{t}{T}H_{final} + \frac{T-t}{T}H_{initial} + \sum_{k=1}^{M}\sum_{n=1}^{N}\left(X_n^{Q_k}\cdot\mathcal{F}_{\mathcal{S}_X}\left[X_n^{Q_K}\right] + Z_n^{Q_k}\cdot\mathcal{F}_{\mathcal{S}_Z}\left[Z_n^{Q_k}\right]\right)$$

if the code is not separable:

$$H = \frac{t}{T}H_{final} + \frac{T-t}{T}H_{initial} + \sum_{k=1}^{M}\sum_{n=1}^{N}\left(X_n^{Q_k}\cdot\mathcal{F}_{\mathcal{S}_X}\left[X_n^{Q_k}\right] + Y_n^{Q_k}\cdot\mathcal{F}_{\mathcal{S}_Y}\left[Y_n^{Q_k}\right] + Z_n^{Q_k}\cdot\mathcal{F}_{\mathcal{S}_Z}\left[Z_n^{Q_k}\right]\right)$$

where $H_{initial}$ is an easily prepared initial state Hamiltonian and H_{final} is the target Hamiltonian whose ground state encodes the solution to our problem of interest and where we have used the standard linear interpolation Hamiltonian to encode the adiabatic evolution between initial and final states. Notice that the error correcting terms are written as double sums over each encoded logical qubit and that we have removed the term corresponding to the "penalty" Hamiltonian given in [33]. The coupling terms and noises are identical to the ordinary, time-dependent models described in

the previous chapters.

As a toy model, we can simulate adiabatic evolution on a single qubit. Following [16] we choose the initial Hamiltonian:

$$H_B = \frac{1}{2} - \frac{1}{2}\sigma_x$$

and the final Hamiltonian

$$H_B = \frac{1}{2} + \frac{1}{2}\sigma_z$$

We can encode the single qubit in any stabilizer code. For simplicity, we start out with the 3 qubit bit-flip code. In both of these plots, the noise Γ ranges from 0 to .1 with evenly spaced increments:

Table 5.1: Noisy adiabatic evolution with and without error correction

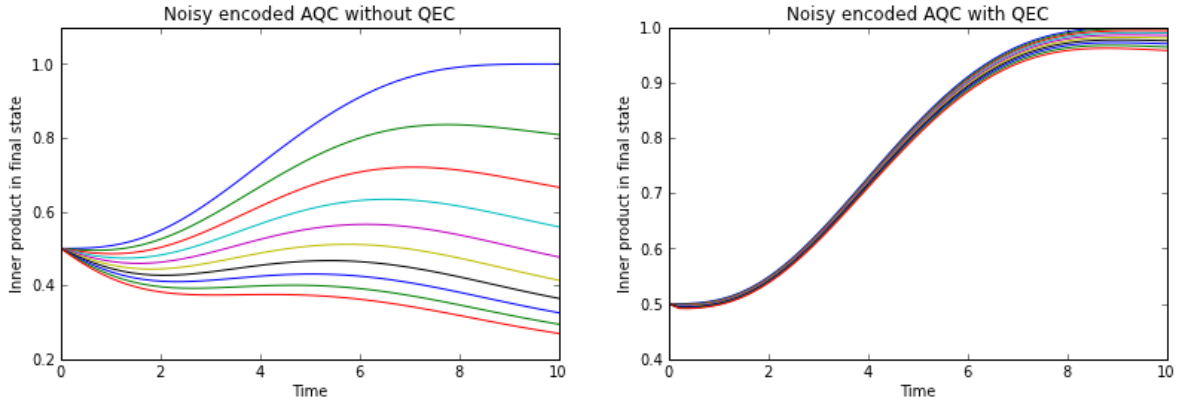

Of course, these results are simply for a toy model with a single qubit, but they suggest that in thinking about possible ways of using autonomous quantum memories for the sake of computation, the gate model is not the only choice. However, note that we have simply used a phenomenological master equation in characterizing the encoded adiabatic evolution, which necessarily means that we have chosen to ignore what in this case are relevant atomic dynamics. For instance, since the qubit model in the

autonomous quantum memories I have described in this thesis encodes logical information in degenerate ground states, it would not be suitable for adiabatic evolution. Important work along these lines would involve designing realistic pre-limit models for the register qubits as well as mechanisms for implementing adiabatic evolution.

Appendix A

AC Stark Shift Compensation for Quantum Memories

The physical mechanism used by the quantum memories proposed in [34, 36] and discussed here in Chapter 4 rely on Raman resonance conditions for issuing corrective feedback. While this is an elegant mechanism, the Raman interaction also introduces AC Stark shifts to the qubit ground states that break the degeneracy between the joint qubit states. In [34], the authors have proposed several mechanisms to counteract these effects, one of which attempts to engineer the atomic level structure of the qubits so as to cancel the AC Stark shift on each component, and the other is to modify the network so as to minimize the effects of the Stark shifts.

In the first approach, we assume a more complicated level structure which contains two additional exited states $\{|H\rangle, |G\rangle\}$, which are coupled to the ground states $\{|h\rangle, |g\rangle\}$ with the opposite detuning $-k\Delta$. Equivalently, instead of presuming additional excited states, we could simply have two additional free field modes, both of which couple to $|r\rangle$ with the opposite detuning. In either case, the pre-limit SLH model would have the following form:

$$Q_{R^+}^{(k)} = \left(I_2, \begin{bmatrix} \sqrt{2\gamma}(\sigma_{hr} + \sigma_{Hr}) \\ \sqrt{2\gamma}(\sigma_{gr} + \sigma_{gG}) \end{bmatrix}, k^2\Delta(\Pi_r - \Pi_H - \Pi_G) \right) \tag{A.1}$$

$\|Q_1Q_2Q_3\|R_1R_2\rangle$	SS(Q1)	SS(Q2)	SS(Q3)
$\|hhh\|hh\rangle$	0	0	-2Ω
$\|ggg\|hh\rangle$	-2Ω	0	0
$\|hgg\|gh\rangle$	-2Ω	0	0
$\|ghh\|gh\rangle$	-1Ω	-1Ω	0
$\|hgh\|gg\rangle$	-1Ω	-1Ω	0
$\|ghg\|gg\rangle$	0	-1Ω	-1Ω
$\|hhg\|hg\rangle$	0	-1Ω	-1Ω
$\|ggh\|hg\rangle$	0	0	-2Ω

Table A.1: The table displays the network configuration for each of 8 possible error states and the corresponding AC Stark shift experienced by each qubit, under the Hamiltonian in Equation 4.37. Using the mechanism described above, when the relays correctly represent the error state, the joint qubit state will experience a total -2Ω AC Stark shift.

In this case, the limiting SLH model after applying the adiabatic elimination theorem, would be:

$$\left(I, 0, -\frac{\gamma}{\Delta}(\beta_1\beta_2^*\sigma_{gh} + \beta_1^*\beta_2\sigma_{gh}^*)\right) \tag{A.2}$$

In other words, the limiting SLH model with the additional excited states, or additional free field couplings, gives rise to the same SLH model as in equation (4.14), but without the first two terms of the Hamiltonian.

An alternate approach, which is ultimately what is used in the network calculations in [34] (see Section 4.2.4), is to choose Raman transitions and the corresponding intensities so that the net AC Stark shift on any joint qubit state is equal to -2Ω (see Table A.1). Consequently, dephasing of the codewords only takes place in the interval in between changes in the qubit parities. Thus, increasing the probe strength α results in a decrease of codeword dephasing during these intervals. The benefit of this approach over the one previously described is a simpler set of network components.

Appendix B

The Bacon-Shor Code

B.1 An intuitive explanation of subsystem codes

The presence of the"gauge subsystem" in the Bacon-Shor code is a critical factor in enabling the autonomous quantum memories I presented in the preceding sections. Here I give an intuitive overview of the operation of this code, and some detailed calculations which elucidate the structure of the state space and the nature of the logical operators. My hope is that these sections provide a very concrete and digestible set of explanations to complement the more representation theoretic flavor of [4, 43].

To understand the structure of the 9-qubit Bacon-Shor code, we start with the stabilizer group for 9-qubit Shor code:

Q	Q_1	Q_2	Q_3	Q_4	Q_5	Q_6	Q_7	Q_8	Q_9
M_1	Z	Z	I	I	I	I	I	I	I
M_2	I	Z	Z	I	I	I	I	I	I
M_3	I	I	I	Z	Z	I	I	I	I
M_4	I	I	I	I	Z	Z	I	I	I
M_5	I	I	I	I	I	I	Z	Z	I
M_6	I	I	I	I	I	I	I	Z	Z
M_7	X	X	X	X	X	X	I	I	I
M_8	I	I	I	X	X	X	X	X	X

As the Shor code is formed by concatenating the 3-qubit bit-flip code with the 3-qubit phase-flip code, it is traditionally thought of as being the simplest code capable of protecting a single logical qubit against arbitrary single-qubit errors. However, in examining the first 6 stabilizer generators, we see that the Shor code is in fact capable of protecting the logical qubit for more than just single qubit errors. Note that each pair of Z-parity measurements takes place on disjoint code blocks. This implies that not only can the code correct for arbitrary single qubit errors, but it can also correct for correlated phase errors that take place on disjoint code blocks. Of course, these errors are not really errors at all, as the net overall phase is unchanged. This observation suggests that we can in fact collapse the first 6 stabilizer generators into 2 and maintain the same degree of protection for the encoded qubit:

Q	Q_1	Q_2	Q_3	Q_4	Q_5	Q_6	Q_7	Q_8	Q_9
M_1	Z	Z	I	Z	Z	I	Z	Z	I
M_2	I	Z	Z	I	Z	Z	I	Z	Z
M_3	X	X	X	X	X	X	I	I	I
M_4	I	I	I	X	X	X	X	X	X

We now have a simpler stabilizer code with only 4 error syndromes to measure, rather than 6. But what has happened to the overall structure of the Hilbert space? The following simple picture of stabilizer codes illustrates the matter. A stabilizer code is effectively a *classical* code, and we can think of the the error syndromes as giving us classical bits of information which, when taken in total, allows us to localize a specific error. In particular, for a stabilizer code which encodes a single logical qubit into N physical qubits, each error syndrome (taking the values ± 1) gives us a single classical bit of information, which effectively divides the Hilbert space in 2. Thus after acquiring k error syndromes, the Hilbert space dimension is $2^N/2^k = 2^{N-k}$. It should come as no surprise, then, for all of the non-subsystem codes we have encountered so far– the 3-qubit bit-flip/phase-flip code, the 5-qubit code, and 7-qubit code, and the 9-qubit Shor code– the number of stabilizer generators has always been $k = N - 1$, so that the Hilbert space dimension after acquiring all k error syndromes is simply 2, i.e., the Hilbert space of a single qubit.

What then is going on with our modified Shor code which encodes a single logical qubit into 9 physical qubits, but with only 4 stabilizer generators? Applying the above reasoning, we see that the code-space has Hilbert space dimension $2^9/2^4 = 2^5$. We are emphatically *not* encoding 5 logical qubits in this code. What is happening, which I will show more carefully in the next section, is that the code space now includes, in addition to our logical qubit, 4 *gauge qubits*, whose states we do not care about. It is precisely these additional gauge qubits which give rise to the flexibility of subsystem codes, as any logical operators need only act modulo the subsystem structure.

B.2 State space structure

We begin with the 9-qubit code, where, as described above, we collapse the 8 stabilizer generators into the following 4:

$$S_{X1} = X_1X_2X_3X_4X_5X_6 \tag{B.1}$$
$$S_{X2} = X_4X_5X_6X_7X_8X_9 \tag{B.2}$$
$$S_{Z1} = Z_1Z_2Z_4Z_5Z_7Z_8 \tag{B.3}$$
$$S_{Z2} = Z_2Z_3Z_5Z_6Z_8Z_9 \tag{B.4}$$

As described in [4], the corresponding logical operators are given by

$$X_L = X_1X_2X_3 \tag{B.5}$$
$$Z_L = Z_1Z_4Z_7 \tag{B.6}$$

And correspondingly

$$\begin{aligned} Y_L &= \frac{1}{2i}(Z_L X_L - X_L Z_L) && \text{(B.7)} \\ &= \frac{1}{2i}(Z_1 Z_4 Z_7 X_1 X_2 X_3 - X_1 X_2 X_3 Z_1 Z_4 Z_7) && \text{(B.8)} \\ &= \frac{1}{2i}(Z_1 X_1 - X_1 Z_1) X_2 X_3 Z_4 Z_7 && \text{(B.9)} \\ &= Y_1 X_2 X_3 Z_4 Z_7 && \text{(B.10)} \end{aligned}$$

It is straightforward to verify that the following two-body operators commute with the stabilizer generators and the logical operators:

$$\begin{gathered} X_1X_4, X_2X_5, X_3X_6, X_4X_7, X_5X_8, X_6X_9 \\ Z_1Z_2, Z_2Z_3, Z_4Z_5, Z_5Z_6, Z_7Z_8, Z_8Z_9 \end{gathered}$$

Our goal is to understand precisely how the logical operators on the gauge space can act without affecting the logical information stored in the remaining qubits. As a first step, we note that the eigenspace corresponding to the $+1$ eigenvalues of S_{Z1} and S_{Z2} includes:

$$\begin{gathered} |+++++++++\rangle, |---------\rangle \\ |++++++--\rangle, |------++\rangle \\ |+++---++\rangle, |---+++--\rangle \\ |---++++++\rangle, |+++----\rangle \end{gathered}$$

Here, we've assumed a row wise ordering of qubits, $|Q_{11}Q_{12}Q_{13}Q_{21}Q_{22}Q_{23}Q_{31}Q_{32}Q_{33}\rangle$. Similarly, we can write the $+1$ eigenstates of S_{X1} and S_{X2} as follows:

$$\begin{aligned} |LX+\rangle &= \frac{1}{\sqrt{8}}(|+++\rangle + |---\rangle)^{\otimes 3} \\ |LX-\rangle &= \frac{1}{\sqrt{8}}(|+++\rangle - |---\rangle)^{\otimes 3} \end{aligned}$$

We have the following relations for the kets $|LX\pm\rangle$

$$X_L|LX\pm\rangle = \pm|LX\pm\rangle, Z_L|LX\pm\rangle = \pm|LX\mp\rangle \tag{B.11}$$

which allows us to write the vectors $|LZ\pm\rangle$ as

$$\begin{aligned}
|LZ+\rangle &= \frac{1}{\sqrt{2}}(|LX+\rangle + |LX-\rangle \\
&= \frac{1}{\sqrt{2}}(|+++++++++\rangle + |+++---\!--\rangle + \\
&\quad |---+++--\rangle + |-------++\rangle) \\
|LZ-\rangle &= \frac{1}{\sqrt{2}}(|LX+\rangle - |LX-\rangle \\
&= \frac{1}{\sqrt{2}}(|---++++++\rangle + |+++---++\rangle + \\
&\quad |+++++\!--\rangle + |---------\rangle)
\end{aligned}$$

Correspondingly, we have:

$$|LX+\rangle = \frac{1}{\sqrt{2}}(|LZ+\rangle + |LZ-\rangle) \tag{B.12}$$

$$|LX-\rangle = \frac{1}{\sqrt{2}}(|LZ+\rangle - |LZ-\rangle) \tag{B.13}$$

If we look at the two-body operators listed above– the "gauge" operators:

$$X_1X_4, X_2X_5, X_3X_6, X_4X_7, X_5X_8, X_6X_9$$
$$Z_1Z_2, Z_2Z_3, Z_4Z_5, Z_5Z_6, Z_7Z_8, Z_8Z_9$$

we can see that the logical Z operators on the gauge space, that is, the operators $Z_{i,j}Z_{i,j+1}$ leave $|LZ\pm\rangle$ and $|LX\pm\rangle$ invariant.

To see that the logical X operators on the gauge qubits similarly leave the code-space invariant, we compute, as an example, the action of one of the logical X gauge

operators on an element of the code space:

$$\begin{aligned} X_1X_4|LZ+\rangle =& \frac{1}{2}(|-+++-++++\rangle + |-+++---+-\rangle + \\ & |+---++--+\rangle + |+--+--++\rangle) \end{aligned} \tag{B.14}$$

Now we examine the action of the stabilizer generators and logical Z operator on this vector:

$$\begin{aligned} S_{X1}X_1X_4|LZ+\rangle &= X_1X_4|LZ+\rangle \\ S_{X2}X_1X_4|LZ+\rangle &= X_1X_4|LZ+\rangle \\ S_{Z1}X_1X_4|LZ+\rangle &= X_1X_4|LZ+\rangle \\ S_{Z2}X_1X_4|LZ+\rangle &= X_1X_4|LZ+\rangle \\ Z_LX_1X_4 &= X_1X_4|LZ+\rangle \end{aligned}$$

Now we compute the action of the logical X operator on this vector:

$$\begin{aligned} X_LX_1X_4|LZ+\rangle &= \frac{1}{2}(|+---++++\rangle + |+--+----\rangle + \\ &\quad |-+++-+++--\rangle + |-+++--++\rangle) \\ X_1X_4|LZ-\rangle &= \frac{1}{2}(|+---++++\rangle + |-+++--++\rangle + \\ &\quad |-++-+++--\rangle + |+--+----\rangle) \end{aligned}$$

We see therefore that $X_L|LZ+\rangle = X_1X_4|LZ-\rangle$, demonstrating how the gauge operators can act on the state vector while preserving the logical information encoded in the qubit (analogous computations can be done for the remaining gauge operators).

B.3 Localization of errors

We can determine how errors are localized and where to issue corrective feedback by examining the action of the the stabilizer generators on corrupted logical states. For

example, we have the following:

$$\begin{aligned} S_{Z1}X_1|LZ+\rangle &= -|LZ+\rangle \\ S_{Z2}X_1|LZ+\rangle &= +|LZ+\rangle \\ S_{Z1}X_2|LZ+\rangle &= -|LZ+\rangle \\ S_{Z2}X_2|LZ+\rangle &= -|LZ+\rangle \end{aligned}$$

Computing the analogous expression for the remaining qubits, we find that we can succinctly express the action of the stabilizer generators on corrupted states as follows:

$$\{S_{Z1}, S_{Z2}\}X_1 \to \{-,+\}, \{S_{Z1}, S_{Z2}\}X_2 \to \{-,-\}, \{S_{Z1}, S_{Z2}\}X_3 \to \{+,-\}$$
$$\{S_{Z1}, S_{Z2}\}X_4 \to \{-,+\}, \{S_{Z1}, S_{Z2}\}X_5 \to \{-,-\}, \{S_{Z1}, S_{Z2}\}X_6 \to \{+,-\}$$
$$\{S_{Z1}, S_{Z2}\}X_7 \to \{-,+\}, \{S_{Z1}, S_{Z2}\}X_8 \to \{-,-\}, \{S_{Z1}, S_{Z2}\}X_9 \to \{+,-\}$$

And analogously for the phase-flip errors:

$$\{S_{X1}, S_{X2}\}Z_1 \to \{-,+\}, \{S_{X1}, S_{X2}\}Z_2 \to \{-,+\}, \{S_{X1}, S_{X2}\}Z_3 \to \{-,+\}$$
$$\{S_{X1}, S_{X2}\}Z_4 \to \{-,-\}, \{S_{X1}, S_{X2}\}Z_5 \to \{-,-\}, \{S_{X1}, S_{X2}\}Z_6 \to \{-,-\}$$
$$\{S_{X1}, S_{X2}\}Z_7 \to \{+,-\}, \{S_{X1}, S_{X2}\}Z_8 \to \{+,-\}, \{S_{X1}, S_{X2}\}Z_9 \to \{+,-\}$$

Thus, we see that X errors can be localized to a column while Z errors are localized to a row. Examining again the gauge operators,

$$X_1X_4, X_2X_5, X_3X_6, X_4X_7, X_5X_8, X_6X_9$$
$$Z_1Z_2, Z_2Z_3, Z_4Z_5, Z_5Z_6, Z_7Z_8, Z_8Z_9$$

we se that, for example, if we detect a Z error on the first row, by applying a correction to Z_2, the net effect will be the gauge operator Z_1Z_2 or Z_2Z_3, which will restore the logical qubit to the correct state. Analogously, for errors in the second or third row,

we can apply the correction Z_5 or Z_8. For X errors in the first column, we apply X_4, in the second column X_5, and in the third column X_6.

B.4 Syndrome extraction for optimal routing

As described briefly in Section 4.4.5, we can express the stabilizer generators in the following modified form:

$$S_{X1} = (X_1X_4)(X_5X_2)(X_3X_6) \tag{B.15}$$
$$S_{X2} = (X_7X_4)(X_5X_8)(X_9X_6) \tag{B.16}$$
$$S_{Z1} = (Z_1Z_2)(Z_5Z_4)(Z_7Z_8) \tag{B.17}$$
$$S_{Z2} = (Z_3Z_2)(Z_5Z_6)(Z_9Z_8) \tag{B.18}$$

If we apply the usual Hamiltonian correction terms as in the lossless case, i.e.:

$$\{S_{X1}, S_{X2}\} = \{-,+\} \rightarrow Z_1, \{S_{X1}, S_{X2}\} = \{-,-\} \rightarrow Z_4, \{S_{X1}, S_{X2}\} = \{+,-\} \rightarrow Z_7$$
$$\{S_{Z1}, S_{Z2}\} = \{-,+\} \rightarrow X_1, \{S_{Z1}, S_{Z2}\} = \{-,-\} \rightarrow X_2, \{S_{Z1}, S_{Z2}\} = \{+,-\} \rightarrow X_3$$

then we see that the modified syndrome extraction will leave the network dynamics unchanged. On the other hand, incorporating the effects of propagation losses, we see that loss-induced errors will now factor as the product of single qubit logical errors and single qubit gauge errors (the terms in parenthesis). Thus, we see that the gauge subsystem in the Bacon-Shor code allows us to eliminate correlated errors that would otherwise be present in a lossy photonic network.

Bibliography

[1] Luigi Accardi, Alberto Frigerio, and Y.G. Lu. The weak coupling limit as a quantum functional central limit. *Communications in Mathematical Physics*, (131):537–570, 1990. http://projecteuclid.org/DPubS?service=UI&version=1.0&verb=Display&handle=euclid.cmp/1104200937. (p. 35.)

[2] Charlene Ahn, Andrew Doherty, and Andrew Landahl. Continuous quantum error correction via quantum feedback control. *Physical Review A*, 65(4):042301, March 2002. http://link.aps.org/doi/10.1103/PhysRevA.65.042301. (p. 47.)

[3] Panos Aliferis and Andrew Cross. Subsystem fault tolerance with the Bacon-Shor code. *Physical Review Letters*, 98(22):1–4, May 2007. http://link.aps.org/doi/10.1103/PhysRevLett.98.220502. (p. 91.)

[4] Dave Bacon. Operator quantum error-correcting subsystems for self-correcting quantum memories. *Physical Review A*, 73(1):1–13, January 2006. http://link.aps.org/doi/10.1103/PhysRevA.73.012340. (p. 91, 93, 104, and 106.)

[5] Alberto Barchielli. Direct and heterodyne detection and other applications of quantum stochastic calculus to quantum optics. *Quantum Optics Journal of the European Optical Society Part B*, 2:423, 1990. http://iopscience.iop.org.offcampus.lib.washington.edu/0954-8998/2/6/002. (p. 15.)

[6] Alberto Barchielli and Giancarlo Lupieri. Quantum stochastic calculus, operation valued stochastic processes, and continual measurements in quantum mechanics. *Journal of Mathematical Physics*, 26(9):2222, 1985. http://link.aip.org/link/JMAPAQ/v26/i9/p2222/s1&Agg=doi. (p. 41.)

[7] Patrick Billingsley. *Probability and Measure*. Wiley, 1979. (p. 16.)

[8] Luc Bouten, John Stockton, Gopal Sarma, and Hideo Mabuchi. Scattering of polarized laser light by an atomic gas in free space: A quantum stochastic differential equation approach. *Physical Review A*, 75(5):1–8, 2007. http://link.aps.org/doi/10.1103/PhysRevA.75.052111. (p. 5 and 36.)

[9] Luc Bouten, Ramon Van Handel, and Matthew R. James. An introduction to quantum filtering. *SIAM Journal on Control and Optimization*, 46(6):2199–2241, 2006. http://epubs.siam.org/doi/abs/10.1137/060651239. (p. 15 and 47.)

[10] Luc Bouten, Ramon van Handel, and Andrew Silberfarb. Approximation and limit theorems for quantum stochastic models with unbounded coefficients. *Journal of Functional Analysis*, 254(12):3123–3147, June 2008. http://linkinghub.elsevier.com/retrieve/pii/S0022123608000876. (p. 23, 49, 52, 56, 66, 77, and 81.)

[11] Bradley A Chase, Heather L Partner, Brigette D Black, Benjamin Q Baragiola, Robert L Cook, and J M Geremia. Magnetic field estimation at and beyond 1/N scaling via an effective nonlinearity. Technical report, 2009. http://arxiv.org/pdf/0708.2730.pdf. (p. 28.)

[12] Claude Cohen-Tannoudji, Jacques Dupont-Roc, and Gilbert Grynberg. *Atom photon interactions: basic processes and applications*. Wiley-VCH, 1998. http://books.google.com/books/about/Atom_Photon_Interactions.html?id=QYl5QgAACAAJ. (p. 7, 12, and 13.)

[13] Jordi Cortadella, Michael Kishinevsky, Alex Kondratyev, Luciano Lavagno, and Politecnico Torino. Petrify: a tool for manipulating concurrent specifications and synthesis of asynchronous controllers. *IEICE Transactions on Information Systems*, E80-D(315), 1997. https://www.google.com/url?sa=t&rct=j&q=&esrc=s&source=web&cd=1&cad=rja&ved=0CDAQFjAA&url=http%3A%2F%2Fciteseerx.ist.psu.edu%2Fviewdoc%2Fdownload%3Fdoi%3D10.1.1.27.3124%26rep%3Drep1%26type%3Dpdf&ei=Md_0UPeNO6KciQLRpIG4DQ&usg=AFQjCNFIM4bnEbLNjIxaIm9pT8k9NOqVIA. (p. 77 and 78.)

[14] Eric Dennis, Alexei Kitaev, Andrew Landahl, and John Preskill. Topological quantum memory. *Journal of Mathematical Physics*, 43(9):4452, 2002. http://link.aip.org/link/JMAPAQ/v43/i9/p4452/s1&Agg=doi. (p. 47.)

[15] L-M Duan and H J Kimble. Scalable photonic quantum computation through cavity-assisted interactions. *Physical Review Letters*, 92(12):127902, 2004. http://link.aps.org/doi/10.1103/PhysRevLett.92.127902. (p. 51.)

[16] Edward Farhi, Jeffrey Goldstone, Sam Gutmann, and Michael Sipser. Quantum Computation by Adiabatic Evolution. 2000. http://arxiv.org/abs/quant-ph/0001106. (p. 98, 99, and 100.)

[17] Peter Fritzson. *Principles of object-oriented modeling and simulation with Modelica*. Wiley-IEEE, 2004. http://books.google.com/books?id=doNqLi7279wC&printsec=frontcover&source=gbs_ge_summary_r&cad=0#v=onepage&q&f=false. (p. 68.)

[18] Crispin W. Gardiner. *Handbook of Stochastic Methods*. Springer, 2004. (p. 23 and 24.)

[19] Crispin W. Gardiner and Matthew Collett. Input and output in damped quantum systems: Quantum stochastic differential equations and the master equation. *Physical Review A*, 31(6):3761–3774, 1985. http://pra.aps.org/abstract/PRA/v31/i6/p3761_1. (p. 29 and 39.)

[20] Crispin W. Gardiner, A. Scott Parkins, and Peter Zoller. Wave-function quantum stochastic differential equations and quantum-jump simulation methods. *Physical Review A*, 46(7), 1992. http://pra.aps.org/abstract/PRA/v46/i7/p4363_1. (p. 6, 12, 13, and 18.)

[21] Crispin W. Gardiner and Peter Zoller. *Quantum Noise: A Handbook of Markovian and Non-Markovian Quantum Stochastic Methods with Applications to Quantum Optics*. Springer, Berlin, 2004. http://books.google.com/books/about/Quantum_Noise.html?id=a_xsT8oGhdgC. (p. 6, 12, 14, and 82.)

[22] Daniel Gottesman. *Stabilizer codes and quantum error correction*. PhD thesis, California Institute of Technology, 1997. http://arxiv.org/abs/quant-ph/9705052. (p. 83, 84, 87, and 93.)

[23] John Gough. Quantum flows as Markovian limit of emission, absorption and scattering interactions. *Communications in Mathematical Physics*, 254(2):489–512, August 2004. http://www.springerlink.com/index/10.1007/s00220-004-1163-y. (p. 35.)

[24] John Gough. Feynman diagrams and the quantum stochastic calculus. *Banach Center Publications*, 73:187–298, 2006. http://arxiv.org/pdf/quant-ph/0411064.pdf. (p. 35.)

[25] John Gough and Matthew R. James. Quantum feedback networks: Hamiltonian formulation. *Communications in Mathematical Physics*, 287(3):1109–1132, December 2008. http://www.springerlink.com/index/10.1007/s00220-008-0698-8. (p. 81.)

[26] John Gough and Matthew R. James. The series product and its application to quantum feedforward and feedback networks. *IEEE Transactions on Automatic Control*, 54(11):2530–2544, November 2009. http://ieeexplore.ieee.org/lpdocs/epic03/wrapper.htm?arnumber=5286277. (p. 38, 75, and 81.)

[27] John E. Gough, Hendra I. Nurdin, and Sebastian Wildfeuer. Commutativity of the adiabatic elimination limit of fast oscillatory components and the instantaneous feedback limit in quantum feedback networks. *Journal of Mathematical Physics*, 51(12):123518, 2010. http://link.aip.org/link/JMAPAQ/v51/i12/p123518/s1&Agg=doi. (p. 77 and 81.)

[28] Matthew A. Hall, Joseph B. Altepeter, and Prem Kumar. All-optical switching of photonic entanglement. *New Journal of Physics*, 14(3):039501, March 2012. http://stacks.iop.org/1367-2630/14/i=3/a=039501?key=crossref.f2a8eff23ea7e33e489633c148cafa3a. (p. 67.)

[29] Ryan Hamerly and Hideo Mabuchi. Advantages of Coherent Feedback for Cooling Quantum Oscillators. *Physical Review Letters*, 109(17):173602, October 2012. http://link.aps.org/doi/10.1103/PhysRevLett.109.173602. (p. 3 and 98.)

[30] R. L. Hudson and K. R. Parthasarathy. Quantum Ito's formula and stochastic evolutions. *Communications in Mathematical Physics*, 93(3):301–323, 1984. http://link.springer.com/article/10.1007%2FBF01258530?LI=true#page-1. (p. 18 and 35.)

[31] Fedor Jelezko and Jörg Wrachtrup. Focus Issue on Diamond-Based Photonics and Spintronics. *New Journal of Physics*, 14(105024), 2012. http://iopscience.iop.org/1367-2630/14/10/105024/cites. (p. 67.)

[32] N. Cody Jones, Rodney Van Meter, Austin Fowler, Peter McMahon, Jungsang Kim, Thaddeus Ladd, and Yoshihisa Yamamoto. Layered architecture for quantum computing. *Physical Review X*, 2(3):1–27, July 2012. http://link.aps.org/doi/10.1103/PhysRevX.2.031007. (p. 91.)

[33] Stephen P Jordan, Edward Farhi, and Peter W Shor. Error Correcting Codes For Adiabatic Quantum Computation. http://arxiv.org/pdf/quant-ph/0512170v3.pdf. (p. 98 and 99.)

[34] Joseph Kerckhoff, Luc Bouten, and Andrew Silberfarb. Physical model of continuous two-qubit parity measurement in a cavity-QED network. *Physical Review A*, pages 1–4, 2009. http://pra.aps.org/abstract/PRA/v79/i2/e024305. (p. 25, 51, 71, 82, 90, 102, and 103.)

[35] Joseph Kerckhoff, Hendra I. Nurdin, Dmitri S. Pavlichin, and Hideo Mabuchi. Designing quantum memories with embedded control: photonic circuits for autonomous quantum error correction. *Physical Review Letters*, 105(4):040502, July 2010. http://prl.aps.org/abstract/PRL/v105/i4/e040502. (p. 46, 47, 49, 51, 72, 77, 78, 81, 88, 90, 93, and 94.)

[36] Joseph Kerckhoff, Dmitri S. Pavlichin, Hamid Chalabi, and Hideo Mabuchi. Design of nanophotonic circuits for autonomous subsystem quantum error correction. *New Journal of Physics*, 13(5):055022, May 2011. http://stacks.iop.org/1367-2630/13/i=5/a=055022?key=crossref.d99fc3128b0b06539af630d6d0e8aa1b. (p. 47, 77, 82, 91, 92, 93, and 102.)

[37] Alexi Yu Kitaev. Fault-tolerant quantum computation by anyons. *Annals of Physics*, 303(2):1–27, 2008. http://www.sciencedirect.com/science/article/pii/S0003491602000180. (p. 47.)

[38] Andreas Klappenecker. Clifford code constructions of operator quantum error-correcting codes. *Information Theory, IEEE*, pages 9–13, 2008. http:

//ieeexplore.ieee.org/xpls/abs_all.jsp?arnumber=4675716. (p. 98.)

[39] Andreas Klappenecker. Clifford subsystem codes. *Information Theory Proceedings (ISIT), 2010*, pages 2667–2671, 2010. http://ieeexplore.ieee.org/xpls/abs_all.jsp?arnumber=5513672. (p. 98.)

[40] Andreas Klappenecker and Rötteler Martin. Clifford Codes. In Ranee K. Brylinski and Goong Chen, editors, *Mathematics of Quantum Computation*, chapter 1, pages 1–21. Chapman and Hall. http://citeseerx.ist.psu.edu/viewdoc/summary?doi=10.1.1.21.1064. (p. 98.)

[41] Andreas Klappenecker and M Rötteler. Beyond Stabilizer Codes II: Clifford Codes. pages 1–9. http://arxiv.org/pdf/quant-ph/0010076.pdf. (p. 98.)

[42] Andreas Klappenecker and Martin Rötteler. Remarks on Clifford codes. *Information Theory, 2004. ISIT Proceedings.*, pages 1–10, 2004. http://ieeexplore.ieee.org/xpls/abs_all.jsp?arnumber=1365391. (p. 98.)

[43] David Kribs, Raymond Laflamme, and David Poulin. A unified and generalized approach to quantum error correction. *Physical Review Letters*, 94(180501):5, December 2004. http://arxiv.org/abs/quant-ph/0412076. (p. 91 and 104.)

[44] Hideo Mabuchi. Derivation of Maxwell-Bloch-type equations by projection of quantum models. *Physical Review A*, (1):4. http://arxiv.org/abs/0803.2887, volume = 78, year = 2008. (p. 17.)

[45] Hideo Mabuchi. Cavity-QED models of switches for attojoule-scale nanophotonic logic. *Physical Review A*, 80(4):1–4, October 2009. http://link.aps.org/doi/10.1103/PhysRevA.80.045802. (p. 58, 78, and 82.)

[46] Hideo Mabuchi. Continuous quantum error correction as classical hybrid control. *New Journal of Physics*, 11(10):105044, October 2009. http://stacks.iop.org/1367-2630/11/i=10/a=105044?key=crossref.90b742f51abf111dc49ad9b7aac50606. (p. 47 and 94.)

[47] Hideo Mabuchi. Nonlinear interferometry approach to photonic sequential logic. *Applied Physics Letters*, 99(15):153103, 2011. http://link.aip.org/link/APPLAB/v99/i15/p153103/s1&Agg=doi. (p. 67.)

[48] Arvind Mithal and Xiaowei Shen. Using term rewriting systems to design and verify processors. *IEEE Micro Special Issue on Modeling and Validation of Microprocessors*, 1999. http://csg.csail.mit.edu/pubs/memos/Memo-419/memo-419.pdf. (p. 70.)

[49] Anne E. B. Nielsen. Fighting decoherence in a continuous two-qubit odd- or even-parity measurement with a closed-loop setup. *Physical Review A*, 81(1):012307, January 2010. http://link.aps.org/doi/10.1103/PhysRevA.81.012307. (p. 51.)

[50] Michael Nielsen and Isaac Chuang. *Quantum Information and Quantum Computation*. Cambridge University Press, Cambridge, 1st edition, 2004. http://books.google.com/books/about/Quantum_Computation_and_Quantum_Informat.html?id=65FqEKQOfP8C. (p. 3, 83, 84, and 87.)

[51] Jeremy O'Brien, Brian Patton, Masahide Sasaki, and Jelena Vuckovic. Focus Issue on Integrated Quantum Optics. *New Journal of Physics*, 15(035016), 2013. http://iopscience.iop.org/1367-2630/15/3/035016/. (p. 67.)

[52] Bernt Øksendal. *Stochastic Differential Equations*. Springer, 2003. http://books.google.com/books?id=VgQDWyihxKYC&printsec=frontcover#v=onepage&q&f=false. (p. 14 and 16.)

[53] K. R. Parthasarathy. *An Introduction to Quantum Stochastic Calculus*. Birkhauser, Berlin, 1992. http://books.google.com/books/

about/An_Introduction_to_Quantum_Stochastic_Ca.html?id=zqTvAAAAMAAJ. (p. 18 and 42.)

[54] Volnei A. Pedroni. *Circuit design with VHDL*. MIT Press, Cambridge, 2004. http://books.google.com/books/about/Circuit_Design_with_Vhdl.html?id=b5NEgENaEn4C. (p. 68.)

[55] John Preskill. Fault-tolerant quantum computation. 1997. http://arxiv.org/abs/quant-ph/9712048. (p. 91.)

[56] Gopal Sarma, Ryan Hamerly, Nikolas Tezak, Dmitri Pavlichin, and Hideo Mabuchi. Transformation of quantum photonic circuit models by term-rewriting. *IEEE Photonics*, 5(1), 2013. http://arxiv.org/abs/1206.1104. (p. 5, 47, 69, 71, 75, 77, 80, 81, 89, 91, and 93.)

[57] Gopal Sarma and Hideo Mabuchi. Gauge subsystems, separability, and robustness of autonomous quantum memories. *New Journal of Physics*, 15(035014), 2013. http://arxiv.org/abs/1212.3564. (p. 5.)

[58] Gopal Sarma, Andrew Silberfarb, and Hideo Mabuchi. Quantum stochastic calculus approach to modeling double-pass atom-field coupling. *Physical Review A*, 78(2):1–5, August 2008. http://arxiv.org/abs/0804.0806http://link.aps.org/doi/10.1103/PhysRevA.78.025801http://pra.aps.org/abstract/PRA/v78/i2/e025801. (p. 5.)

[59] Bilal Shaw, Mark Wilde, Ognyan Oreshkov, Isaac Kremsky, and Daniel Lidar. Encoding one logical qubit into six physical qubits. *Physical Review A*, 78(1):012337, July 2008. http://link.aps.org/doi/10.1103/PhysRevA.78.012337. (p. 93.)

[60] Jacob Sherson. *Quantum Memory and Teleportation Using Macroscopic Gas Samples*. PhD thesis, University of Aarhus, 2006. (p. 29.)

[61] Jacob Sherson and Klaus Mø lmer. Polarization squeezing by optical Faraday rotation. *Physical Review Letters*, 97(14):1–4, October 2006. http:

//link.aps.org/doi/10.1103/PhysRevLett.97.143602. (p. 28, 29, 30, 39, and 40.)

[62] Peter W Shor. Polynomial-Time Algorithms for Prime Factorization and Discrete Logarithms on a Quantum Computer. *Proceedings of the 35th Annual Symposium on Foundations of Computer Science*, 26(5):124–134, 1995. http://arxiv.org/abs/quant-ph/9508027. (p. 3.)

[63] Andrew Silberfarb and Ivan Deutsch. Continuous measurement with traveling-wave probes. *Physical Review A*, 68(1):013817, July 2003. http://link.aps.org/doi/10.1103/PhysRevA.68.013817. (p. 13.)

[64] John K Stockton. *Continuous Quantum Measurement of Cold Alkali-Atom Spins*. PhD thesis, California Institute of Technology, 2006. (p. 23 and 24.)

[65] Nikolas Tezak, Armand Niederberger, Dmitri S. Pavlichin, Gopal Sarma, and Hideo Mabuchi. Specification of photonic circuits using Quantum Hardware Description Language. *Philosophical Transactions of the Royal Society of London A*, 370:5270–5290, 2012. http://arxiv.org/abs/1111.3081. (p. 5, 67, 68, 75, 80, and 81.)

[66] Donald Thomas and Phillip Moorby. *The Verilog Hardware Description Language*. Springer, Berlin, 2001. http://www.springer.com/engineering/circuits+%26+systems/book/978-1-4020-7089-1. (p. 68.)

[67] Nicholas Thomas-Peter, Nathan K. Langford, Animesh Datta, Lijian Zhang, Brian J. Smith, J B Spring, Ben J. Metcalf, Hendrik B. Coldenstrodt-Ronge, M Hu, Joshua Nunn, and Ian A. Walmsley. Integrated photonic sensing. *New Journal of Physics*, 13(5):055024, May 2011. http://stacks.iop.org/1367-2630/13/i=5/a=055024?key=crossref.c5d25538a6c8d0c17737c932d6a40588. (p. 67.)

[68] C. J. Van Rijsbergen, editor. *Term Rewriting Systems (Cambridge Tracts in Theoretical Computer Science vol 55)*. Cambridge University Press, Cambridge,

2004. http://books.google.com/books/about/Term_Rewriting_Systems.html?id=7QQ5u-4tRUkC. (p. 70.)

[69] David Williams. *Probability with Martingales*. Cambridge University Press, 1991. (p. 16.)

[70] Wolfram Research. Mathematica. 2012. http://www.wolfram.com. (p. 68.)

[71] Alexandre Yakovlev and Albert Sangiovanni-Viicentelti. A unified signal transition graph model for asynchronous control circuit synthesis. In *International Conference on Computer-Aided Design*, page 104, 1992. http://ieeexplore.ieee.org/xpl/articleDetails.jsp?arnumber=279390&contentType=Conference+Publications. (p. 77 and 78.)

[72] Masahiro Yanagisawa and Hidenori Kimura. Transfer function approach to quantum control- part I: dynamics of quantum feedback systems. *IEEE Transactions on Automatic Control*, 48(12):2107–2120, December 2003. http://ieeexplore.ieee.org/lpdocs/epic03/wrapper.htm?arnumber=1254080. (p. 38.)

[73] Masahiro Yanagisawa and Hidenori Kimura. Transfer function approach to quantum control- part II: control concepts and applications, 2003. http://ieeexplore.ieee.org/lpdocs/epic03/wrapper.htm?arnumber=1254081. (p. 38.)

[74] Kevin C Young and Mohan Sarovar. Equivalence and limitations of error suppression techniques for adiabatic quantum computing. http://arxiv.org/pdf/1208.6371v1.pdf. (p. 98.)